HIGH RESOLUTION STUDY OF THE CONFORMATIONAL LANDSCAPE OF BIOMOLECULES IN THE GAS PHASE

by

Tri V. Nguyen

B.S., University of Charleston, 1997

M.B.A., University of Pittsburgh, 2005

Submitted to the Graduate Faculty of

Arts and Sciences in partial fulfillment

of the requirements for the degree of

Doctor of Philosophy

University of Pittsburgh

2005

UNIVERSITY OF PITTSBURGH

FACULTY OF ARTS AND SCIENCES

This dissertation was presented

by

Tri V. Nguyen

It was defended on

November 16, 2005

and approved by

Dr. Joseph Grabowski

Dr. Hrvoje Petek

Dr. Sunil Saxena

Dr. David W. Pratt
Committee Chairperson

HIGH RESOLUTION STUDY OF THE CONFORMATIONAL LANDSCAPE OF BIOMOLECULES IN THE GAS PHASE

Tri V. Nguyen, Ph.D.

University of Pittsburgh, 2005

Abstract.

Rotationally resolved electronic spectroscopy has been used to map the conformational landscape of isolated biomolecules in the gas phase. A multivariate analysis based on experimental measurements supplemented by *ab initio* calculations provides a detailed description of the low energy regions of the potential energy surface (PES) in both the ground and excited states. Our findings lead to interesting insights into the interactive forces shaping the contours of the PES and the dynamics of interconversion pathways. A novel perspective centered on the electron distribution is presented to address the issue of the correlation of shape and functionality.

FOREWORD

I would like to convey my gratitude to Dr. Pratt for his help and guidance during my studies. The many conversations we shared have really broadened my views about science and life. He has been a constant source of inspiration.

I also would like to thank the many members of the Pratt group. In particular, Dr. Jason Ribblett helped me tremendously by lessening the steepness of the "high resolution" learning curve. Dr. Timothy Korter and Dr. David Borst have shown me the inquisitiveness and attention to details needed to approach any project. Dr. Cheolwha Kang has been of great help dealing with the intricacies of theory and quantum mechanics. I also want to thank Jennifer Reese and Alexei Nikolaev who helped me with program decoding and writing. I would like to especially thank my officemate and great friend, Dr. John Yi, with whom I spent countless hours in the labs searching for that elusive perfect spectrum with no mode hop and infinite signal to noise ratio.

I want to thank Dr. Jon Hougen and Dr. David Plusquellic for their assistance and hospitality at NIST and Dr. Michael Pugh for his help during my stay at Bloomsburg University.

I would like to thank my parents and siblings who have been very supportive during my years at school. Finally, I want to thank two special persons who have been very dear to me and without whom I could not have accomplished so much: Em Nga va Em Ngoc, all I can say is thank you.

TABLE OF CONTENTS

LIST OF TABLES

LIST OF FIGURES

1. Introduction.

The topographical determination of the conformational landscape of macromolecules has been a challenging task due to the multitude of possible degrees of freedom, often resulting in an ensemble average. We use rotationally resolved electronic spectroscopy to map the conformational subspace of isolated biomolecules in the gas phase. By targeting a specific molecule or group of molecules, we gain unique and quantitative information on the conformational preferences in both the ground and excited states. This approach leads to a simplification of the complex potential energy surface by focusing on the molecules at the point of contact and demands a rigorous multivariate analysis to gain an understanding of the correlation between dynamics, energetics, structure and function. Measurements of the electronic transition moment and depiction of the excited state conformational landscape help in understanding the functionality of biological systems. One such example is in the field of molecular recognition where the key feature might be a structural change altering the effectiveness of the process being triggered by an interaction with light, and the subsequent sampling of a different conformational subspace.

In Chapter 2, we use the detailed results obtained from rotationally resolved electronic spectroscopy to study the role of symmetry. In particular, we based our study on Platt's rule on the S_1-S_0 transitions. Divinylbenzene was the molecule of choice due to the high symmetry present in its different isomers. Our findings show that the polarization of the electronic transition moment and the energetic ordering of the L_a and L_b states are influenced not only by the parent symmetry group but also by the direction of the symmetry axis.

In Chapter 3, we continue with the theme of symmetry as we investigate the effect of breaking symmetry on molecular systems. We focus on the intramolecular forces responsible for the conformational properties of indole acetic acid and indole propionic acid. In particular, we

are interested in the properties of the flexible side chains and its interaction with the indole chromophore. These molecules also serve as a nice stepping stone into the study of large three-dimensional biomolecules.

In Chapter 4, we continue our survey of biomolecules present at the point of contact in biological systems with tryptamine, an analogue of the amino acid tryptophan and a structural precursor of hallucinogens such as serotonin and LSD. We provide a complete description of the conformational landscape by assigning each transition to a unique structure. Furthermore, we are able to identify a possible hindered motion interconverting conformers *via* a two-dimensional pathway of a cross section of the potential energy surface.

The topic discussed in Chapter 5 is the dipole moment. This intrinsic property is important predictor in biological processes such as donor/acceptor tandem systems. By applying an electric field to the molecular beam, we determine the charge distribution of cross section of the energy landscape of tryptamine. We measure the magnitude and direction of the permanent electric dipole moment in both the ground and excited states for four tryptamine conformers. We also introduce an interesting perspective on the "through-bond" *vs*. "through-space" interactions via the topic of induced dipole moment.

In Chapter 6, we build on the knowledge accumulated in the study of tryptamine in Chapter 4 to investigate the solvent effect with a study of the tryptamine-water complex. The interesting finding is that the double hydrogen bonded system collapses the complex conformational landscape of tryptamine into a single dimer structure effectively locking the conformational system. An in-depth analysis results in both the position and the orientation of the water moiety.

In summary, our study indicates that the overall shape of polyatomic molecules is governed by weak interactions between distinctive parts of the molecules. These interactions are particularly important in tunning the elements within the side chain, thus leading to a convoluted conformational landscape. We also show that an increase in size does not necessarily result in a more complex landscape. These forces lower the number of possible structures present in the molecular beam by favoring specific conformers. This feature is also exemplified in the constraint imposed by the water moiety in leading to a single tryptamine-water complex. Finally, the Stark measurements suggest that a separate but not necessarily conflicting approach should be considered in addressing the behavior, characteristic and function of biomolecules.

2. Rotationally resolved electronic spectroscopy of some divinylbenzenes in the gas phase. Platt's rule revisited.

Tri V. Nguyen, Jason W. Ribblett[a], and David W. Pratt[b]

[a] Department of Chemistry, Ball State University, Muncie, Indiana 47306 USA.

[b] Department of Chemistry, University of Pittsburgh
Pittsburgh, Pennsylvania 15260 USA.

2.1. Abstract.

Platt's rule, as interpreted by Heilbronner and Murrell, states that "if a (an aromatic) molecule has a two-fold symmetry axis passing through an atom, then (electronic) transitions to *a* states are polarized parallel to that axis, and transitions to *b* states at right angles to this". We have observed and assigned the fully resolved electronic spectra of three divinylbenzenes, and used this rule to assign the character of their lowest excited electronic states in cases where the molecule has an in-plane C_2 axis.

Published in *Chemical Physics*, **283** (2002) 279.

2.2. **Introduction.**

Symmetry is an important property of molecular systems. The presence or absence of symmetry has many ramifications. An interesting example can be found in the electronic absorption spectra of substituted benzenes. Here, it was recently discovered that different conformers of the same molecule exhibit differently oriented electronic transition moments (TM's) in the molecular frame [1]. This effect was later traced to a mixing of the side chain orbitals with the π-orbitals of the ring, caused by an "off-axis" substituent that breaks a C_2 axis of symmetry lying in the aromatic plane [2]. These conformationally induced changes in the electronic structures of isolated molecules have developed into an important diagnostic of molecular structure and dynamics [3,4].

A mixing of the ring π-orbitals can lead to a reordering of the electronic states. Thus, the origin band in the S_1-S_0 transition of phenylacetylene is a pure *b*-type band [5], evidencing an S_1 state that is ^1L_b in character [6]. Most monosubstituted benzenes have lowest ^1L_b states in the gas phase. But the corresponding band of styrene is an *a*-type band [5], evidencing a lowest ^1L_a state. Breaking an in-plane C_2 axis of symmetry inverts the order of the ^1L_a and ^1L_b states in the isolated molecule.

We hypothesize that the normal ordering of the two states (^1L_b lower than ^1L_a) can be recovered in an "off-axis" molecule by introducing a second substituent that restores the C_2 axis. We test this hypothesis here by recording and analyzing the high resolution S_1-S_0 electronic spectra of three divinylbenzenes, deducing from these analyses the orientation of the electronic TM in the molecular frame, and thereby determining which of the two S_1 states lies lower in energy. The molecule of choice was 1,4-divinylbenzene (DVB), which can exist in two isomeric forms, shown below:

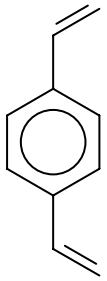

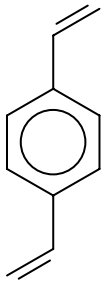

cis-1,4-DVB *trans*-1,4-DVB

We reasoned that *cis*-1,4-DVB would have a lowest ^1L_b state, whereas *trans*-1,4-DVB would have a lowest ^1L_a state (its C_2 axis is perpendicular to the plane). Unfortunately, whereas the latter prediction was confirmed, the former was not, owing to our inability to observe the spectrum of *cis*-1,4-DVB. However, a similar study of two 1,3-DVB's (adventitiously present in the commercial sample) confirmed our initial hypothesis; restoring the in-plane C_2 axis lowers the ^1L_b state below ^1L_a, providing a new application of Platt's rule [6] to substituted benzenes.

2.3. **Experiment.**

DVB was purchased from Fluka and used without further purification. The sample was 80% pure. Previous gas chromatography analyses [7] have shown that a typical commercially available sample of DVB contains a 2:1:1:1 ratio of 1,3-DVB, 1,4-DVB, 3-ethylstyrene, and 4-ethylstyrene, respectively, as well as a small amount (0.01%) of the inhibitor *p-t*-butylcatechol. The vibrationally resolved S_1-S_0 excitation spectrum of a similar sample was obtained using a pulsed jet apparatus. At room temperature, the sample was seeded into He gas at 90 psi and expanded into a chamber kept at 10^{-5} torr through a 1 mm diameter orifice pulsed valve (General Valve Series 9) operating at 10 Hz. Molecules were excited by a frequency-doubled dye laser

(Quanta Ray Model PDL-1) pumped by a Nd^{+3}:YAG (Model DCR-1A) laser also operating at 10 Hz. The dye laser was frequency doubled into the UV by a potassium dihydrogen phosphate (KDP) crystal. The spectral resolution of the dye laser is 0.6 cm^{-1} in the ultraviolet. The following dyes were used; LDS 751, LDS 698, a mixture of DCM-Kiton Red, Rhodamine 610, and Rhodamine 590. The laser beam crossed the supersonic jet about 2.5 cm downstream of the nozzle. The fluorescence signal was collected by a photomultiplier (EMI 98139B) using a single lens system, recorded by a boxcar integrator, and processed by a data acquisition system (MASSCOMP MCS561). Calibration of the spectrum was performed by recording the 1 cm^{-1} markers from a solid etalon.

The high resolution apparatus has been described elsewhere [8]. The sample was heated to ~ 78º C, seeded into 2 psi of He, and expanded into a vacuum through a 240 μm nozzle. The molecular beam was formed by passing the expansion through a 1 mm skimmer 2 cm downstream of the nozzle and crossed with a modified CW ring dye laser 15 cm downstream of the nozzle, giving a Doppler-limited resolution of ~ 18 MHz. The fluorescence was collected by a PMT and stored on the MASSCOMP data acquisition system. Absolute frequency calibration was performed by simultaneously recording the I_2 signal and frequency markers from a stabilized etalon with a spectral range of 299.7520 ± 0.0005 MHz.

The rotationally resolved spectra were analyzed using a modified version of ASYROT [9] that employs Watson's asymmetric rotor Hamiltonian [10]. Fits of the spectra were made using a standard least squares analysis and previously described fitting strategies [8]. *Ab initio* calculations were performed using the Gaussian 98 suite [11] of electronic structure programs.

2.4. **Results and Interpretation.**

Figure 2-1 shows the laser induced fluorescence (LIF) excitation spectrum of the commercial sample of DVB in the region 290 – 318 nm. Clearly evident is the large number of bands that defy simple interpretation. The strongest bands are at 31409 cm^{-1} (Band A), 32164 cm^{-1} (Band B), and 32553 cm^{-1} (Band C). Accompanying these are numerous weaker bands extending all the way to 34000 cm^{-1}, well below the S_1-S_0 origin of styrene at 34759 cm^{-1} [5]. It is likely that more than one isomer (or conformer) of DVB is present, but how these are related is not obvious from Fig. 2-1. No prominent Franck-Condon progressions exist to aid in this analysis.

Rotationally resolved electronic spectroscopy is an extremely powerful tool for distinguishing one isomer or conformer of a molecule from another. This is because the different equilibrium structures have different moments of inertia. Previously, we have used this technique in studies of 1- and 2-hydroxynaphthalene [12], 2-hydroxypyridine [13], hydroquinone [14], 2-vinylnaphthalene [15], and even linear polyenes [16]. Here, we apply it to the divinylbenzenes.

Figure 2-2 shows the rotationally resolved fluorescence excitation spectrum of Band A in DVB at 31409 cm^{-1}. The bottom two traces are simulations with and without the addition of a lineshape function. Band A exhibits ~ 2000 resolved lines and was fit by assigning 287 transitions. The resulting standard deviation is 2.64 MHz. The lineshape of each transition has a Voigt profile composed of ~ 18 MHz (FWHM) for the Doppler-broadened Gaussian component and ~ 20 MHz (FWHM) for the lifetime-broadened Lorentzian component. The corresponding fluorescence lifetime is about 8 ns.

Figure 2-3 shows the corresponding spectrum of Band B located at 32164 cm^{-1} along with the fit of a magnified portion of the Q-branch. The standard deviation of the fit of 290

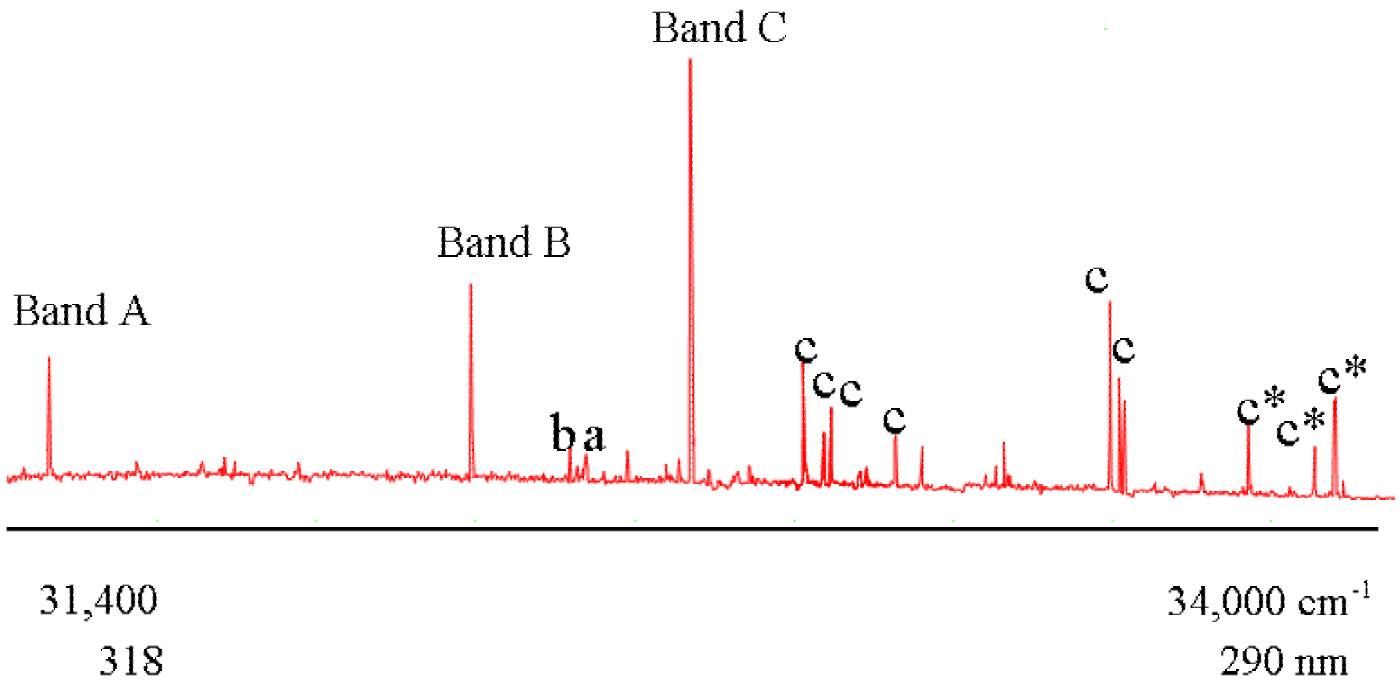

Figure 2-1. Vibrationally resolved fluorescence excitation spectrum of DVB, showing the assignment of higher vibrational bands to specific isomers/conformers (asterisks denote bands with strong perturbations at higher K_a's).

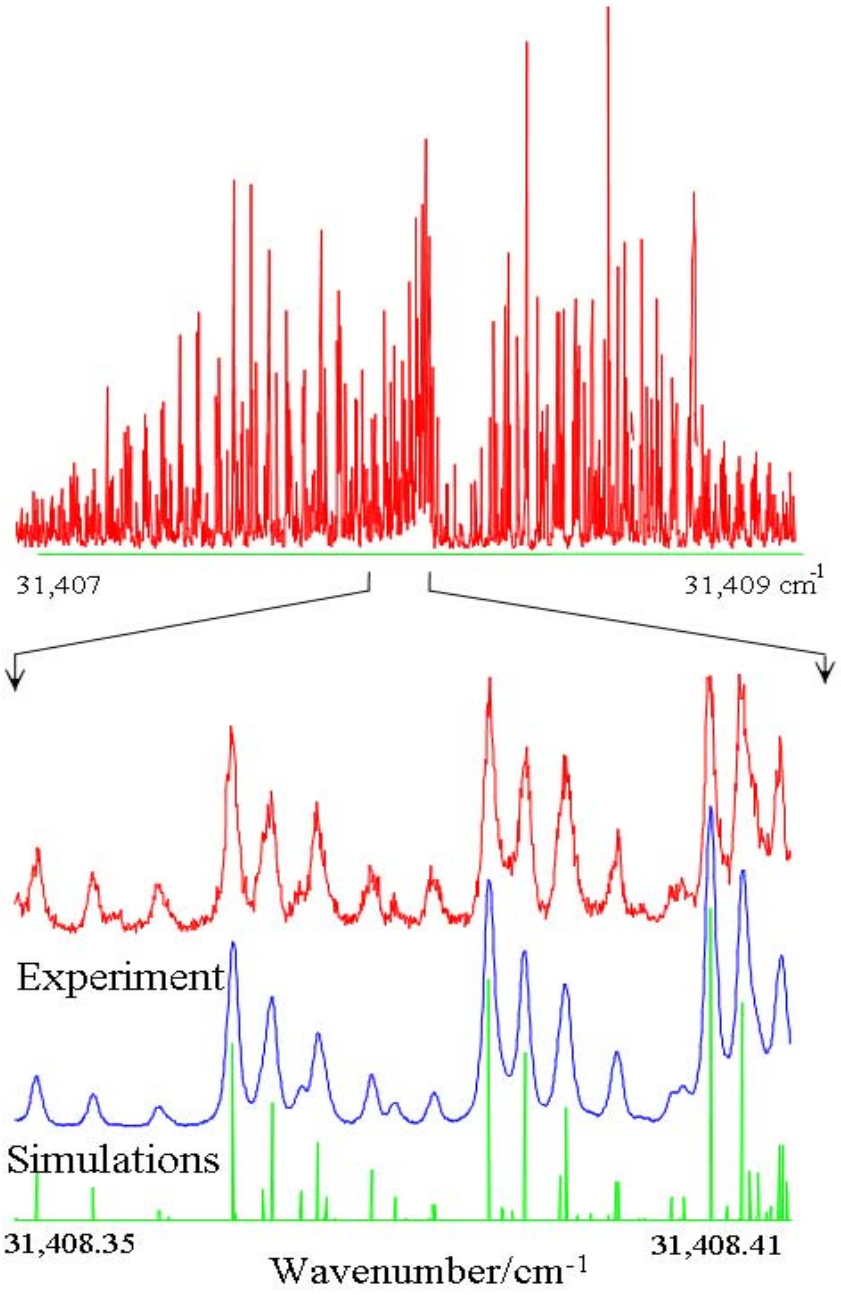

Figure 2-2. Rotationally resolved fluorescence excitation spectrum of Band A recorded in a molecular beam. The bottom traces show an expanded section of the Q-branch and two computer simulations, with and without a convoluted lineshape function.

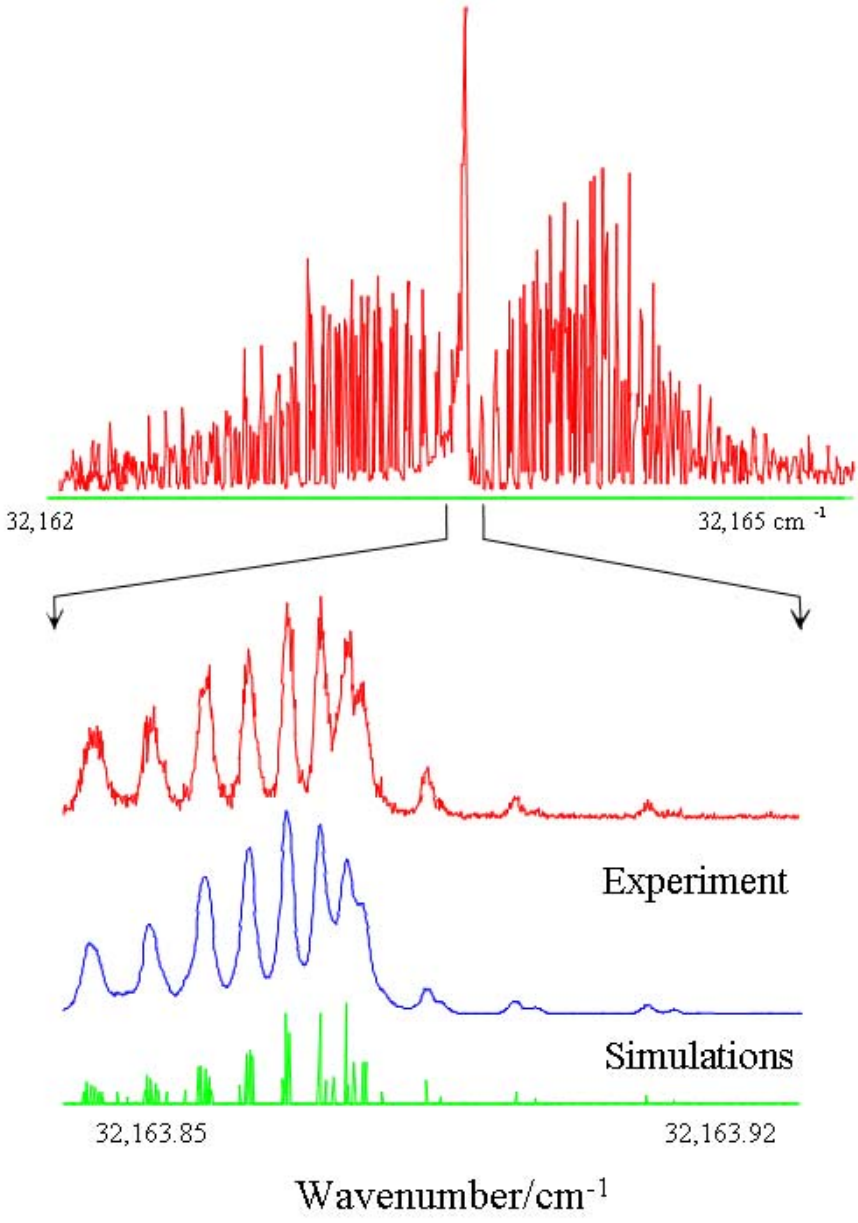

Figure 2-3. Rotationally resolved fluorescence excitation spectrum of Band B recorded in a molecular beam. The bottom traces show an expanded section of the Q-branch and two computer simulations, with and without a convoluted lineshape function.

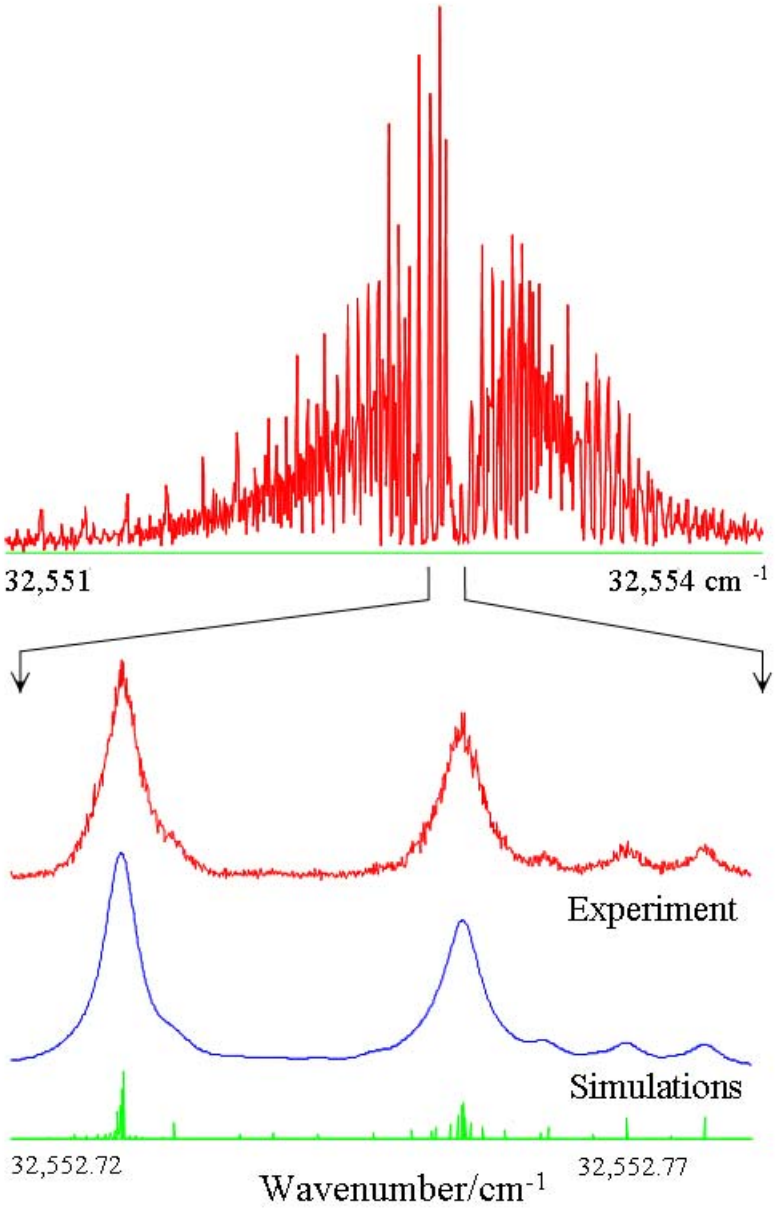

Figure 2-4. Rotationally resolved fluorescence excitation spectrum of Band C recorded in a molecular beam. The bottom traces show an expanded section of the Q-branch and two computer simulations, with and without a convoluted lineshape function.

transitions is 2.55 MHz. The shapes of single rovibronic lines again could be simulated with a Voigt profile having an ~ 18 MHz Gaussian component and a ~ 20 MHz Lorentzian component (around 8 ns).

Figure 2-4 shows the spectrum of Band C which is located at 32553 cm^{-1}. In this case, the assignment of 314 lines resulted in a standard deviation of 3.99 MHz. The Lorentzian component of the lineshape is about 62 MHz, which indicates a much shorter lifetime (about 3 ns). Similar procedures were used to fit the rotationally resolved spectra of all of the weaker bands marked with lower case letters in Fig. 2-1.

Even a cursory examination of the fits in Figs. 2-2-4 reveals that the spectra of Bands A-C are very different at high resolution. Therefore, either the rotational constants, the changes in the rotational constants, and/or the TM orientations of the three bands must be very different. The orientation of the TM in the inertial coordinate system of each species can be determined from the relative intensities of the different rovibronic lines in its spectrum. *a*-, *b*-, and *c*-type transitions exhibit different selection rules [17]. In the present instance, all bands examined at high resolution (including the weaker bands shown in Fig. 2-1) exhibit only *a*-type transitions. No *b*- or *c*-type transitions could be detected. Therefore, whatever species are responsible for these bands, all have TM orientations parallel to their *a*-inertial axes. The different appearances of the spectra at high resolution must therefore have their origins in different moments of inertia.

2.5. Discussion.

The major results of this study are the rotational constants of the carriers of these spectra in their ground (S_0) and excited (S_1) states and the orientation of their respective S_1-S_0 electronic transition moments. In what follows, we discuss each of these results in turn, and show how we can use the data obtained to assign the observed transitions to specific structures, to determine

the nature of their S_1-S_0 transitions, and to probe the geometry changes that occur when the photon is absorbed.

Table 2-1 lists the rotational constants of the three main transitions of DVB; Bands A, B, and C. These constants are intrinsic properties of the 3-D structure of any isolated molecule in the gas phase. By inspection of the ground state values in Table 2-1, it is clear that they differ greatly between the different bands. For example, A increases by more than 1000 MHz on going from Band A (1947 MHz) to B (3386 MHz) to C (4716 MHz). The disparity between these values is well outside the error bars of our experiment (a maximum of ±14 MHz for Band C). The fact that these constants differ so much indicates the presence of molecules with distinctive structures.

Of course, three rotational constants are not sufficient to determine the complete structure of an isolated molecule. Help from theory and a few chemical assumptions are necessary to obtain a conclusive assignment of the bands Table 2-2 lists the calculated rotational constants of five different DVB isomers and conformers, based on optimizations of their ground state geometries at the B3LYP 6-31G* level. Comparisons of these values with those determined experimentally (Table 2-1) shows conclusively that Bands A, B, and C should be assigned to the DVB isomers/conformers shown below:

Table 2-1. **Inertial parameters of three divinylbenzenes in their ground (S_0) and excited (S_1) electronic states.**

Parameter	Band A	Band B	Band C
A", MHz	1947.2 (0.4)	3386 (3)	4716 (14)
B", MHz	1074.7 (0.1)	786.1 (0.1)	701.7 (0.1)
C", MHz	694.0 (0.1)	639.2 (0.1)	612.1 (0.1)
ΔI, u$Å^2$	-1.78 (0.13)	-1.54 (0.20)	-1.72 (0.36)
κ	-0.393	-0.833	-0.956
$\Delta A'$, MHz	-40.2 (0.1)	-8.8 (0.1)	-159.1 (0.1)
$\Delta B'$, MHz	8.8 (0.1)	-10.8 (0.1)	1.4 (0.1)
$\Delta C'$, MHz	-2.9 (0.1)	-8.3 (0.1)	-2.3 (0.1)
ΔI, u$Å^2$	-0.39 (0.12)	-0.48 (0.15)	-0.84 (0.17)
κ'	-0.355	-0.895	-0.953
Origin, cm^{-1}	31409	32164	32553
Band Type	*a* (±9º)	*a* (±7º)	*a* (±9º)
N	387	290	314
OMC, MHz	2.64	2.55	3.99
T, K	3 (1)	3 (1)	3 (1)

Table 2-2. **Calculated (B3LYP 6-31G*) rotational constants of five divinylbenzenes in their ground electronic states.**

Parameter	**13*cc***	**13*ct***	**13*tt***	**14*c***	**14*t***
A", MHz	1947.2	2546.4	3374.2	4296.1	4750.4
B", MHz	1062.4	891.6	781.4	712.5	695.5
C", MHz	687.4	660.4	634.5	611.2	607.0
κ"	-0.405	-0.755	-0.893	-0.945	-0.953

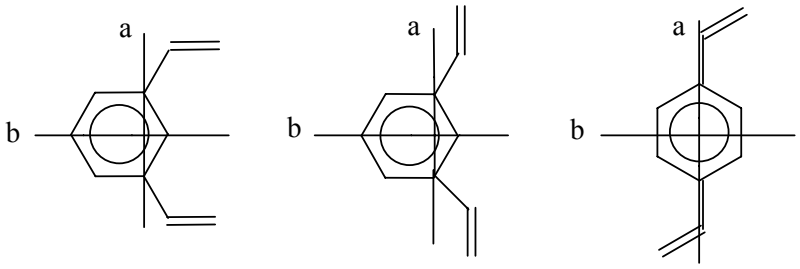

13*cc* 13*tt* 14*t*

Here, 13*cc* and 13*tt* are two conformers of 1,3-DVB, with the two vinyl groups *cis*, *cis* or *trans*, *trans*; 14*t* is a single conformer of 1,4-DVB, with the two vinyl groups *trans* to each other.

Examination of these structures shows clearly why their rotational constants are so different. For example, the relative magnitudes of the A rotational constants increase in the order A (13*cc*) < A (13*tt*) < A (14*t*) because fewer heavy atoms are displaced from the *a* axis on going from one structure to the next, reducing their moments about *a* ($A = h/8\pi^2 I_a$). Similarly, B (and C) decrease in the same order, because the displacement of heavy atoms from *b* (*c*) increases across the series. The assignment of the remaining weaker transitions in Fig. 2-1 follows a similar procedure. Possible assignments for these bands include other transitions in the vibrational manifolds of 13*cc*-, 13*tt*-, or 14*t*-DVB, other conformers/isomers of DVB, or entirely different structures.

Table 2-3 lists the determined values of the rotational constants deduced from fits of nine of these weaker bands. Comparisons of these values with the calculated values in Table 2-2 shows that bands marked with a lower case "a" in Fig. 2-1 all have the same ground state constants (within error) as 13*cc*-DVB. Similarly, the bands marked with the "b" and "c" designations have the same ground state constants as 13*tt*-DVB and 14*t*-DVB, respectively. All weaker bands studied in this way may therefore be assigned as vibronic bands built upon the

Table 2-3. **Inertial parameters of all examined vibronic bands in the S_1-S_0 fluorescence excitation spectrum of divinylbenzene.**[a]

ΔE	A"	B"	C"	ΔA	ΔB	ΔC	ΔI'
0 (13*cc*)	1947.2 (0.4)	1074.7 (0.1)	694.0 (0.1)	-40.2 (0.1)	8.8 (0.1)	-2.9 (0.1)	-0.34 (0.12)
+956	1945.7 (0.6)	1074.7 (0.1)	694.0 (0.1)	-44.5 (0.1)	11.7 (0.1)	-0.5 (0.1)	-2.32 (0.1)
+957	1946.2 (0.6)	1074.7 (0.1)	694.3 (0.1)	-43.0 (0.1)	10.5 (0.1)	-1.7 (0.1)	-1.51 (0.11)
0 (13*tt*)	3386 (3)	786.1 (0.1)	639.2 (0.1)	-8.8 (0.1)	-10.8 (0.1)	-8.3 (0.1)	-0.48 (0.15)
+173	3392 (6)	786.2 (0.1)	639.2 (0.1)	1.3 (0.1)	-10.1 (0.1)	-8.5 (0.1)	1.14 (.15)
0 (14*t*)	4716 (14)	701.7 (0.1)	612.1 (0.1)	-159.1 (0.1)	1.4 (0.1)	-2.3 (0.1)	-0.84 (0.17)
+211	4730 (4)	701.7 (0.1)	612.1 (0.1)	-193.8 (0.1)	2.1 (0.1)	-1.0 (0.1)	-2.43 (0.17)
+245	4719 (19)	701.7 (0.1)	612.1 (0.1)	-182.8 (0.1)	2.1 (0.1)	-1.3 (0.1)	-2.09 (0.17)
+258	4710 (9)	701.8 (0.1)	612.1 (0.1)	-131.9 (0.1)	1.6 (0.1)	-2.6 (0.1)	0.22 (0.17)
+376	4703 (22)	701.8 (0.1)	612.1 (0.1)	-191.3 (0.1)	1.7 (0.1)	-1.5 (0.1)	-2.81 (0.17)
+770	4711 (9)	701.8 (0.1)	612.1 (0.1)	-158.2 (0.1)	0.7 (0.1)	-2.5 (0.1)	-1.34 (0.17)
+786	4741 (28)	701.7 (0.1)	612.1 (0.1)	-187.4 (0.4)	1.8 (0.1)	-1.5 (0.1)	-1.79 (0.17)

[a] ΔE is the excitation energy above the S_1-S_0 origin band of each designated isomer/conformer. All constants are in MHz except for ΔI', in amu Å^2.

origin bands A, B, and C. Differences in the excited state rotational constants of these bands reflect differences in their intrinsic excited state vibrational motions.

The B3LYP calculations place both 1,4-DVB's at about 2000 cm^{-1} lower in energy than the 1,3-DVB's, with 14*c* and 14*t* being roughly degenerate. Therefore, it is not clear why the spectrum of 14*c* is not observed. Among the 1,3-DVB's, 13*tt* is calculated to be the most stable, with 13*cc* and 13*ct* lying at ~ 60 cm^{-1} higher in energy. Experimentally, Band C (14*t*) is the strongest, followed by Band B (13*tt*) and Band A (13*cc*), in qualitative accord with theory.

We turn now to a discussion of the observed TM orientations in these substituted benzenes. 14*t*-DVB exhibits an *a*-type origin band in its S_1-S_0 spectrum. Hence, its S_1 state is a ^1L_a state with its TM oriented roughly parallel to the points of attachment of its substituent groups. The *a* axis in 14*t*-DVB is not an in-plane C_2 axis, so ^1L_a lies below ^1L_b in the isolated molecule (a similar situation exists in styrene [5]). 13*cc* and 13*tt* also exhibit *a*-type origin bands. However, the *a* axes in these two conformers are roughly perpendicular to the points of attachment of their substituent groups. And this axis, the *b*-axis, *is* a C_2 axis, so the S_1 states of the two 1,3-DVB's are "^1L_b" in character, not "^1L_a". Thus, restoring the missing C_2 axis of a monosubstituted benzene by attaching a second substituent restores the normal order of the ^1L_a and ^1L_b states. This confirms our original hypothesis.

Valuable insight into the factors that are responsible for these effects are provided by the *ab initio* calculations. Shown in Figure 2-5 are the CIS/6-31G* calculated one-electron molecular orbitals (MO's) of styrene (STY), the three DVB's, and phenylacetylene (PA). Their corresponding energies are listed in Table 2-4. Both the orbitals and their energies are labeled according to the scheme below, which shows the nodal planes of the nominally degenerate HOMO's (ψ_2 and ψ_3) and LUMO's (ψ_4 and ψ_5) of benzene itself:

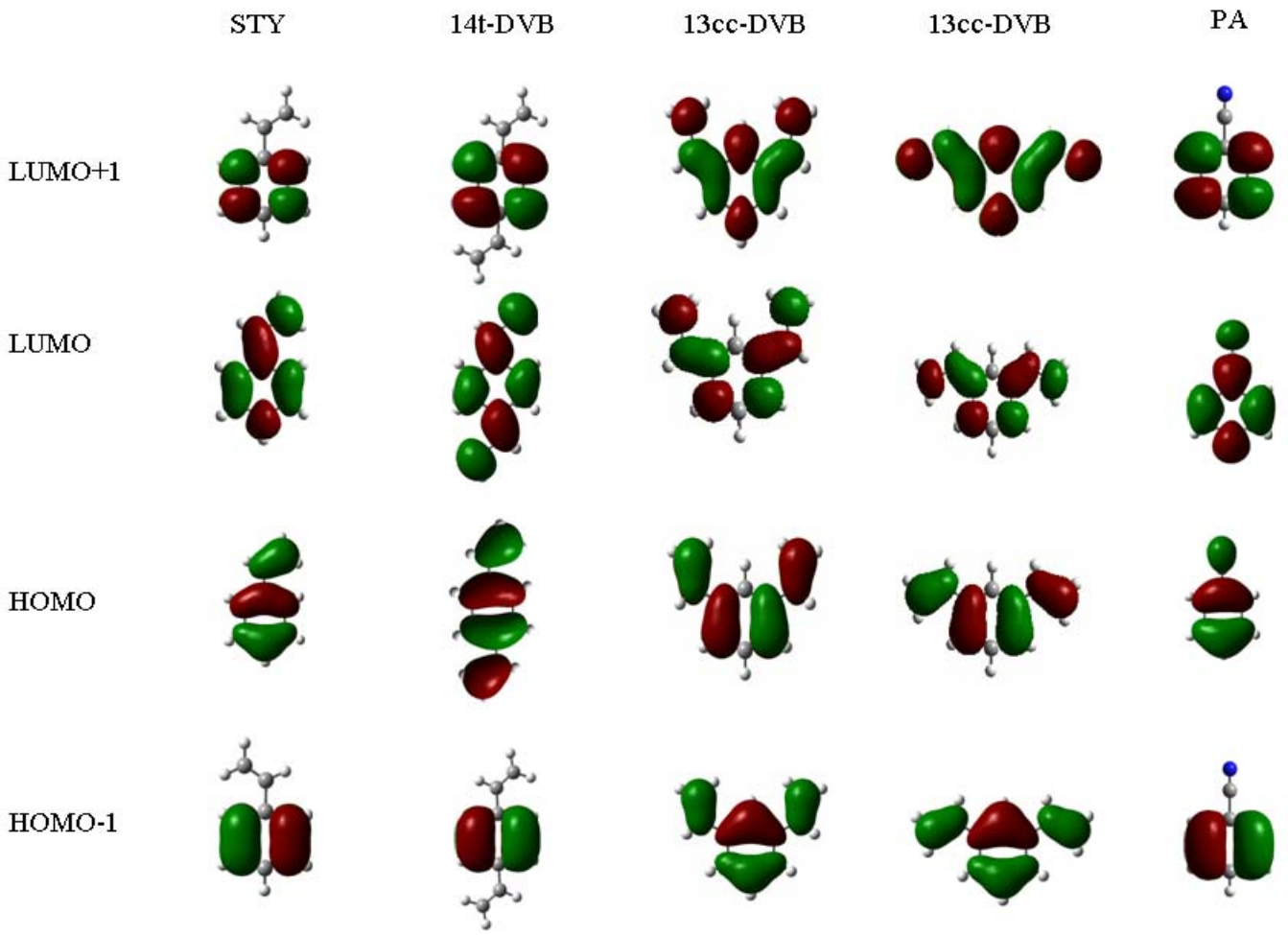

Figure 2-5. CIS/6-31G* calculated one-electron molecular orbitals of styrene, the three divinylbenzenes studied in this work, and phenylacetylene.

Table 2-4. **One-electron energies (in eV) of the molecular orbitals of styrene, three divinylbenzenes, and phenylacetylene according to CIS/6-31G*.**

Orbital	STY	**14*t***	**13*cc***	**13*tt***	PA
Ψ_5	4.05	3.96	0.85	2.52	3.85
Ψ_4	3.04	2.30	2.94	3.50	3.07
Ψ_3	-8.21	-7.63	-8.46	-8.53	-8.61
Ψ_2	-9.08	-9.14	-7.99	-7.93	-9.28

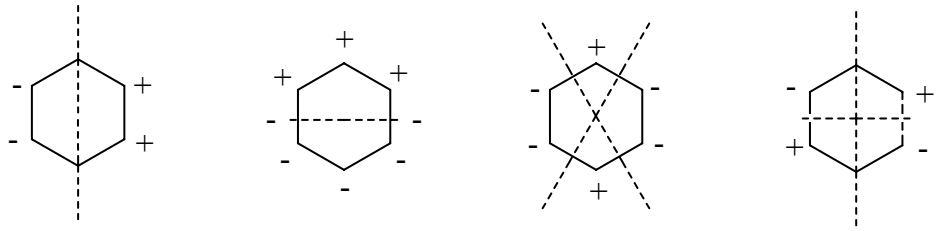

ψ_2 ψ_3 ψ_4 ψ_5

These degeneracies are lifted in all substituted benzenes, but the resulting pattern of MO's differs from one molecule to the next. Consider STY and 14*t*-DVB. Here, as shown in Fig. 2-5 and Table 2-4, the energy ordering of the MO's is $\epsilon_2 < \epsilon_3 < \epsilon_4 < \epsilon_5$. ψ_3 and ψ_4 contain significant out-of-phase contributions from orbitals localized on the vinyl group(s), which destabilizes bonding MO's and stabilizes antibonding MO's. According to CIS, the S_1-S_0 transition in STY can be represented by the linear combination 0.27 ($\psi_2\psi_5$) + 0.63 ($\psi_3\psi_4$), with a 10% contribution from $\psi_1\psi_6$ [5]. Similarly, the S_1-S_0 transition in 14*t*-DVB can be represented by the linear combination 0.06 ($\psi_2\psi_5$) +0.90 ($\psi_3\psi_4$), with a 3% contribution from ψ_1 ψ_6. Two one-electron excitations contribute to the S_1 state of each molecule, unequally in both cases. But the transition densities of both excitations oscillate in directions parallel to *a*.

The situation is very different in the two 1,3-DVB's. All four MO's ($\psi_2 \ldots \psi_5$) contain significant out-of-phase contributions from orbitals localized on the vinyl groups. Thus, the energy ordering of the MO's is different, with $\epsilon_3 < \epsilon_2 < \epsilon_5 < \epsilon_4$.

Two principal one-electron excitations again contribute to the S_1 states of both molecules. According to CIS, the S_1-S_0 transition in 13*cc*-DVB can be represented by the linear combination 0.53 ($\psi_2\psi_5$) + 0.47 ($\psi_3\psi_4$), and that in 13*tt*-DVB can be represented by 0.82 ($\psi_2\psi_5$) + 0.15 ($\psi_3\psi_4$) (with a 3% contribution from $\psi_1\psi_6$). These results are qualitatively similar to the results for STY and 14*t*-DVB. However, the principal symmetry axis in the 1,3-DVB's is *b*, rather than *a*. Thus, CIS predicts *b*-axis polarized transitions in both 13*cc*-DVB and 13*tt*-DVB. Experimentally, *a*-

axis polarized transitions are observed in both cases, in clear disagreement with theory. A similar situation exists in PA [5].

The connection between the observed polarizations of electronic transitions and the assignments of the states themselves was first explored by Platt [6] in his particle-on-a-ring model of the electronic spectra of cata-condensed hydrocarbons [18]. A simple example is benzene; its two lowest energy states are ^1L_a and ^1L_b, where the subscripts *a* and *b* refer to the polarizations of their respective bands. The *a* state is associated with MO's having nodes that bisect the bonds of the molecule, whereas the MO's of the *b* state have nodes that pass through the atoms, as shown below:

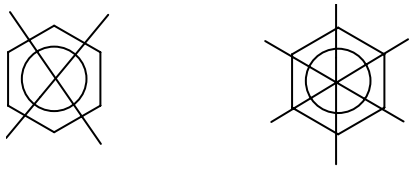

^1L_a ^1L_b

Hence, the transitions to L_a and L_b are polarized along the vertical and horizontal axes, respectively. (These are forbidden in benzene itself). More generally, if there is a two-fold symmetry axis, the labels *a* and *b* can be used to distinguish symmetry with respect to that axis, *a* being used for states which give transitions that are parallel to the two-fold axis, and *b* for states which give transitions that are perpendicular to this axis. This is the rule of Platt, as interpreted by Heilbronner and Murrell [19]. Only the two 1,3 DVB's have a two-fold symmetry axis passing through an atom, the *b*-inertial axis in both cases. Their S_1-S_0 transition moments are both oriented along *a*. Hence, the S_1 states of both 1,3 DVB's are ^1L_b in character.

Our initial expectation was that restoring the in-plane C_2 axis in 14*c* would complement the result from 14*t*. The MOs for 14*c* are similar to the ones for 14*t* (*cf*. Fig. 2-5). According to

the Platt model, an L_a transition involves the excitations ψ_3 ψ_4 and ψ_2 ψ_5, while an L_b transition involves ψ_3 ψ_5 and ψ_2 ψ_4. The only transition moment connecting ψ_3 ψ_5 and ψ_2 ψ_4 has A_1 symmetry and is aligned along the *b*-axis (C_2 axis) of 14*c*, resulting in an L_b state. Connecting ψ_3 ψ_4 and ψ_2 ψ_5, a transition along the *a*-axis has B_1 symmetry and results in an L_a excited sate. Unfortunately, we were unable to detect the spectrum of 14*c*; however, this analysis holds true for any C_{2v} molecule. Since both *meta* conformers of DVB have C_{2v} symmetry, the same analyses indicate that the transitions are L_b in character since they are polarized along the *a*-axis.

Assignment of the S_1 states of 13*cc*- and 13*tt*-DVB as ^1L_b states, and the S_1 state of 14*t*-DVB as a ^1L_a state, helps explain the large differences in the ΔA, ΔB, and ΔC values of the three species. Recall that L_a states have wavefunction maxima at atoms whereas L_b states have wavefunction maxima at the centers of bonds (see above). Thus, 14*t*-DVB should have a relatively large negative value of ΔA, and relatively small negative values of ΔB and ΔC, owing to a ring expansion that preferentially lengthens perpendicular C-C bonds compared to parallel ones [5]. This is what is observed; ΔA = -159, ΔB = 1.4, and ΔC = -2.3 MHz. These values are very similar to those of styrene; ΔA = -182, ΔB = -14, and ΔC = -19 MHz. The somewhat more positive values in 14*t*-DVB may be attributed to increased conjugation with the attached vinyl groups [20].

The two 1,3-DVB's are qualitatively different. 13*cc*-DVB has ΔA = -40, ΔB = 9, and ΔC = -3 MHz. The principal bond lengthening occurs in directions perpendicular to *a*. Clearly, this must involve the two –CH=CH_2 groups, as ψ_4 and ψ_5 both have nodes between the two carbon atoms. 13*tt*-DVB has ΔA = -9, ΔB = -11, and ΔC = -8 MHz. The three nearly equal values suggest, again, involvement of the vinyl groups, except that the resulting displacements now make nearly equal projections along both *a* and *b*. But the degree of conjugation between

the double bond of the vinyl group and the electrons of the benzene ring must be somewhat different in the two conformers, since 13*tt* is substantially blue shifted from 13*cc* (~ 750 cm^{-1}) in the excitation spectra. Studies of isotopically substituted DVB's will be necessary to fully resolve these issues.

Finally, we note that all three DVB's are planar in both electronic states, since their inertial defects ($\Delta I = I_c - I_a - I_b$) are negative and relatively small (*cf.* Table 2-1). The same is true in styrene ($\Delta I(S_0) =$ -0.70, $\Delta I(S_1) =$ -0.29 u$Å^2$ [5].) The main contributors to negative inertial defects are low wavenumber out-of-plane vibrational modes, principally C (ring) –C (substituent) torsional modes in styrene [21] and the three DVB's. Their inertial defects are all less negative in the S_1 state, suggesting that these modes become more rigid, compared to the S_0 state, owing to increased conjugation with the ring [20]. One effect of the less negative inertial defect in the S_1 state of styrene is to produce a vibrational progression. It is possible that similar progressions are responsible for the weaker bands of the three DVB's in Fig. 2-1.

2.6. **Acknowledgments.**

We thank J. M. Hollas and C. S. Parmenter for helpful comments on the manuscript. This work has been supported by NSF (CHE-9728636 and CHE-9987048), to whom we are grateful.

2.7. References.

[1]. P. W. Joireman, R. T. Kroemer, D. W. Pratt, and J. P. Simons, J. Chem. Phys. **1996**, 105, 6075.

[2]. R. T. Kroemer, K. R. Liedl, J. A. Dickinson, E. G. Robertson, J. P. Simons, D. R. Borst, and D. W. Pratt, J. Am. Chem. Soc. **1998**, 120, 12573.

[3]. E. G. Robertson and J. P. Simons, Phys. Chem. Chem. Phys. **2001**, 3, 1.

[4]. D. R. Borst, P. W. Joireman, D. W. Pratt, E. G. Robertson, and J. P. Simons, J. Chem. Phys., in press.

[5]. J. W. Ribblett, D. R. Borst, and D. W. Pratt, J. Chem. Phys. **1999**, 111, 8454.

[6]. J. R. Platt, J. Chem. Phys. **1949**, 17, 484.

[7]. J. A. Swift, A. Pivovar, A. Reynolds, and M. D. Ward, J. Amer. Chem. Soc. **1998**, 120, 5887.

[8]. W. A. Majewski, J. F. Pfanstiel, D. F. Plusquellic, and D. W. Pratt, *Laser Techniques in Chemistry*. T. R. Rizzo, A. B. Myers, Eds. J. Wiley & Sons: New York, **1995**; p. 101.

[9]. F. W. Birss and D. A. Ramsay, Comput. Phys. Commun. **1984**, 38, 83.

[10]. J. K. G. Watson, in *Vibrational Spectra and Structure*, edited by J. R. Durig (Elsevier, Amsterdam, 1977), Vol. 6, p. 1.

[11]. Gaussian 98, Revision A.4, M. J. Frisch, G. W. Trucks, H. B. Schlegel, G. E. Scuseria, M. A. Robb, J. R. Cheeseman, V. G. Zakrzewski, J. A. Montgomery, Jr., R. E. Stratmann, J. C. Burant, S. Dapprich, J. M. Millam, A. D. Daniels, K. N. Kudin, M. C. Strain, O. Farkas, J. Tomasi, V. Barone, M. Cossi, R. Cammi, B. Mennucci, C. Pomelli, C. Adamo, S. Clifford, J. Ochterski, G. A. Petersson, P. Y. Ayala, Q. Cui, K. Morokuma, D. K. Malick, A. D. Rabuck, K. Raghavachari, J. B. Foresman, J. Cioslowski, J. V. Ortiz, B. B. Stefanov, G. Liu, A. Liashenko, P. Piskorz, I. Komaromi, R,. Gomperts, R. L. Margin, D. J. Fox, T. Keith, M. A. Al-Laham, C. Y. Peng, A. Nanayakkara, C. Gonzalex, M. Challacombe, P. M. W. Gill, B. Johnson, W. Chen, M. W. Wong, J. L. Andres, C. Gonzalez, M. Head-Gordon, E. S. Replogle, and J. A. Pople, Gaussian, Inc., Pittsburgh, PA, 1998.

[12]. J. R. Johnson, K. D. Jordan, D. F. Plusquellic, and D. W. Pratt, J. Chem. Phys. **1990**, 93, 2258.

[13]. A. Held, B. B. Champagne, and D. W. Pratt, J. Chem. Phys. **1991**, 95 8732.

[14]. S. J. Humphrey and D. W. Pratt, J. Chem. Phys. **1993**, 99, 5078.

[15]. J. F. Pfanstiel and D. W. Pratt, J. Phys. Chem. **1995**, 103, 7258.

[16]. J. F. Pfanstiel, D. W. Pratt, B. A. Tounge, and R. L. Christensen, J. Phys. Chem. A. **1999**, 103, 2337.

[17]. J. M. Hollas, *High Resolution Spectroscopy*, Butterworths, London, 1982.

[18]. A useful review may be found in M. Orchin and H. H. Jaffé, *Symmetry, Orbitals, and Spectra*, Wiley-Interscience, New York, 1971.

[19]. E. L. Heilbronner and J. N. Murrell, Mol. Phys. **1963**, 6, 1.

[20]. T. Cvitas, J. M. Hollas, and G. H. Kirby, Mol. Phys. **1970**, 19, 305.

[21]. J. M. Hollas and T. Ridley, J. Mol. Spectrosc.**1981**, 89, 232.

3. On the energy landscapes of 3-indole acetic acid and 3-indole propionic acid. A study of side chain flexibilities in their S_0 and S_1 electronic states.

Tri V. Nguyen, John T. Yi, and David W. Pratt*

Department of Chemistry, University of Pittsburgh
Pittsburgh, PA 15260 USA.

3.1. Abstract.

The tandem of 3-indole acetic acid (IAA) and 3-indole propionic acid (IPA) is ideally suited for a detailed study of the intramolecular forces responsible for the conformational properties of species containing side chains. Toward this end, high resolution $S_1 \leftarrow S_0$ excitation spectra of the three origin bands in IAA and the two origin bands in IPA were recorded and analyzed. Each origin is assigned to a unique conformer. A discussion of the resulting energy landscape is given.

Submitted to *Physical Chemistry Chemical Physics.*

3.2. Introduction.

The shapes of biomolecules play a significant role in living systems. For example, an intricate network of hydrogen bonds coordinates the process of protein folding.[1] The forces (dipole-dipole, induced dipole, *etc*.) that are responsible for the formation of these bonds operate at the point of contact within and/or between large biomolecules. Often, the making and/or breaking of such bonds triggers a cascade of much larger movements. Thus, studies of the three-dimensional structures of such molecules at these points of contact are fundamental to our understanding of biological processes. Spectroscopy in the gas phase is an ideal tool for such studies because it makes possible a more detailed examination of the individual "end-parts" of interest by isolating them from the surrounding environment.

The focus in this work is on 3-indole acetic acid (IAA) and 3-indole propionic acid (IPA). These molecules play a variety of biological roles. For example, IAA is a natural plant auxin that regulates various physiological and functions. It has been the subject of many studies in the agricultural field because it plays an important role in plant growth.[2,3] Further improvements in overall activity would benefit from a more complete understanding of receptor-auxin binding, and how this binding might be affected by changes in the conformation of the attached R-CH_2-COOH side chain.

In recent years, it has been suggested that the energy landscapes of molecules with large side chains (> 20 atoms) encompassing various functional groups are much simpler than anticipated based on the sheer number of possible degrees of freedom available.[4] IAA and IPA are very good candidates for testing this proposal, and for probing the forces that are responsible for the flexibility of such side chains. This is because their side chains are sufficiently simple to track the specific interactions within them as well as with the indole ring while still retaining

complexity. IAA has two functional groups connected by three dihedral angles (χ_1, χ_2, and ψ), as shown in Scheme I. IPA has one additional dihedral angle (χ_3), as shown in Scheme II.

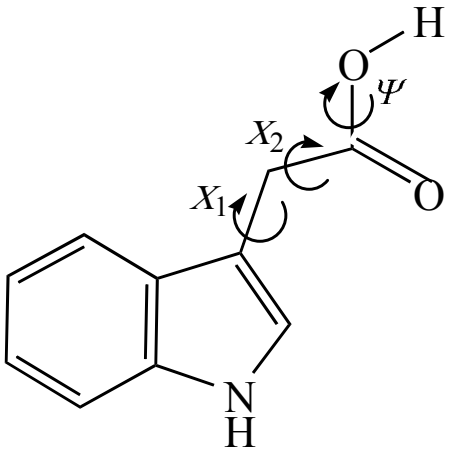

Scheme I

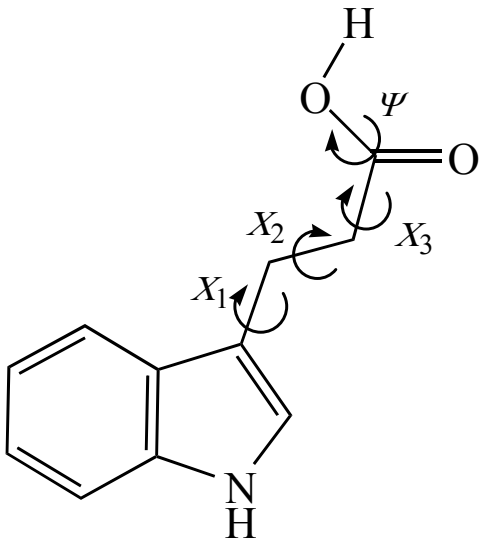

Scheme II

The preferred conformations of their side chains depend upon the relative strengths of the interactions between these groups and their angular dependence. Further, adding an additional CH_2 group in IPA provides another layer of information about these interactions.

The vibrationally resolved electronic spectrum of IAA was first reported by Park, *et al*.[5] In their work, three main transitions situated near 35 000 cm^{-1} were assigned as the origins of different conformers based on power saturation studies. Connell, Corcoran, Joireman, and Felker[6,7] performed conformational analyses of IAA and IPA using the rotational coherence spectroscopy (RCS) technique. A large variety of other studies have also been reported, some using sophisticated theoretical methods.[8,9] Recently, Clarkson, *et al*. [10] have measured the energy thresholds to the conformational isomerization along different coordinates.

Rotationally resolved electronic spectroscopy is an ideal tool for distinguishing conformers on the basis of both their structural and electronic properties. This technique has been previously applied to the study of conformational dynamics of flexible side chains in molecules like benzoic acid,[11] 1-naphthoic acid,[12] *p*-methoxy-phenethylamine,[13] and tryptamine.[14] Here, we use the sensitivity of this technique to probe the flexibilities of the -CH_2COOH and -CH_2-CH_2COOH side chains in IAA and IPA, respectively. We present the fully resolved spectra of their $S_1 \leftarrow S_0$ origin bands. Along with *ab initio* calculations, the inertial parameters that are derived from analyses of these spectra allow for an identification of the most stable structures and the forces that are responsible for their three-dimensional shapes.

3.3. Experiment.

3-Indole acetic acid and 3-indole propionic acid were purchased from Sigma-Aldrich and used as received. Vibrationally resolved $S_1 \leftarrow S_0$ excitation spectra were obtained using a pulsed jet apparatus. At room temperature, the sample was seeded into He gas at ~ 50 psi and expanded into a chamber kept at 10^{-5} Torr through a 1 mm diameter orifice pulsed valve (General Valve Series 9) operating at 10 Hz. Molecules were excited by a frequency-doubled dye laser (Quanta Ray Model PDL-1) pumped by a Nd^{+3}:YAG (Model DCR-1A) laser also operating at 10 Hz. The dye laser (Rhodamine 590) was frequency doubled into UV by a β-barium borate (BBO) crystal. The spectral resolution of the dye laser was 0.6 cm^{-1} in the ultraviolet. The laser beam crossed the supersonic jet about 2.5 cm downstream of the nozzle. The fluorescence signal was collected by a photomultiplier tube (PMT, EMI 98139B) using a single lens system, recorded by a boxcar integrator, and processed by a data acquisition system (QUICK DATA ACQ 1.05). Calibration of the spectrum was performed by recording the markers (1 cm^{-1}) from a solid etalon.

The high resolution apparatus has been described elsewhere.[15] The sample was heated to ~ 150 ºC, seeded into ~ 100 Torr of He, and expanded into a vacuum through a 240 μm nozzle. The molecular beam was expanded through a 1 mm skimmer 2 cm downstream of the nozzle into a differentially pumped vacuum system and crossed 15 cm downstream of the nozzle with a modified continuous wave ring dye laser operating with R6G and intracavity doubled in BBO, yielding ~ 200 μW of ultraviolet radiation. The fluorescence was detected using special collection optics consisting of two spherical mirrors positioned above and below the intersection of the molecular and laser beams. To maximize the efficiency, the focus of the top mirror is located at the intersection of the two beams while the bottom mirror is focused at a 2 mm hole drilled in the center of the top mirror. The emitted signal was collected by a PMT. This spatially selective setup results in a collection efficiency of 33% and a Doppler-limited resolution of ~ 18 MHz. Absolute frequency calibration was performed by simultaneously recording the fluorescence spectrum of I_2 (accuracy ~ 30 MHz) and the laser interference fringes from a stabilized etalon with a spectral range of 299.7520 ± 0.0005 MHz at the fundamental of the dye. Rotationally resolved spectra were analyzed using the Windows' based program jb95[16] which employs Watson's asymmetric rotor Hamiltonian.[17] *Ab initio* calculations were performed using the Gaussian 98 suite of electronic structure programs.[18]

3.4. Results.

The low resolution fluorescence excitation spectrum of IAA shows three strong and sharp origin bands labeled A, B, and C by Connell, *et al*.[6] Band A is the most intense transition and is located at 35,039 cm^{-1}. The weaker band B is shifted to the red by 21 cm^{-1}. Band C has the lowest intensity and is 11 cm^{-1} higher in energy, relative to band A.

Figure 3-1 shows the high resolution fluorescence excitation spectrum of band A of IAA at 35,039.84 cm^{-1}. The spectrum spans ~ 2.6 cm^{-1} and contains prominent P, Q, and R branches. A cursory examination reveals a pronounced spreading of the Q branch into the lower frequency P branch. Initially, approximately 4500 *a*- and *b*-type transitions were generated based on the inertial parameters from *ab initio* calculations to account for this effect. Subsequently, a least-squares fitting procedure was used to optimize the frequency assignments throughout the three branches. This fit showed that all of the intensity in the experimental spectrum could be accounted for by *a*-type transitions as illustrated by the lower traces in Fig. 3-1. Added *b*- and *c*-type transitions did not improve the fit, The OMC (observed minus calculated) frequency difference of the overall fit is 3.0 MHz, yielding a standard deviation of 1.1 MHz for the ground state A rotational constant and standard deviations of 0.1 MHz for the remaining rotational constants. Lineshape profiles of individual rovibronic lines are characterized by a Doppler-broadened component of 18 MHz (Gaussian) and a lifetime-broadened component of 45 MHz (Lorentzian).

Figures 3-2 and 3-3 show the rotationally resolved spectra of bands B and C of IAA. These bands do not exhibit the spread-out Q branch characteristic of band A but have P and R branches on either side of a well-defined central Q branch. Fits of bands B and C were accomplished using the same general procedures; both bands also are pure *a*-type bands. The inertial parameters of the fits of all observed bands of IAA are listed in Table 3-1.

Figure 3-4 shows the vibrationally resolved $S_1 \leftarrow S_0$ fluorescence excitation spectrum of IPA. The spectrum shows the same intensity pattern as previously reported.[7,8,19-25] Band A, the most intense and the higher energy band, is an origin band located at ~ 34,963 cm^{-1}. Band B is a second electronic origin band and is shifted to the red of band A by 45 cm^{-1}. The two series of

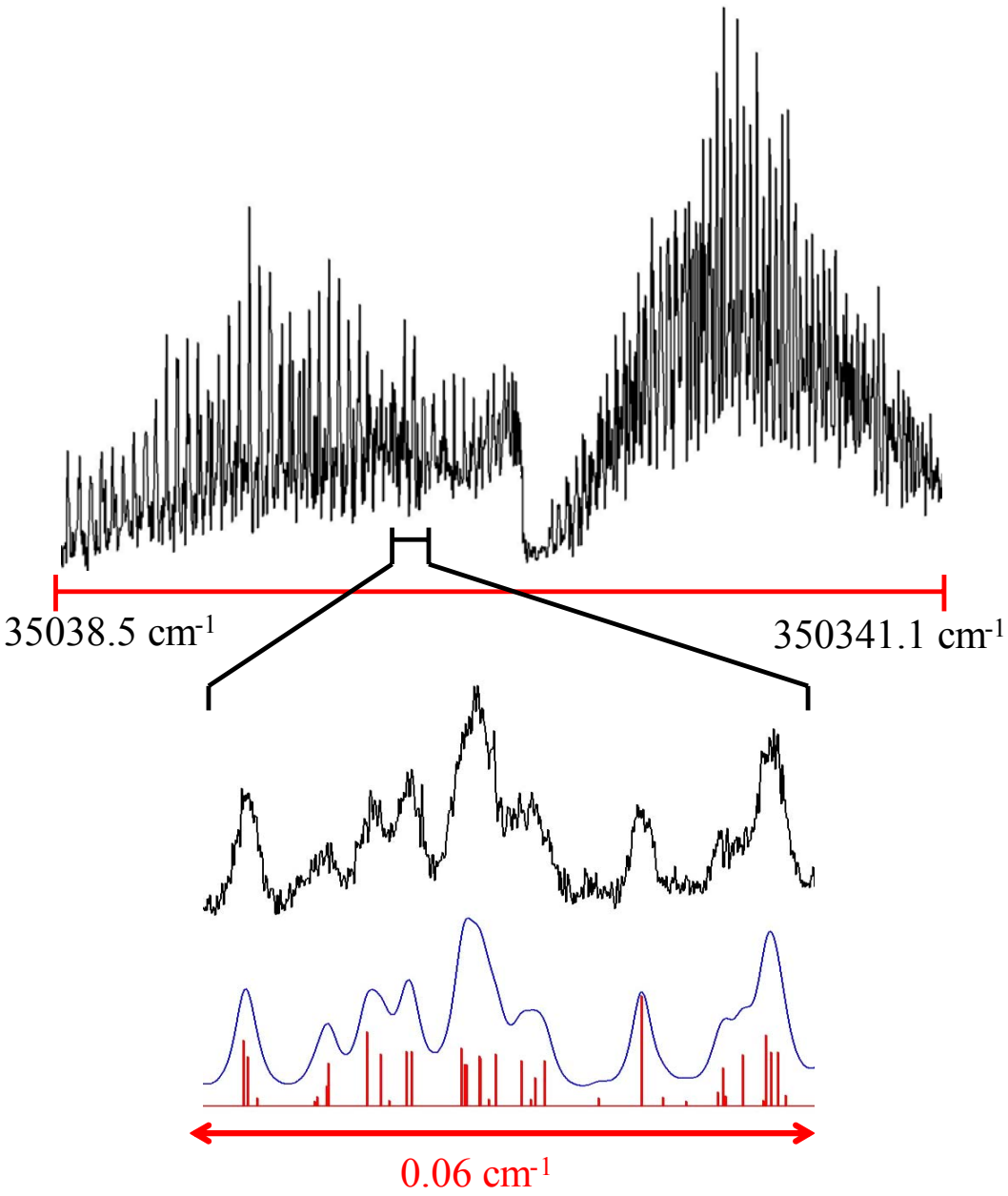

Figure 3-1. Rotationally resolved fluorescence excitation spectrum of band A of IAA in a molecular beam.

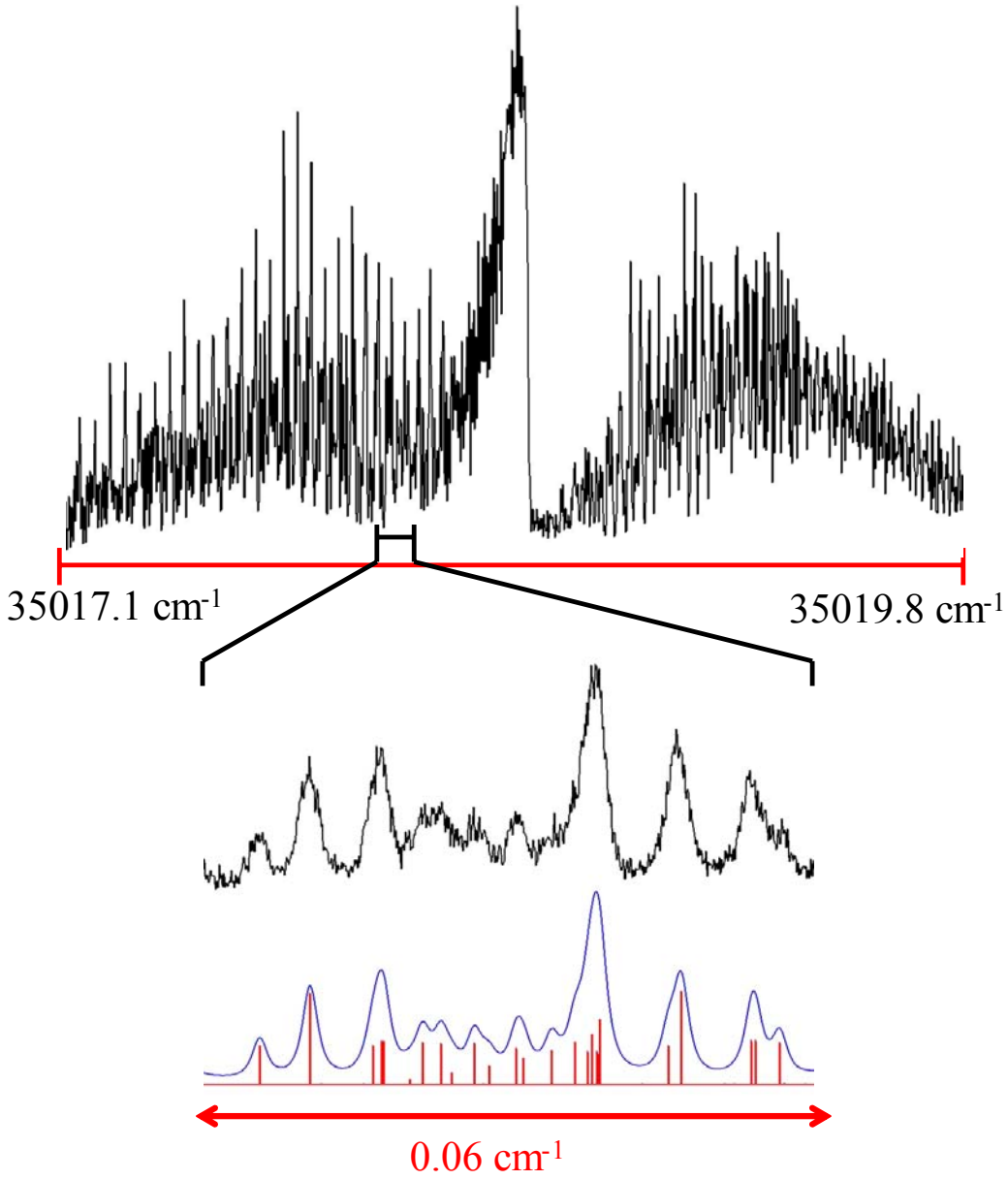

Figure 3-2. Rotationally resolved fluorescence excitation spectrum of band B of IAA in a molecular beam.

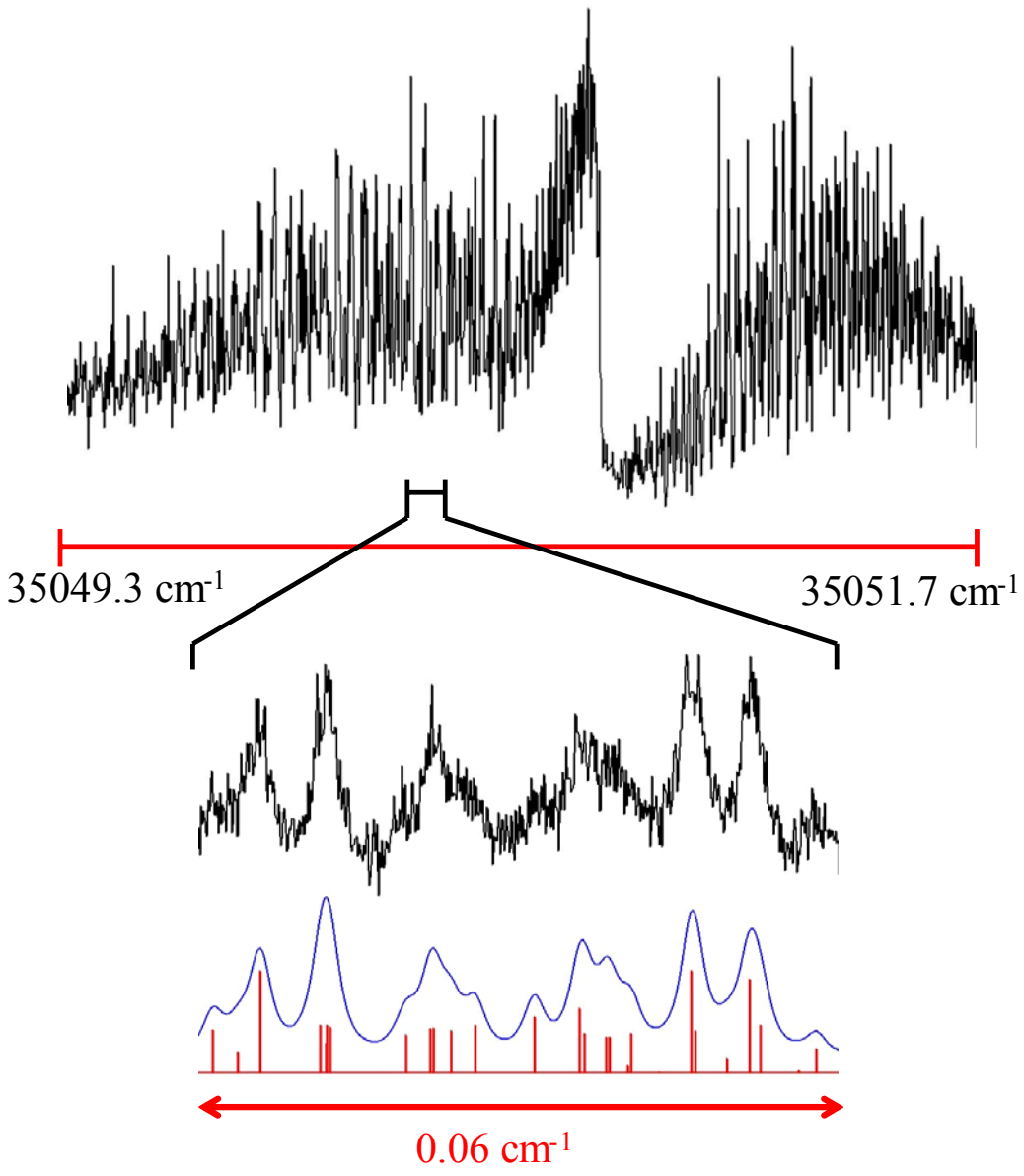

Figure 3-3: Rotationally resolved fluorescence excitation spectrum of band C of IAA in a molecular beam.

Table 3-1. **Inertial parameters of three 3-indole acetic acid in their ground (S_0) and excited (S_1) electronic states.[a]**

Parameter	Band A	Band B	Band C
A" (MHz)	2078.3 (1.1)	1438.8 (0.6)	1518.9 (0.7)
B" (MHz)	453.8 (0.1)	602.1 (0.1)	578.3 (0.1)
C" (MHz)	373.5 (0.1)	464.6 (0.1)	453.0 (0.1)
$\Delta I''$ ($\mu Å^2$)	-3.65	-102.97	-90.98
κ''	-0.91	-0.72	-0.76
ΔA (MHz)	-25.8 (0.1)	-8.5 (0.1)	-14.2 (0.1)
ΔB (MHz)	-2.8 (0.1)	-4.7 (0.1)	-5.5 (0.1)
ΔC (MHz)	-2.7 (0.1)	-3.1 (0.1)	-3.5 (0.1)
$\Delta I'$ ($\mu Å^2$)	-3.69	-104.35	-93.68
κ'	-0.90	-0.72	-0.77
Origin (cm^{-1})	35039	35018	35051
Band Type	*a*	*a*	*a*
N	183	149	136
OMC (MHz)	3.01	3.67	3.87
Temp (K)	15 (±2)	15 (±2)	15 (±2)

[a]ΔA, ΔB, and ΔC are the differences in the ground and excited state rotational constants, $\Delta A = A(S_1) - A(S_0)$, *etc.* ΔI is the inertial defect, $\Delta I = I_c - I_a - I_b$. κ is the asymmetry parameter, $\kappa = (2B - A - C)/(A - C)$.

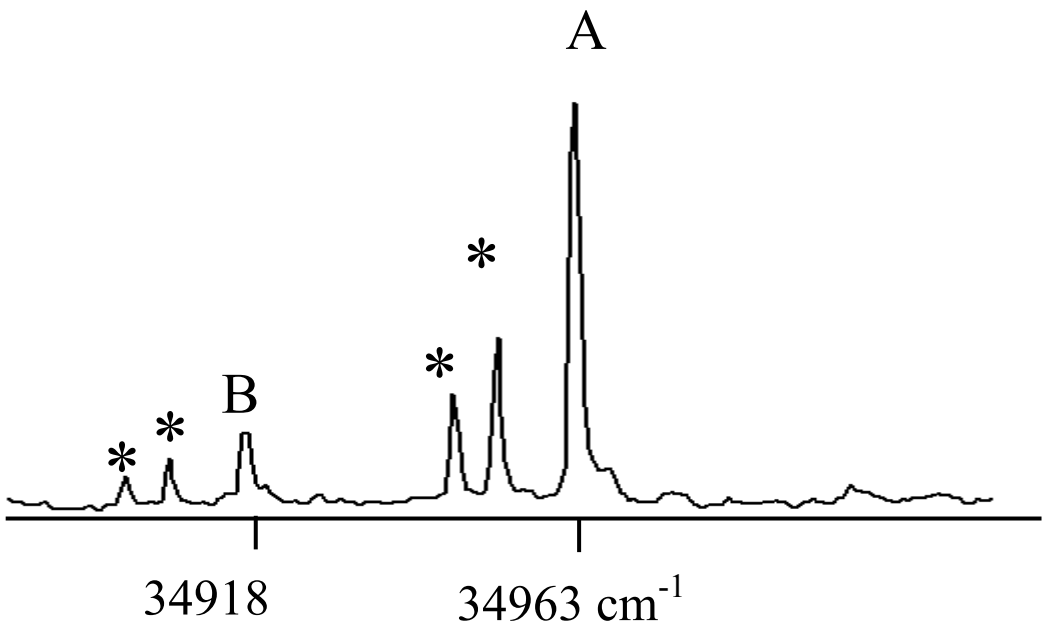

Figure 3-4. Fluorescence excitation spectrum of IPA cooled in a supersonic free jet. The origins of the transitions due to the two conformers are marked as A and B in order of decreasing intensities. Also shown is the origin band of the water cluster.

transitions located to the red of each origin band and marked by asterisks in Fig. 3-4 have been identified as water complex bands.[5]

Figures 3-5 and 3-6 show the rotationally resolved fluorescence excitation spectra of bands A and B of IPA. Like the spectra of bands B and C of IAA, each of these spectra spans about 2.5 cm^{-1} and exhibits well-defined P and R branches on either side of a strong central Q branch. However, bands A and B of IPA are not pure *a*-type bands. For example, an intensity analysis of band A revealed that this band is a hybrid band with 82% *a* character, 8% *b* character, and 10 +/- 2 % *c* character. The lower traces in Fig. 3-5 illustrate the quality of this fit. Similar effects were observed in band B (*cf*. Fig. 3-6). The final fits of these two bands utilized 173 and 214 assigned lines and resulted in OMC values of 2.99 and 3.38 MHz, respectively. The FWHM's of single transitions in the two spectra are ~ 28 MHz with Gaussian components of 18 MHz and Lorentzian components of 18 MHz. Table 3-2 summarizes the inertial parameters of bands A and B of IPA. Our excited state rotational constants for these bands are similar (within error) to the ones obtained by Connell, *et al*.[20] (A' = 1373, B' = 415 and C' = 372 MHz for band A and A' = 1441, B' = 349 and C' = 300 MHz for band B).

In general, each of the fits of the high resolution spectra of IAA and IPA described above employed a mixture of low and high J lines (with a maximum J of 45) among the 200 or so transitions assigned in each spectrum. Thus, it can be safely concluded that rigid rotor Hamiltonians adequately account for all observed features in the spectra to within the quoted OMC values. These values are in all cases substantially less than the observed single rovibronic level linewidths.

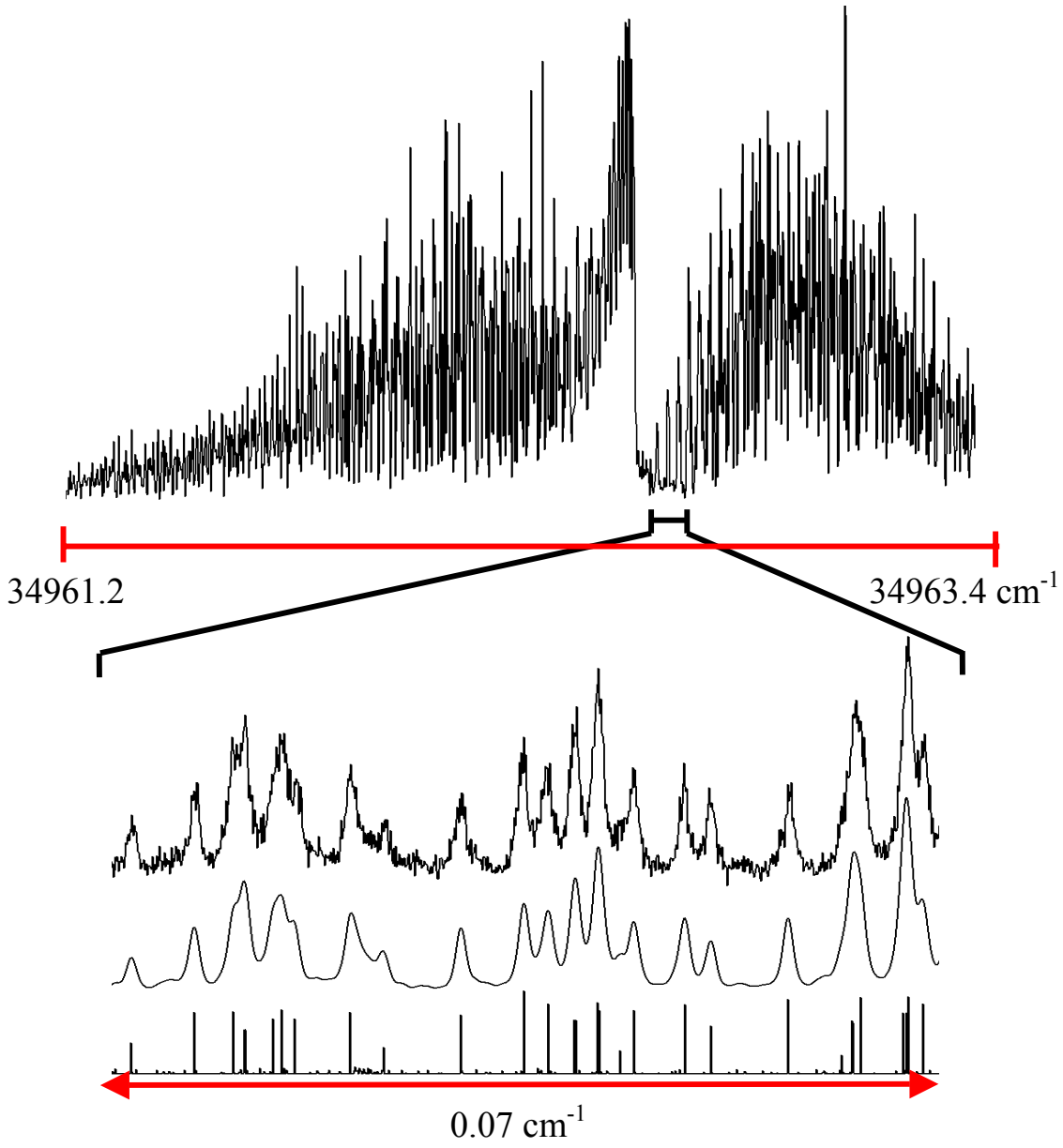

Figure 3-5: Rotationally resolved fluorescence excitation spectrum of band A of IPA in a molecular beam.

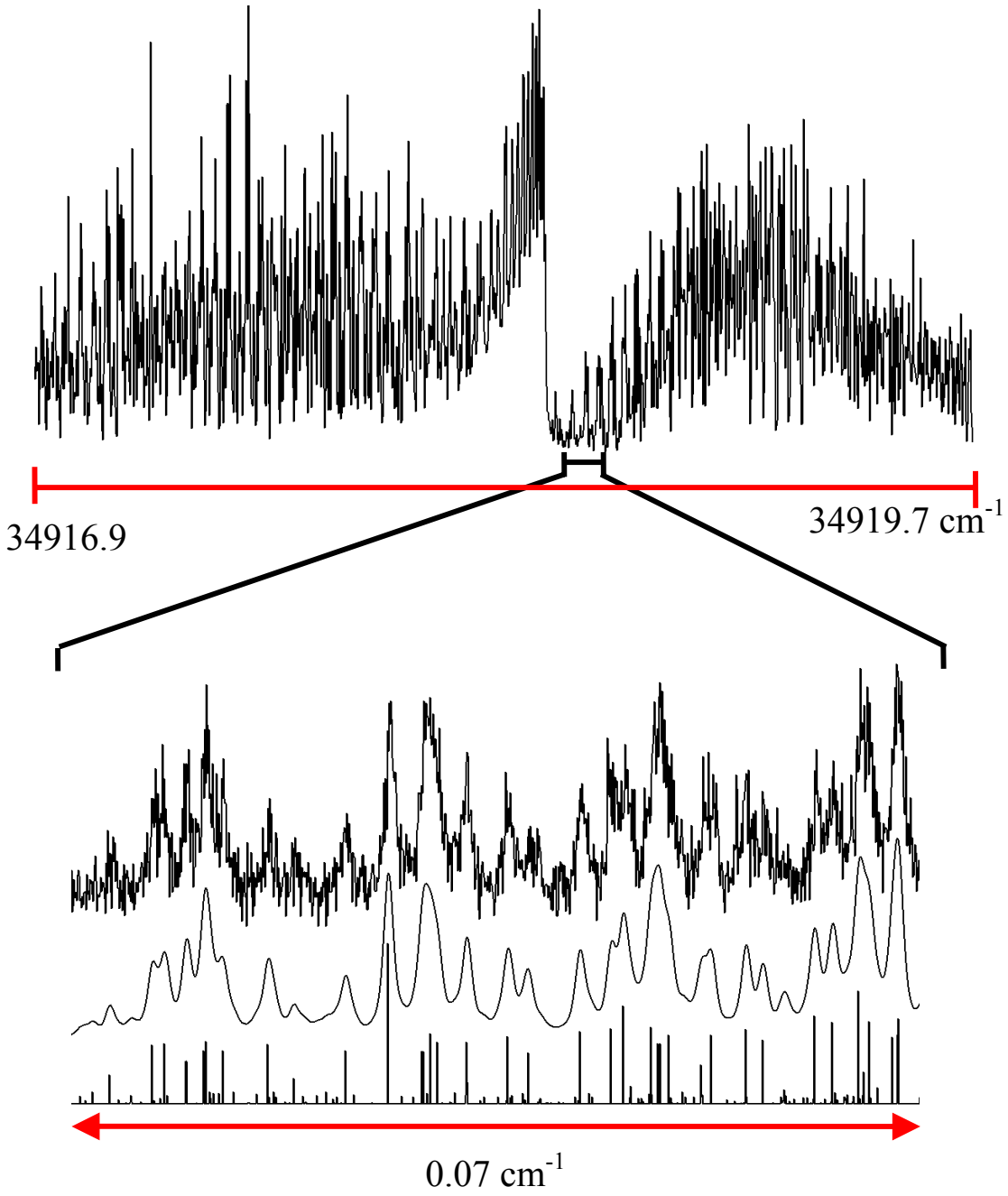

Figure 3-6. Rotationally resolved fluorescence excitation spectrum of band B of IPA in a molecular beam.

Table 3-2. **Inertial parameters of three 3-indole propionic acid in their ground (S_0) and excited (S_1) electronic states.**

Parameter	Band A	Band B
A"(MHz)	1388.3 (2.4)	1461.27 (2.7)
B"(MHz)	415.1 (0.1)	350.01 (0.1)
C"(MHz)	372.9 (0.1)	301.86 (0.1)
$\Delta I"(\mu Å^2)$	-226.17	-115.55
K"	-0.917	-0.917
ΔA(MHz)	-17.9 (2.4)	-13.7 (2.7)
ΔB(MHz)	-1.3 (0.1)	-1.2 (0.1)
$\Delta C'$(MHz)	-2.2 (0.1)	-0.9 (0.1)
$\Delta I' (\mu Å^2)$	-226.73	-119.04
K'	-0.914	-0.917
Origin (cm^{-1})	34962.60	34916.33
a/b/c-band type	82/8/10	74/12/14
N	173	214
OMC (MHz)	2.99	3.38
Temp (^{0}K)	5 (±0.5)	5(±0.5)

3.5. Discussions.

In what follows, the derived values of the rotational constants of the five observed bands in IAA and IPA are first used to identify the conformers responsible for these bands, by comparing their experimental rotational constants with theoretical ones. Then, the key interactions that lead to the stabilization of certain conformers relative to others are discussed by comparing the results for the two molecules. An intriguing aspect of these results is that IPA, which has more degrees of freedom than IAA owing to its additional CH_2 group, apparently has fewer stable structures. Finally, we examine the effects that interactions with the indole ring have on the known conformational properties of the attached alkyl chains.

The possible stable conformers of each molecule were first identified using a model kit, followed by a low-level (3-21G*) calculation to find the most stable ones. Subsequent to this, their relative energies and optimized geometries were determined at the MP2/6-31G(d,p) level of theory.[18]

Figure 3-7 shows the predicted structures of the five lowest energy conformers of IAA. Table 3-3 lists their calculated ground state inertial parameters and relative energies. The nomenclature used to distinguish the conformers is as follows. A three-fold rotation about χ_1, around the C_{ring}-C_α bond, changes the position of the side chain from in the plane of the indole ring (Inp) to out of the plane of the indole ring (Oop); the two possible in-plane positions are designated Inp-Py and Inp-Ph, depending on whether the carbonyl group is on the pyrrole or the phenyl side of the molecule. A three-fold rotation about χ_2, around the C_α-C_β bond, changes the position of the hydroxyl group; the Inp conformers that result are designated In or Out, and the Oop conformers that result are called Py, Anti, and Ph. A two-fold rotation about ψ, around the C-O(H) bond, changes the relative orientations of the carbonyl and hydroxyl groups, *cis* or *trans.*

Table 3-3. Calculated (MP2 6-31G(d,p)) rotational constants of five conformers of 3-indole acetic acid in their ground electronic states.

	Inp-Py-In	**Inp-Py-Out**	**Oop-Ph**	**Oop-Py**	**Oop-Anti**
A"(MHz)	2061.5	2072.6	1436.3	1498.0	1589.8
B"(MHz)	456.6	453.5	609.8	590.2	554.8
C"(MHz)	374.6	372.9	467.4	458.2	439.8
$\Delta I"(\mu \text{ Å}^2)$	-3.0	-3.0	-99.5	-90.6	-79.7
ΔE (cm^{-1})	1141	0	170	293	493

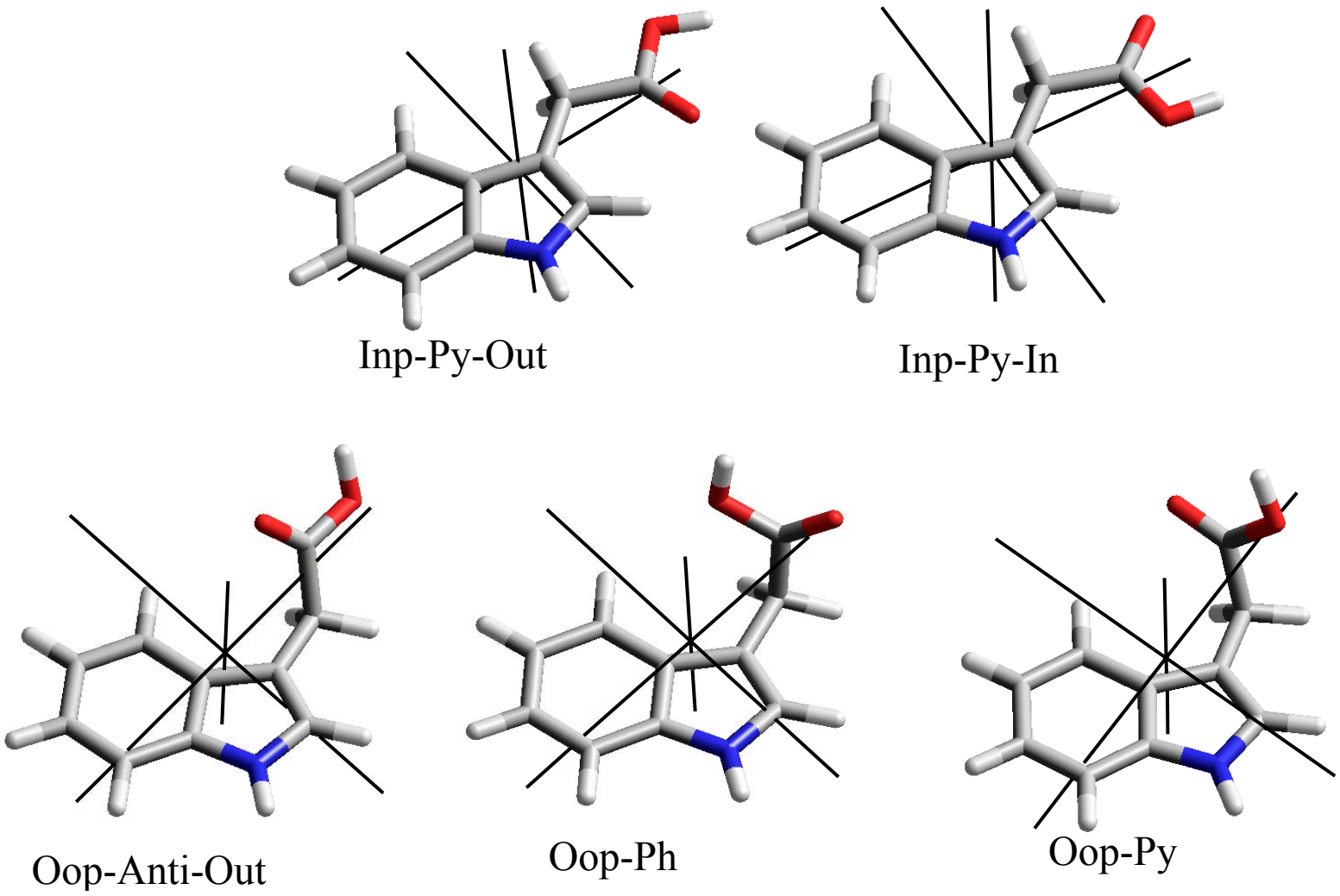

Figure 3-7: The five conformers of IAA as calculated at the MP2 6-31G(d,p) level. See text for details on nomenclature.

The five lowest energy conformers of IAA all have *cis* configurations of the carboxyl groups and are Inp-Py-In, Inp-Py-Out, Oop-Py, Oop-Anti, and Oop-Ph (*cf*. Fig. 3-7). The fact that all low energy structures are *cis* is consistent with what is currently known about the structures of a wide variety of organic acids in the condensed phase.[26]

The observed ground state inertial defects of IAA fall into two classes; a value near 0 $\mu Å^2$ for band A and values near -100 $\mu Å^2$ for bands B and C. Comparing these to the predicted values in Table 3-3 clearly shows that the acetic acid side chain is in the plane of the indole ring in the conformer responsible for band A and out of the plane of the indole ring in the conformers responsible for bands B and C. Further, the conformers responsible for bands B and C have smaller A rotational constants and larger B rotational constants and therefore must have the $–CH_2$-COOH side chain in Oop-Py and Oop-Ph (rather than Anti) positions.

Assignment of the conformers within each class requires a careful examination of the inertial parameters coupled with a direct comparison with theoretical values. We start with the conformer responsible for band A which has a side chain in the plane of the indole ring. Theory predicts two possible conformers, Inp-Py-In and Inp-Py-Out, which differ in the position of the acid group by a two-fold rotation about the C_α-C_β bond. The differences between the experimental and predicted values are smaller for Inp-Py-Out ($\Delta A'' = 5.7$, $\Delta B'' = 0.3$, and $\Delta C'' =$ 0.6 MHz) than for Inp-Py-In ($\Delta A'' = 16.9$, $\Delta B'' = -2.8$, and $\Delta C'' = -1.1$ MHz). Hence, band A is assigned to conformer Inp-Py-Out. This finding is corroborated by theory which shows that Inp-Py-Out is energetically more stable than Inp-Py-In by 1141 cm^{-1}. The likely source for this difference in energy is an attractive interaction between the carbonyl oxygen and hydrogen atom H2 on the pyrrole ring; the OH oxygen should be much less attractive in this regard.

Similarly, the smallest differences between the experimental constants of band B and the theoretical constants of the different conformers are found for the Oop-Ph structure ($\Delta A'' = 2.5$, $\Delta B'' = -7.7$, and $\Delta C'' = 2.8$ MHz; $\Delta\Delta I'' = -3.5 \mu Å^2$). The smallest differences between the experimental constants of band C and the theoretical constants of the different conformers are found for the Oop-Py structure ($\Delta A'' = 20.9$, $\Delta B'' = -12.0$, and $\Delta C'' = -5.2$ MHz; $\Delta\Delta I'' = -0.4$ $\mu Å^2$). Energetically, these two conformers lie at 170 and 293 cm^{-1} with respect to the global minimum Inp-Py-Out structure, a reasonable result given the likely existence of a putative –OH-pi interaction involving the ring pi electrons.

Figure 3-8 shows the seven lowest energy conformers of IPA as calculated at the MP2/6-31(d,p) level of theory.[18] Table 3-4 lists the ground state inertial parameters and relative energies obtained from these calculations. Unlike IAA, IPA exhibits no relatively stable in-plane structures; the lowest energy conformers all have out-of-plane side chains. Following the convention established by Carney and Zwier [27] for tryptamine, we use the symbols Gauche and Anti to describe folded and extended side chains, Py and Ph to label OH groups that are pointing towards the pyrrole and phenyl rings and In, Out and Up to denote the position of the hydroxyl hydrogen with respect to the indole ring (*cf*. Fig. 3-8).

The experimental rotational constants along with the derived inertial parameters listed in Table 3-2 are compared with the theoretical results listed in Table 3-4 and serve as the basis for the unique conformational assignment of IPA. These constants are a direct reflection of the three-dimensional structure of the isolated molecule in the gas phase. We first note that the ground state values in Table 3-2 differ greatly between the two bands. For example, the A rotational constant differs by 73 MHz on going from band A (1388 MHz) to band B (1461 MHz) in IPA. The difference between these values is well outside the error bars of our experiment (a

Table 3-4. **Calculated (MP2 6-31G(d,p)) rotational constants of seven conformers of 3-propionic acetic acid in their ground electronic states.**

	GPhOut	**GPhIn**	**GPyOut**	**GPyIn**	**AntiUp**	**AntiPh**	**AntiPy**
A"(MHz)	1107.4	1094.2	1355.0	1376.2	1455.5	1472.9	1484.0
B"(MHz)	569.4	586.8	450.3	424.0	351.4	361.9	361.3
C"(MHz)	457.1	451.6	410.0	381.9	303.0	303.8	298.4
$\Delta I"(\mu Å^2)$	-238.4	-204.0	-262.7	-236.0	-117.4	-76.3	-46.0
$\Delta E\ (cm^{-1})$	1084	886	621	0	72	445	449

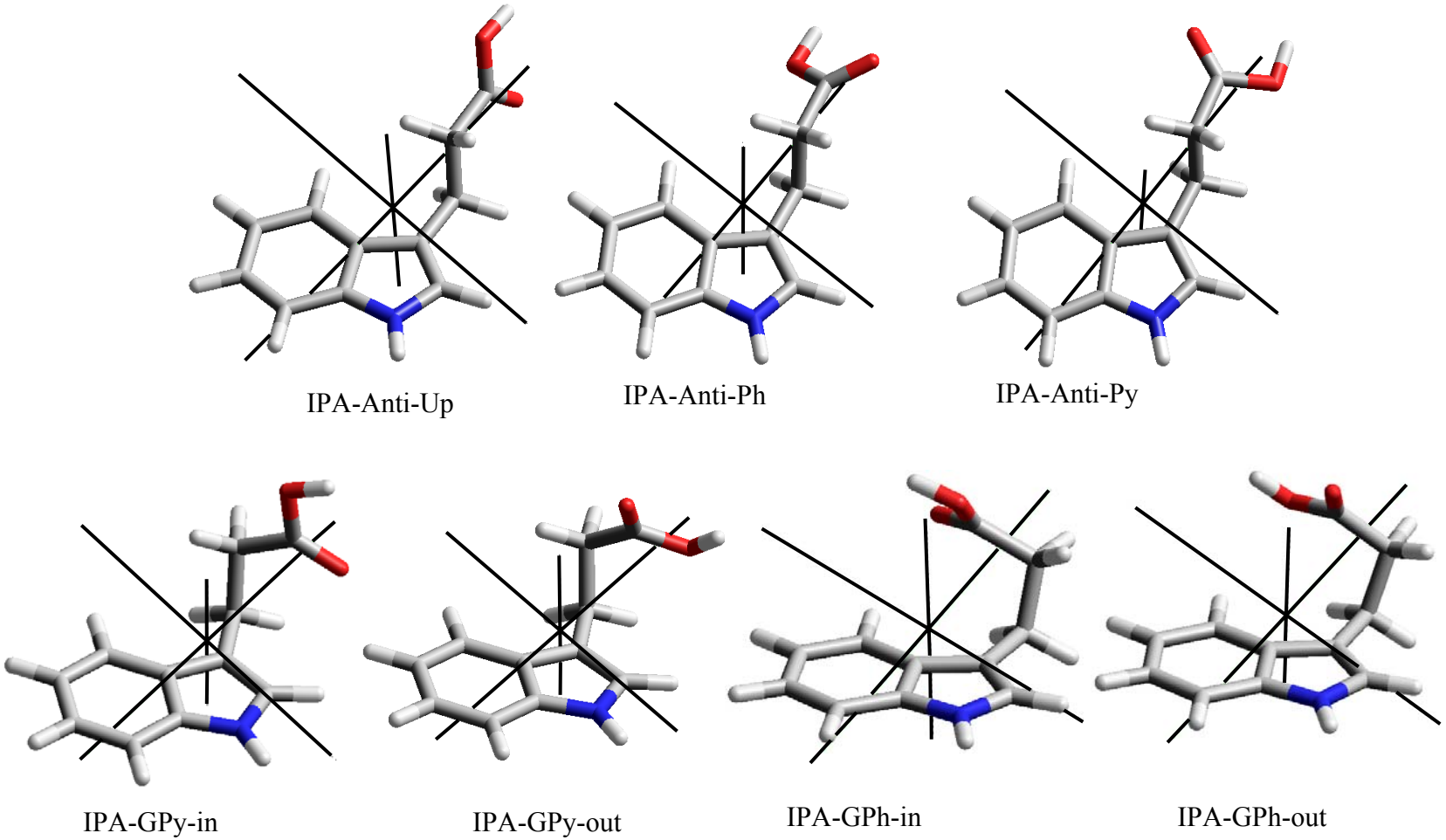

Figure 3-8: The seven conformers of IPA as calculated at the MP2 6-31G(d,p) level.

maximum of 2.7 MHz for band B). Additionally, the conformers responsible for bands A and B have large and negative values of the inertial defect ΔI in the ground state, specifically – 226 μÅ^2 for band A and - 115 μÅ^2 for band B. Both conformers must have out-of-plane acid side chains. The data in Table 3-4 show that conformers with the side chain in the Gauche position have inertial defect values of ~ 200 μÅ^2 whereas conformers with the side chain in the Anti position have inertial defect values of ~100 μÅ^2. Thus, conformer A must have a folded side chain and conformer B must have an extended one.

Next, we determine the orientation of the acid group within each class. Among the Gauche structures, only the GPy conformers have theoretical rotational constants and inertial defects that are close to the observed ones. The differences are smaller for GPyIn (ΔA″ = 12.1, ΔB″ = -8.8, and ΔC″ = -9.0 MHz; ΔΔI″ = 9.7 μÅ^2) than for GPyOut (ΔA″ = 33.3, ΔB″ = -35.1, and ΔC″ = -37.1 MHz; ΔΔI″ = 36.5 μÅ^2). The latter differences are well outside of experimental error. Therefore, we assign band A to conformer GPyIn. An analogous comparison between the results for band B and the Anti conformers (ΔA″ = 5.7, ΔB″ = -1.4, and ΔC″ = -1.1 MHz; ΔΔI″ = 1.8 μÅ^2 for AntiUp; ΔA″ = -11.6, ΔB″ = -11.9, and ΔC″ = -2.0 MHz; ΔΔI″ = -39.2 μÅ^2 for AntiPh and ΔA″ = -22.7, ΔB″ = -11.3, and ΔC″ = 3.4 MHz; ΔΔI″ = -69.5 μÅ^2 for AntiPy) leads to the assignment of band B to conformer AntiUp. GPyIn and AntiUp are predicted to be the two lowest energy conformers of IPA within its own sub-family. The remaining five conformers are expected to lie at significantly higher energy, greater than 300 cm^{-1}. The key to the stabilization of GPyIn and AntiUp is the direct overlap of the two sp^3 lone pairs of the oxygen atom in the OH group with the two adjacent hydrogen atoms of the $C_\beta H_2$ group.

The hybrid band ratios for each of the conformers are listed in Table 3-1. An examination of these data shows that these ratios are quite similar for each conformer of IPA.

Thus, the position and orientation of the side chain does not significantly affect the orientation of the S_1 - S_0 transition moment (TM). This transition is localized on the indole chromophore. Indole itself exhibits an *ab* hybrid band with a TM that makes an angle of 38.3° with the *a*-axis.[28] The additional mass of the propionic side chain rotates this TM vector into the *abc* coordinate system of IPA by angles which are largely the same for both observed conformers. Similarly, all observed conformers exhibit similar values of ΔA, ΔB, and ΔC, indicating that the structural changes upon excitation mainly occur in the indole ring system. The same pattern is observed for the Gauche conformers of IAA. The reorientation effect from the additional mass of the side chain does not entirely account for the observed TM orientation in the Inp-Py-Out conformer. Apparently, this is due to a perturbation of the electron distribution of the indole chromophore by the intramolecular hydrogen bond.

IAA and IPA can be viewed as a propionic acid (PA) molecule substituted with an indole side chain, at C_β in IAA and at C_α in IPA. Therefore, it is interesting to consider the energy landscape from this point of view. Only one conformer of PA was detected in early gas phase diffraction and microwave spectroscopy studies,[29-31] the T_t conformer shown in Fig. 3-9. Recently, Macoas, *et al.*[32] have studied PA by means of *ab initio* calculations, IR absorption spectroscopy and narrow-band NIR excitation in solid Ar. They found that only the T_t conformer is present in the deposited argon matrix. However, they were also able to produce three additional conformers (T_g□, C_t and C_g□) by vibrational excitation of the T_t conformer. T and C denote *trans* and *cis* orientations of the OH group with respect to the methylene carbon, and t and g denote *trans* and *gauche* positions of the OH group with respect to the methylene carbon (*cf.*, Fig. 3-9). These newly produced conformers are short-lived species and readily

interconvert back to the T_t conformer in the absence of irradiation. This fast conversion from the *cis* to the *trans* conformer in the dark has also been observed in acetic acid.[33,34]

Indole substitution has several effects on PA; the conformational landscape is enriched due to the asymmetric ring system of indole and novel (and possibly (de)stabilizing) forces are introduced. The overwhelming stability of the *trans* conformer stemming from the *intra*molecular hydrogen bond between the hydroxyl hydrogen and the carbonyl oxygen is conserved in IPA and IAA as well. All conformers present in the molecular beam have a *trans* hydroxyl group.

In IPA, the AntiUp conformer has the propionic side chain away and isolated from indole and is analogous to the T_t conformer. Unlike the Gauche conformer in PA, which readily converts back to T_t, GPyIn is a stable Gauche conformer of IPA. To gain a better understanding of the interactive forces present in IPA, we examine the experimental fluorescence excitation spectrum (*cf*., Fig. 3-1). We note that the stronger and more blue shifted origin band in the spectrum is assigned to GPyIn. The additional feature in GPyIn is the carbonyl group pointing toward the pyrrole ring, thus allowing for an *intra*molecular hydrogen bond between the carbonyl oxygen and the pyrrole hydrogen. This hydrogen bond is stronger than the hydrogen bonds found within the propionic side chain of AntiUp. The significance of these secondary interactions is seen in the large energy shift and the intensity ratio between AntiUp and GpyIn and the low population of conformers which lack this interaction in the molecular beam.

The importance of *intra*molecular forces is even more pronounced in IAA due to the closer proximity of the indole ring system. For example, Inp-Py-Out differs from Inp-Py-In by a two-fold rotation around the C_α-$C_{carbonyl}$ bond. The former has the carbonyl oxygen pointing towards the pyrrole hydrogen and an *intra*molecular hydrogen bond is formed. The stability of

Inp-Py-Out is further enhanced by the formation of a five-membered "ring-like" structure with the side chain. This is a reasonable assumption as the C=O----HC_2 distance is 2.363 Å, a typical length for a hydrogen bond. In contrast, Inp-Py-In lacks these interactions and is not present in the molecular beam. Thus, the energy landscape of propionic acid is greatly influenced by the proximity of the attached indole ring in both molecules. Similar effects have been observed in tryptamine.[14]

3.6. Summary.

High resolution $S_1 \leftarrow S_0$ fluorescence excitation experiments on IAA and IPA have been performed in the collision-free environments of a supersonic jet and a molecular beam. Rotational constants obtained from fits of the observed bands have been used, in combination with high level *ab initio* calculations, to determine which conformers of the two molecules were present in these environments, and which were not, thereby defining the principal features of their energy landscapes. The results show that the shape of this landscape fundamentally depends on stabilizing intramolecular interactions between the side chains and the ring systems in both IAA and IPA. These forces are therefore expected to be important in biological systems.

3.7. Acknowledgements.

This work has been supported by NSF (CHE-0315884).

3.8. References.

1. Voet, D. and Voet, J. *Biochemistry.* (John Wiley & Sons, Inc., New York, 1995).

2. Davies, P. J. *Plant Hormones and Their Role in Plant Growth and Development.* (M. Nijhoff, Dordrecht, **1987**).

3. Thiemann, K. V. *Hormone Action in the Whole Life of Plants*. (Univ. of Massachusetts Press, Amherst, **1977**).

4. Dian, B. C.; Florio, G. M.; Clarkson, J. R.; Longarte, A.; Zwier, T. S. *J. Chem. Phys*. **2004**, 120, 9033.

5. Park, Y. D.; Rizzo, T. R.; Peteanu, L. A.; Levy, D. H. *J. Chem. Phys*. **1986**, 84, 6539.

6. Connell, L. L.; Corcoran, T. C.; Joiremans, P. W.; Felker, P. M.. *Chem. Phys. Lett*. **1990**, 166, 510.

7. Felker, P. M.. *J. Phys. Chem*. **1992**, 96, 7844.

8. Sipior, J.; Sulkes, M. *J. Chem. Phys*. **1988**, 88, 6149; Sipior, J.; Sulkes, M. *J. Chem. Phys*. **1993**, 98, 9389; Sulkes, M. *J. Comp. Chem*. **1995**, 16, 973.

9. Ramek, M.; Tomić, S.; Kojić-Prodić, B. *Int. J. Quant. Chem*. **1996**, 22, 75.

10. Clarkson, J. R.; Baquero, E.; Zwier, T. S. *J. Chem. Phys*. **2005**, 122, 214312/1.

11. Hepworth, P. A.; McCombie, J.; Simons, J. P.; Pfanstiel, J. F.; Ribblett, J. W.; Pratt, D. W. *Chem. Phys. Let.* **1995**, 236, 571

12. Jagannathan, S. and Pratt, D. W. *J. Chem. Phys*. **1994**, 100, 1874.

13. Yi, J. T.; Robertson, E. G. and Pratt, D. W. *Phys. Chem. Chem. Phys.* **4** (2002) 5244.

14. Nguyen, T. V.; Korter, T. M. and Pratt, D. W. *Mol. Phys.* **103** (2005) 1603.

15. Majewski, W. A.; Pfanstiel, J. F.; Plusquellic, D. F. and Pratt, D. W. *Laser Techniques in Chemistry*. T. R. Rizzo, A. B. Myers, Eds. J. Wiley & Sons: New York, **1995**; p. 101.

16. Described in Plusquellic, D.F.; Suenram, R.D.; Mate, B.; Jensen, J.O.; Samuels, A.C. *J. Chem. Phys.* **2001***, 115*, 3057.

17. J. K. G. Watson, in *Vibrational Spectra and Structure*, edited by J. R. Durig (Elsevier, Amsterdam, 1977), Vol. 6, p. 1.

18. Gaussian 98, Revision A.10, M. J. Frisch, G. W. Trucks, H. B. Schlegel, G. E. Scuseria, M. A. Robb, J. R. Cheeseman, V. G. Zakrzewski, J. A. Montgomery, Jr., R. E. Stratmann, J. C. Burant, S. Dapprich, J. M. Millam, A. D. Daniels, K. N. Kudin, M. C. Strain, O. Farkas, J. Tomasi, V. Barone, M. Cossi, R. Cammi, B. Mennucci, C. Pomelli, C. Adamo, S. Clifford, J. Ochterski, G. A. Petersson, P. Y. Ayala, Q. Cui, K. Morokuma, D. K. Malick, A. D. Rabuck, K. Raghavachari, J. B. Foresman, J. Cioslowski, J. V. Ortiz, B. B. Stefanov, G. Liu, A. Liashenko, P. Piskorz, I. Komaromi, R,. Gomperts, R. L. Margin, D. J. Fox, T. Keith, M. A. Al-Laham, C. Y. Peng, A. Nanayakkara, C. Gonzalex, M. Challacombe, P. M. W. Gill, B. Johnson, W. Chen, M. W. Wong, J. L. Andres, C. Gonzalez, M. Head-Gordon, E. S. Replogle, and J. A. Pople, Gaussian, Inc., Pittsburgh, PA, 1998.

19. Joireman, P. W.; Connell, L. L.; Ohline, S. M. and Felker, P. M. *J. Chem. Phys.,* 96, (1992), 4118.

20. Connell, L. L.; Corcoran, T. C.; Joireman, P. W and Felker, P. M. *J. Phys. Chem.*, **94,** (1990),1229.

21. Teh, C. K.; Sipior, J. and Sulkes, M. *J. Phy. Chem.*, **93**, (1989), 5393.

22. Peteanu, L. and Levy, D. H. *J. Phys. Chem.,* **92**, (1988), 6554.

23. Sipior, J.; Sulkes, M.; Auerbach, R. and Boivinean, M. *J. Phy, Chem.,* **91**, (1987), 2016.

24. Rizzo, T. R.; Park, Y. D. and Levy, D. H. *J. Chem. Phys.,* **85**, (1986), 6945.

25. Phillips, L. A.; Levy, D. H. *J. Chem. Phys.* **1986**, *85*, 1327.

26. Chiari, G.; Fronczek, F. R.; Davis, S. T.; Gandour, R. D. *Acta Cryst., (B): Structural Crystallography and Crystal Chemistry,* **1981**, B37, 1623.

27. Carney , J.R., and Zwier, T. S., *Chem. Phys. Lett.,* **341**, 2001, 77.

28. Berden, G.; Meerts, W. L.; Jalviste, E. *J. Chem. Phys.* **1995**, *103*, 9596.

29. Derissen, J.L. *J. Mol. Struct.* **1971**, 7, 81.

30. Stiefvater, O.L. *J. Chem. Phys.* **1975**, 62, 233.

31. Stiefvater, O.L. *J. Chem. Phys.* **1975**, 62, 244.

32. Maçôas, E. M. S.; Khriachtchev, L.; Pettersson, M.; Fausto, R.; Räsänen, M. *J. Phys. Chem.A.*. **2005**, 109, 3617.

33. Maçôas, E. M. S.; Khriachtchev, L.; Fausto, R.; Räsänen, M. *J. Phys. Chem.A.*. **2004**, 108, 3380.

34. Maçôas, E. M. S.; Khriachtchev, L.; Pettersson, M.; Fausto, R.; Räsänen, M. *J. Am. Chem. Soc.* **2003**, 125, 16188.

4. Tryptamine in the gas phase. A high resolution laser study of the structural and dynamic properties of its ground and electronically excited states.

Tri V. Nguyen, Timothy M. Korter,[†] and David W. Pratt*
Department of Chemistry, University of Pittsburgh
Pittsburgh, PA 15260 USA.

*Email: pratt@pitt.edu

4.1. Abstract.

High resolution $S_1 \leftarrow S_0$ fluorescence excitation spectra of tryptamine have been observed in the collision-free environment of a supersonic molecular beam. Each origin band has been assigned to a unique conformer of the isolated molecule based on its observed rotational constants. For the first time, subbands have been detected in the rotationally resolved spectra of bands C_{blue} and D. A possible hindered motion is proposed to account for the appearance of these subbands. This motion connects the minima associated with the Antipy and Antiph conformers, and thus explores new regions of the energy landscape of this important biomolecule.

[†] Present address: Department of Chemistry, Syracuse University
Syracuse, NY 13244

Published in *Molecular Physics*, **103** (2005) 1603

4.2. Introduction.

Tryptophan (TRP, Scheme I) fluorescence is a powerful analytical probe frequently used to examine the structure and dynamics of peptides and proteins due to its sensitivity and response to changes in the local environment.[1] Tryptamine (TRA, Scheme II) is an analogue of TRP and thus has been the subject of numerous studies in both the gas and in the condensed phase.

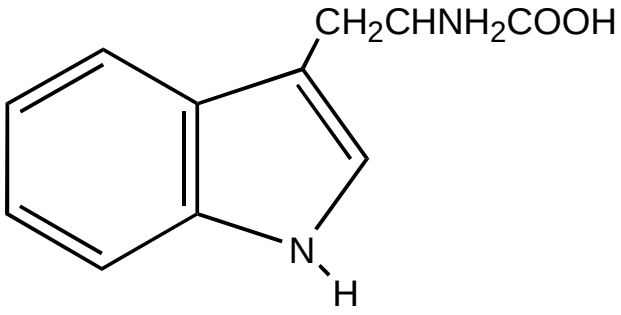

Scheme I

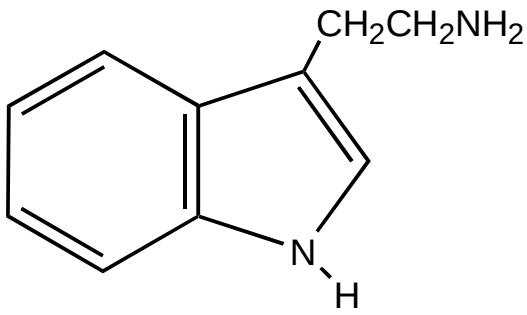

Scheme II

Park, *et al*.[2] were the first to record the vibrationally resolved $S_1 \leftarrow S_0$ fluorescence excitation spectrum of TRA in the gas phase. They showed that multiple origin bands were present in the environment of a supersonic jet. Subsequently, partially resolved contours of these bands[3,4] and those of deuterated tryptamine[5] were used to assign the various conformers of TRA. Rotational coherence measurements extended the analysis and also identified a water complex of TRA.[6-9] A more detailed conformational profile was given once R2PI, RIDIR and UV-UV hole burning investigations were combined with the results from previous studies.[10] However, a complete description of the energy landscape of TRA still has not been achieved.

The complexity of this landscape originates in the flexibility of the ethylamine side chain which has three dihedral angles χ_1, χ_2, and ψ, as shown in Scheme III.

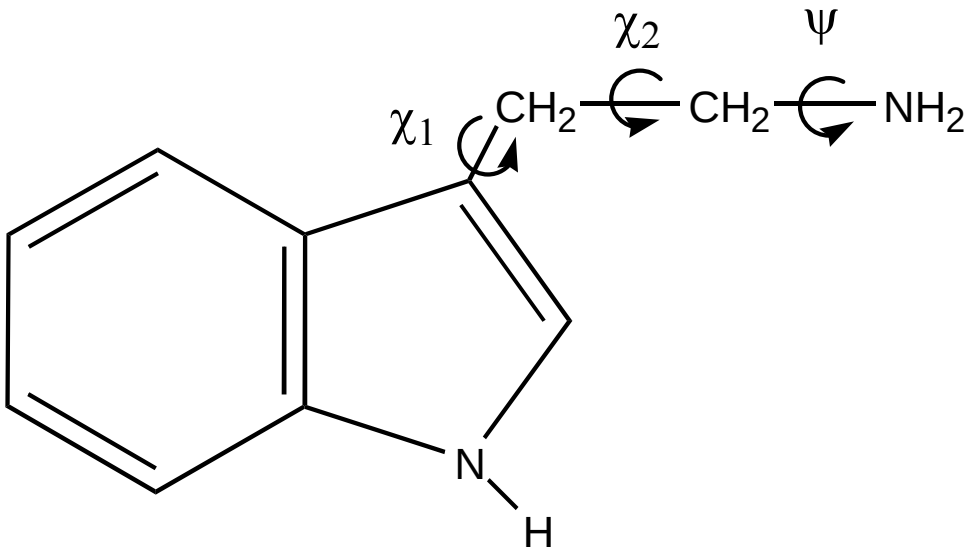

Scheme III

The angle χ_1 describes the out-of-plane character of the whole side chain whereas the angles χ_2 and ψ describe the position and the orientation of the amine group, respectively. A three-fold rotation about χ_2, around the C_α-C_β bond, changes the position of the amine group from pointing towards the pyrrole ring (Gauche-Pyrrole, GPy), away from the pyrrole ring (Anti), and towards the phenyl ring (Gauche-Phenyl, GPh). A three-fold rotation about ψ, around the C_β-N bond, changes the orientation of the amine group. A second designation is introduced within each subgroup based on the position of the lone pair on the nitrogen atom relative to the ring system. For example, the amine group in conformer GPhup points to the side of the phenyl ring with the lone pair on the nitrogen atom pointing up, away from the ring. (The nomenclature used here is identical to that introduced by Carney, *et al*.[10])

In this work, we have used high resolution electronic spectroscopy in the gas phase to assign each origin band to a unique conformer of TRA. Similar techniques were recently applied to assign the seven origin bands in an analogous molecule, *p*-methoxy-phenethylamine (MPEA), which also has an ethylamine side chain.[11] In TRA, seven conformers also have been

unambiguously identified. Additionally, two of these conformers are found to exhibit other facile motions along low frequency coordinates, thereby revealing new properties of the energy landscape of this important biomolecule for the first time.

4.3. Experiment.

Tryptamine was purchased from Sigma-Aldrich and used without further purification**.** The vibrationally resolved $S_1 \leftarrow S_0$ excitation spectrum of TRA was obtained using a pulsed jet apparatus. At room temperature, the sample was seeded into He gas at 500 kPa and expanded into a chamber kept at 10^{-5} Pa through a 1 mm diameter orifice pulsed valve (General Valve Series 9) operating at 10 Hz. Molecules were excited by a frequency-doubled dye laser (Quanta Ray Model PDL-1) pumped by a Nd^{+3}:YAG (Model DCR-1A) laser also operating at 10 Hz. The dye laser was frequency doubled into UV by a potassium dihydrogen phosphate (KDP) crystal. The spectral resolution of the dye laser is 0.6 cm^{-1} in the ultraviolet. The laser beam crossed the supersonic jet about 2.5 cm downstream of the nozzle. The fluorescence signal was collected by a photomultiplier (EMI 98139B) using a single lens system, recorded by a boxcar integrator, and processed by a data acquisition system (QUICK DATA ACQ 1.05). Calibration of the spectrum was performed by recording the markers (1 cm^{-1}) from a solid etalon.

The high resolution apparatus has been described elsewhere.[12] The sample was heated to ~ 150 ºC, seeded into ~ 400 Pa of argon, and expanded into a vacuum through a 240 μm nozzle. The molecular beam was expanded through a 1 mm skimmer 2 cm downstream of the nozzle, into a differentially pumped vacuum system. It was crossed 15 cm downstream of the nozzle with a modified continuous wave ring dye laser operating with R6G and intracavity doubled in BBO, yielding ~ 200 μW of ultraviolet radiation. The fluorescence collection optics consisted

of two spherical mirrors positioned above and below the intersection of the molecular and laser beams. In order to maximize the efficiency, the focus of the top mirror is located at the intersection of the two beams while the bottom mirror is focused at a 2 mm hole drilled in the center of the top mirror. The emitted signal was collected by a PMT. This spatially selective setup results in a collection efficiency of 33% and a Doppler-limited resolution of ~ 18 MHz. Absolute frequency calibration was performed by simultaneously recording the fluorescence spectrum of I_2 (accuracy ~ 30 MHz) and the laser interference fringes from a stabilized etalon with a spectral range of 299.7520 ± 0.0005 MHz in the fundamental of the dye.

4.4. Results.

Figure 4-1 shows the vibrationally resolved $S_1 \leftarrow S_0$ fluorescence excitation spectrum of TRA. The labeling scheme is taken directly from Park, *et al*.[2] in which the ordering A-F is used to designate the six origins of the conformers of TRA based on power saturation studies. Band A, the most intense and highest energy band, is located at ~ 34915 cm^{-1}. The other origin bands are shifted to the red of band A, at - 20 (B), - 31 (D), - 36 (C), - 47 (E), and - 84 cm^{-1} (F) with respect to band A. The presence of a seventh conformer was established when rotational band contour studies showed that band C is actually composed of two overlapping origins.[4] These two bands are called C_{red} and C_{blue} (*cf.*, Fig. 4-1).

Figure 4-2 shows the high resolution fluorescence excitation spectrum of band A. Spanning ~ 1.7 cm-1, the spectrum exhibits typical *a*-type band features, P- and R-branches on either side of an intense central Q-branch. Initially, approximately 4000 *a*- type transitions were generated based on inertial parameters from *ab initio* calculations to account for the observed spectrum.[13]

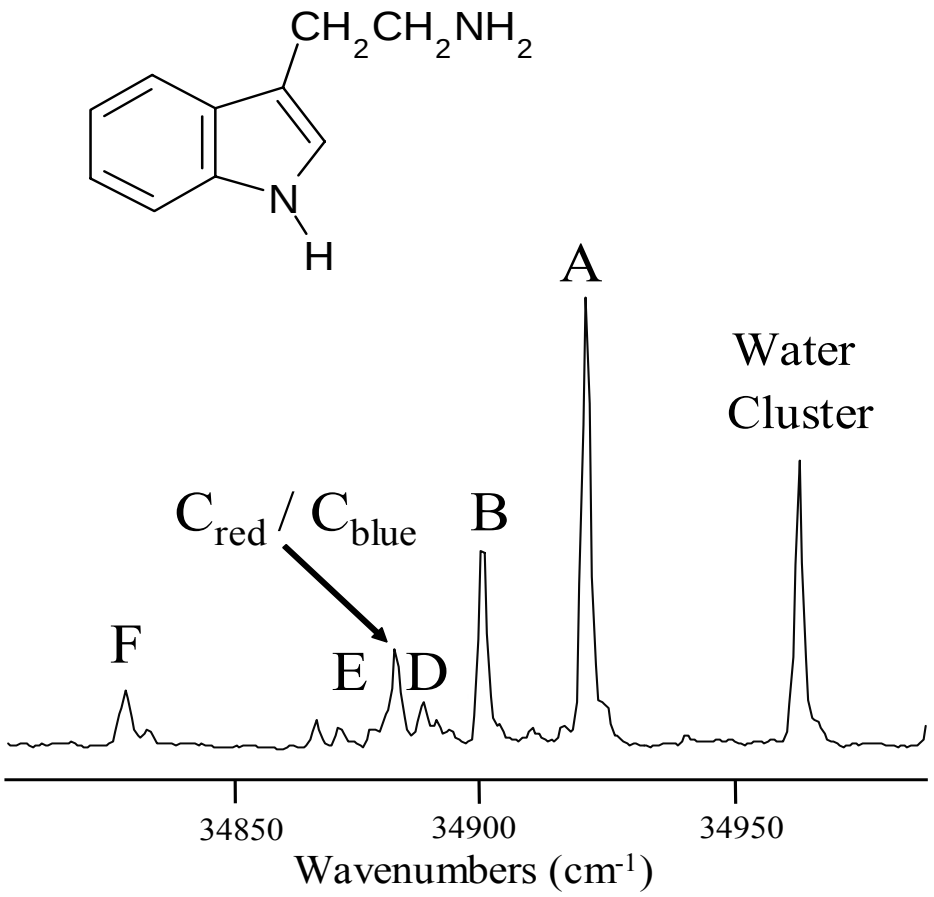

Figure 4-1. Fluorescence excitation spectrum of TRA cooled in a supersonic free jet. The origins of the transitions due to the seven conformers are marked as A-F in order of decreasing intensities. Also shown is the origin band of the single water cluster.

The FWHM of a single transition spans ~ 27 MHz. Quantum number assignments of single transitions in the simulated spectrum to corresponding transitions in the experimental spectrum were made using a Windows' based program, jb95, which employs the Watson Hamiltonian.[14,15] Subsequently, a least-squares fitting procedure was used to optimize these frequency assignments throughout the P-, Q-, and R-branch. Initially, more than 150 transitions were assigned, resulting in an OMC (observed minus calculated) standard deviation for the overall fit of 1.5 MHz, a standard deviation of 0.2 MHz for the ground state A rotational constant, and standard deviations of 0.1 MHz for all remaining rotational constants. However, all of the intensity in the experimental spectrum could not be accounted for only by *a*-type transitions. An intensity analysis was performed in which *b*- and *c*-type transitions were added to the previously generated fit. The hybrid band character determined from this intensity analysis indicates a relative ratio of 88/4/8 for *a/b/c* type selection rules. The lower traces of Fig. 4-2 show an expanded portion of the experimental spectrum of band A along with the frequency fit spectrum to illustrate the quality of the fit. The lineshape profile was characterized by a Doppler-broadened component of 18 MHz (Gaussian) and a lifetime-broadened component of 10 MHz (Lorentzian). The corresponding fluorescence lifetime of 13 ns agrees with previous time-resolved fluorescence decay measurements.[16]

Bands B, E, and F exhibit the same features as band A and were fit using the same general procedure. Slight variations were employed when fitting bands C and D. As expected from previous work,[4] band C was found to exhibit two overlapping bands with different relative intensities as shown in Fig. 4-3. The lower energy band, C_{red}, is more intense than the higher energy band, C_{blue}. The observed separation of these two origin bands (0.6169 cm^{-1}) is consistent with previous results.[4] We then used a feature of jb95 that allows for the addition of two traces.

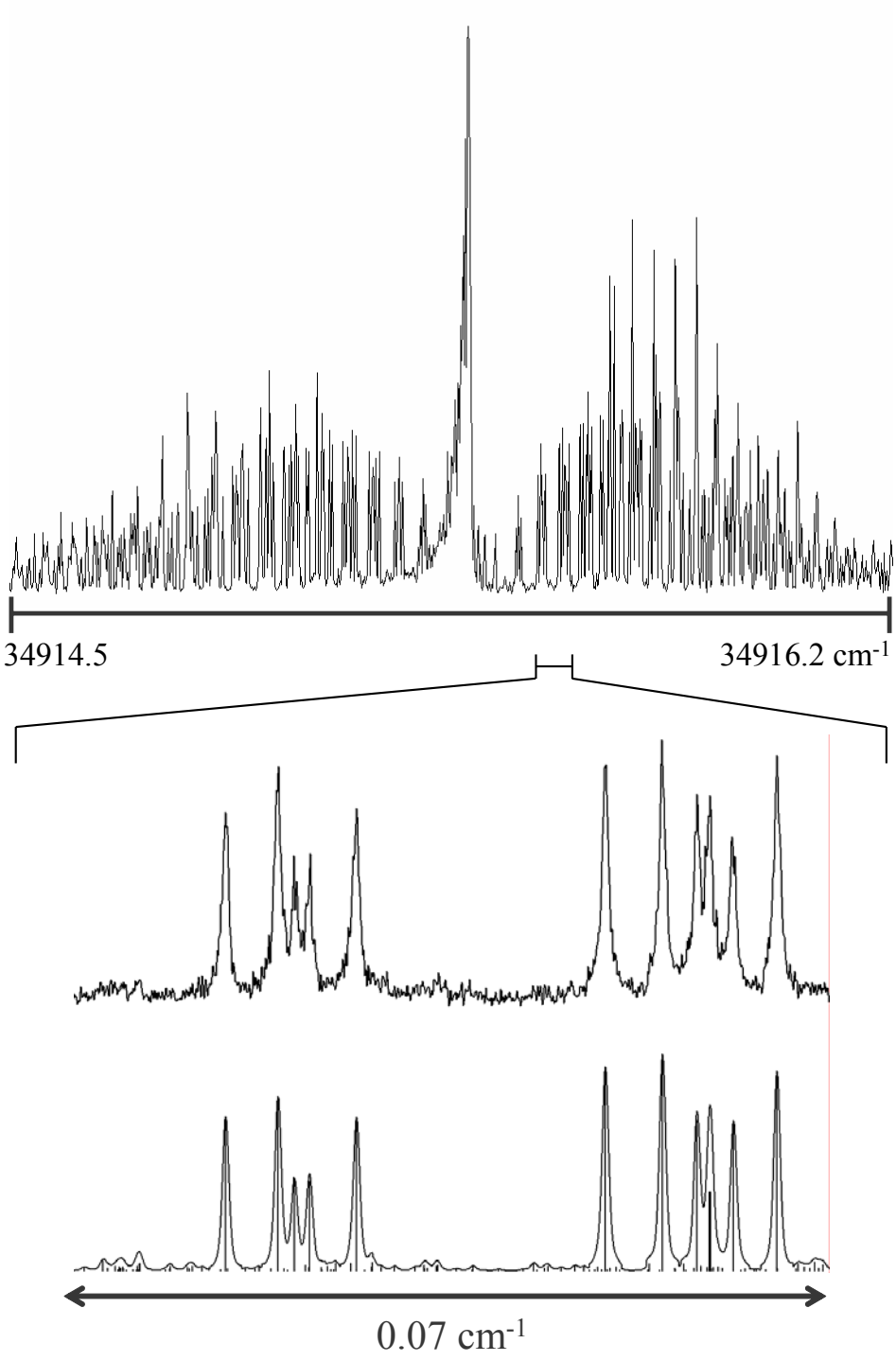

Figure 4-2. Rotationally resolved fluorescence excitation spectrum of band A of TRA in a molecular beam.

to compare the summed intensity of two simulations to an experimental spectrum A careful examination of this result indicated that there was still some "missing" intensity at the higher energy end of the experimental spectrum. A third spectrum was then generated starting with the constants of the C_{blue} conformer and used to fit this remaining intensity by the least squares method. The results showed that C_{blue} is composed of two subbands, $C_{blue\text{-}red}$ and $C_{blue\text{-}blue}$, which are separated by 95 MHz and exhibit a relative intensity ratio of ~ 1:3.

That there are three bands in this region of the spectrum is made unambiguously clear by the data in Fig. 4-3. The second trace in this figure shows an expanded portion of the experimental spectrum taken from the R branch of band C_{red} and the P-branches of bands $C_{blue\text{-}red}$ and $C_{blue\text{-}blue}$. The bottom three traces are simulations of each of these branches. Clearly, the intensity of the entire experimental spectrum can only be completely accounted for when all three simulations are present. Additional evidence for the presence of both bands $C_{blue\text{-}red}$ and $C_{blue\text{-}blue}$ is provided by careful examinations of the spectrum at higher energy, where the contribution of band C_{red} is small.

Band D in Fig. 4-4 shows the same overall shape as bands A, B, E, and F; notably congested P- and R- branches surrounding a strong central Q-branch. However, a generated fit which included *a*-, *b*-, and *c*- type transitions again could not account for all of the intensity in the experimental spectrum. As in the case of band C_{blue}, a second band was found in the vicinity of band D. The lower trace in Fig. 4-4 shows an expanded portion of the R-branch of the experimental spectrum of band D that illustrates this point. The bottom traces show two simulations, D_{red} and D_{blue}, in which the same set of transitions are separated by 95 MHz and exhibit an intensity ratio of ~ 3:1, with the stronger band lying to the red. Fits of these two bands yielded results that were consistent with an independent autocorrelation fit of the experimental

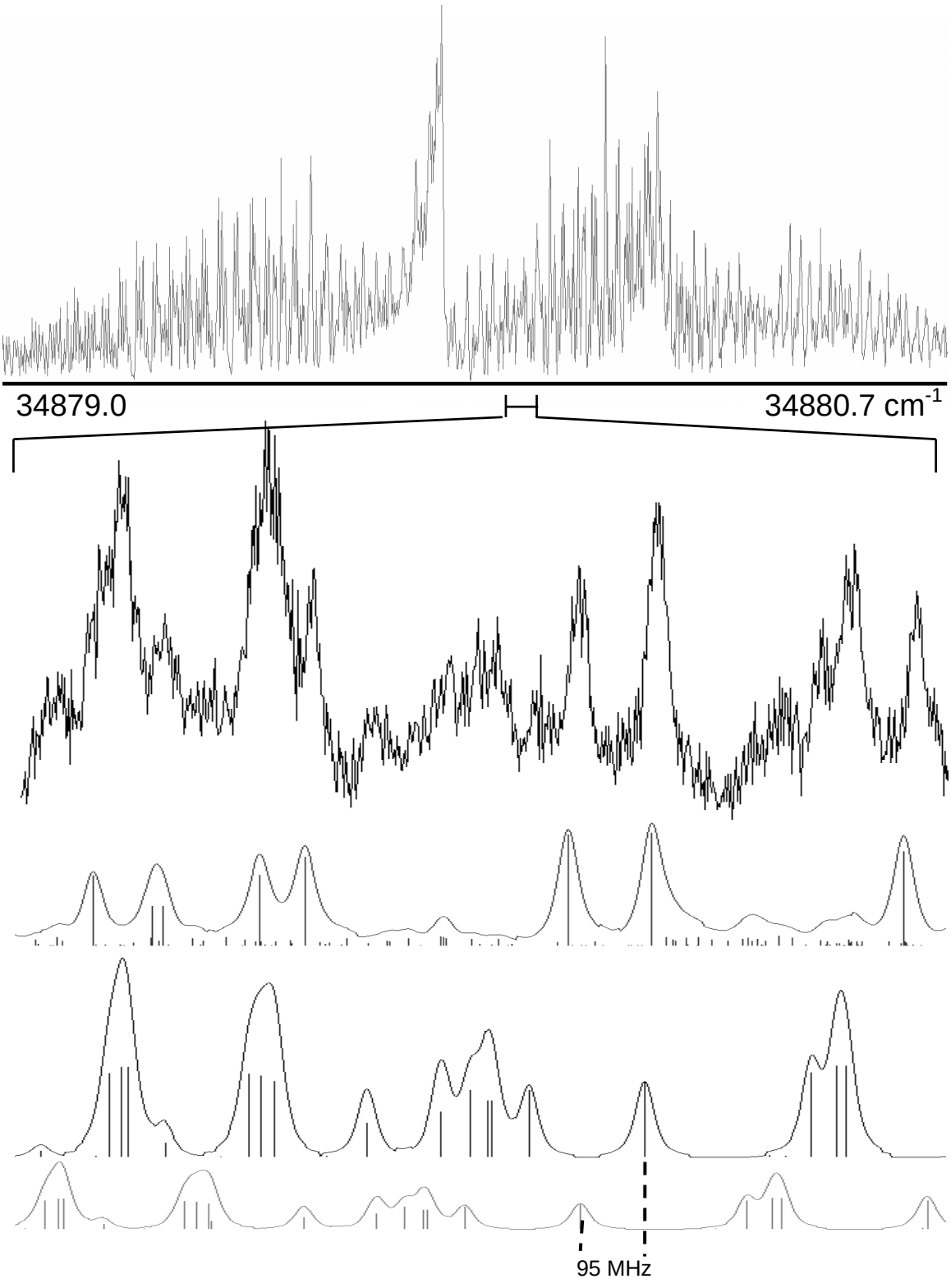

Figure 4-3. Rotationally resolved fluorescence spectrum of band C of TRA in a molecular beam.

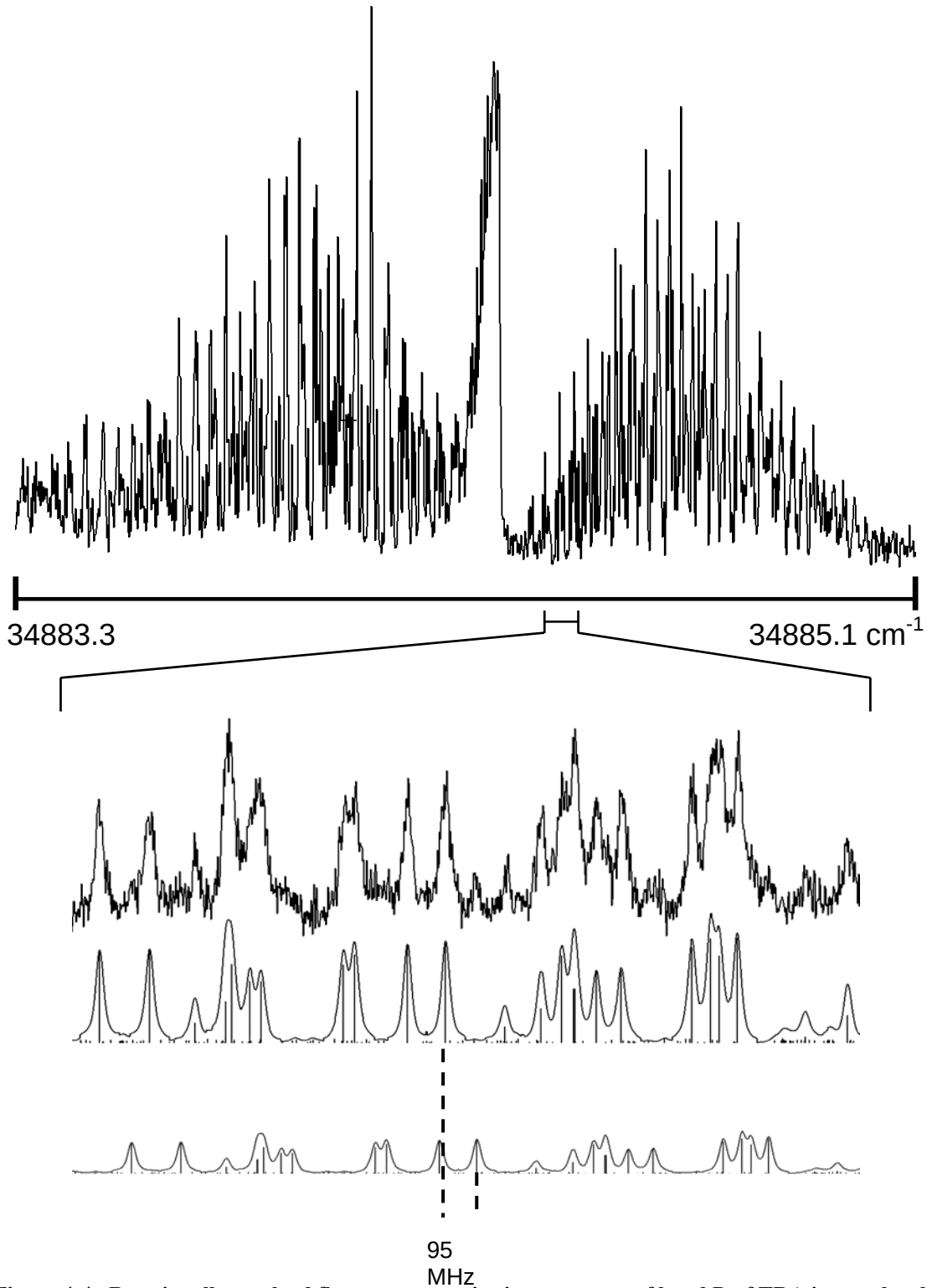

Figure 4-4. Rotationally resolved fluorescence excitation spectrum of band D of TRA in a molecular beam. spectrum.

Figure 4-5 shows comparable portions of the high resolution spectra from the R-branches of bands A-F expanded to full experimental resolution. Also shown are the corresponding set of transitions ($J'=3 \leftarrow J''=2$) generated from the fit. The pattern of lines in each spectrum is clearly different, thus making an assignment of each band to a unique conformer of TRA possible. Table 4-1 lists the inertial parameters of all bands that were derived from this analysis. The listed values, to the extent that comparisons are possible, are consistent with previously measured values,[4,6] but significantly more precise.

4.5. Discussion.

Shown in Fig. 4-6 are the nine lowest energy conformers of TRA as calculated at the MP2/6-31+G** level of theory.[13] Also shown are the inertial axes of each of the conformers. Table 4-2 lists the ground state inertial parameters and relative energies obtained from these calculations.

The experimental rotational constants and derived inertial defects listed in Table 4-1, and a comparison of these with the theoretical results listed in Table 4-2, constitute the basis for the assignment of each origin band of TRA. We begin by noting that all observed bands have large, negative values of the inertial defect ΔI in the ground state, ranging from - 44 to - 120 $\mu\text{Å}^2$. The inertial defect is a measure of the planarity of a molecule and can be extracted from the rotational constants ($\Delta I = I_c - I_a - I_b$; where $I_a = h/8\pi^2A$, $I_b = h/8\pi^2B$, and $I_c = h/8\pi^2C$). An inertial defect of zero indicates that the molecule is completely planar; large and negative ΔI values indicate significant out-of-plane character. Compared to indole (ΔI = - 0.11 $\mu\text{Å}^2$),[3,17-19] the measured inertial defects in TRA (- 44 to - 120 $\mu\text{Å}^2$) clearly show that the ethylamine tail is above (or below) the indole ring in all observed conformers.

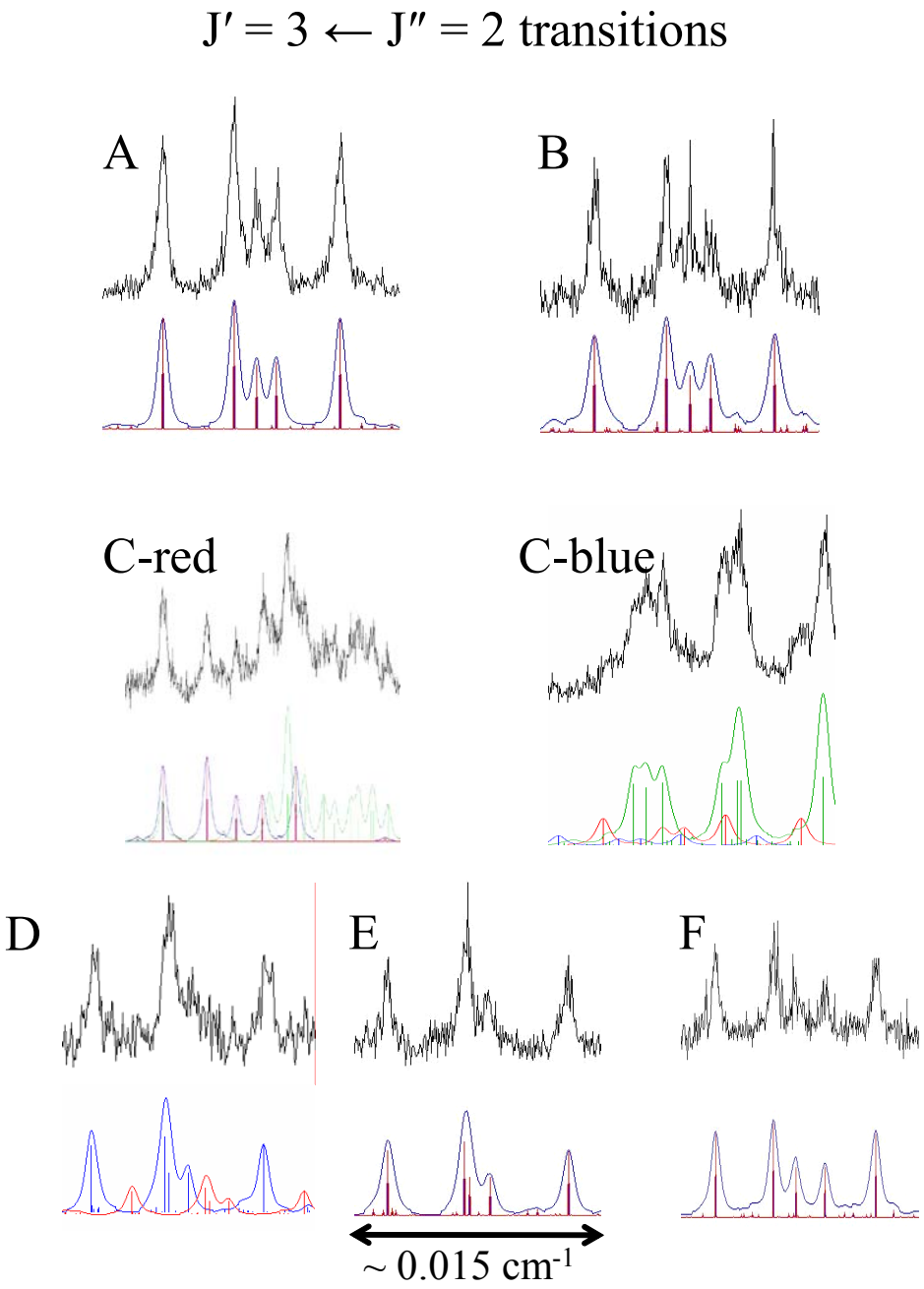

Figure 4-5. Comparable portions of the high resolution spectra of bands A-F at full experimental resolution, extracted from the R-branch. In each band, the top trace is the experimental spectrum, the bottom trace is the simulated spectrum, with an added lineshape function.

Next, we note that the observed inertial defects fall into classes. Five of the observed bands have ΔI values near - 45 $\mu\text{Å}^2$, two have values near - 90 $\mu\text{Å}^2$, and two have values near - 120 $\mu\text{Å}^2$. Comparing these results to the theoretical ones, we see that only the three Anti conformers have ΔI values near - 45 $\mu\text{Å}^2$. We also see that two calculated conformers have ΔI values near - 20 $\mu\text{Å}^2$ (GPyin) and - 70 $\mu\text{Å}^2$ (GPhin). Thus, either the calculations are in error, or the experiments have exposed previously unexplored regions of the energy landscape; *i.e.*, there is not a 1:1 correspondence between the nine observed bands and the nine lowest energy conformers.

Next, we examine differences in the ground state rotational constants listed in Table 4-1. Bands C_{blue} (both $C_{blue\text{-}red}$ and $C_{blue\text{-}blue}$), D (both D_{red} and D_{blue}), and E have larger A rotational constants as well as smaller B rotational constants. Since rotational constants are inversely proportional to moments of inertia, the heavy atoms in the ethylamine chains of the conformers responsible for these bands must be closer to the *a*-axis and further away from the *b*-axis. Therefore, bands C_{blue}, D, and E must be assigned to conformers that have the chain in the Anti position. Analogous arguments show that bands A, B, C_{red}, and F must belong to conformers that have folded ethylamine side chains with the amine group on the side of the pyrrole ring in bands A and B, and on the side of the phenyl ring in bands C_{red} and F.

The determination of the orientation of the amine group within each class demands a careful examination of the rotational constants since the difference between each conformer is essentially a three-fold rotation of two hydrogen atoms about the C_β-N bond. Direct comparisons between the experimental and theoretical ground state rotational constants indicate only that certain conformers are not present in the beam. Thus, while the three rotational constants of bands C_{red} and F are close to the predicted values for GPhout and GPhup, no

observed band has rotational constants close to the predicted values for GPhin. A similar conclusion is reached regarding the GPyin conformer in the Gauche-Pyrrole class. The difference between its calculated A rotational constant and all observed values is greater than 600 MHz. Hence, we conclude that neither GPhin nor GPyin are present in high concentration in the molecular beam.

Since the difference between the conformers within each class is a simple rotation of the NH_2 group about the C_β-N bond, and since this motion is common to all classes, we finally compare the differences between the inertial parameters of all observed bands within a given class to those predicted by theory, to make unique assignments. Table 4-3 lists the experimental and calculated differences in the ground state rotational constants and inertial defects within each class. In the Gauche-Pyrrole family, the experimental differences between conformer A and B are 21.3 MHz for the ground state A″ rotational constant, 0.1 MHz for B″, and 0.6 MHz for C″. The difference in the ground state inertial defects ($\Delta\Delta I''$) is 2.8 $\mu Å^2$. Among the possible pairs of conformers that might be responsible for these differences, only the "out-up" pair gives values that are similar to the experimental ones ($\Delta A''$=30.5, $\Delta B''$=-1.6, and $\Delta C''$=0.4 MHz; $\Delta\Delta I''$=3.1 $\mu Å^2$). Based on this agreement, bands A and B are assigned to conformers GPyout and GPyup respectively. In these comparisons, the signs of the differences are important, since they indicate whether conformer A should be assigned to GPyout or GPyup, or *vice versa*. This comparison also confirms the absence of the GPyin conformer in the beam as the calculated differences for this conformer are much larger than the observed ones.

In the Gauche-Phenyl class of structures, differences of - 12.9, 17.1, and - 0.5 MHz in the A″, B″, and C″ rotational constants and $\Delta\Delta I''$=13.8 $\mu Å^2$ in the inertial defect are observed between bands C_{red} and F. From an examination of the changes between GPhout-GPhup,

Table 4-1. Inertial parameters of seven conformers of TRA in their ground (S_0) and excited (S_1) electronic states[a]

	A	B	C_{red}	$C_{blue\text{-}red}$	$C_{blue\text{-}blue}$	D_{red}	D_{blue}	E	F
S_0									
A (MHz)	1730.6 (0.2)	1709.3 (0.2)	1591.9 (0.3)	1775.0 (2.0)	1774.8 (1.1)	1766.8 (0.3)	1765.1 (0.9)	1761.0(1.4)	1604.9(0.2)
B (MHz)	681.8	681.8	754.6	615.3	615.2	617.5	617.4	615.0	737.6
C (MHz)	551.4	550.8	560.7	475.9	475.9	476.9	476.9	475.8	561.2
ΔI ($\mu Å^2$)	-116.7	-119.5	-85.9	-44.1	-44.4	-44.7	-45.3	-46.6	-99.6
S_1									
A (MHz)	-7.0	-6.7	-6.8	-14.2	-14.2	-13.6	-13.7	-13.0	-12.3
B (MHz)	-9.3	-9.4	-12.7	-5.2	-5.2	-5.4	-5.4	-5.5	-9.3
C (MHz)	-7.0	-6.6	-7.2	-3.5	-3.5	-3.6	-3.5	-3.4	-6.3
ΔI ($\mu Å^2$)	-116.4	-119.9	-87.0	-45.7	-45.7	-46.3	-46.9	-48.4	-100.7
Origin (cm^{-1})	34915.7	34896.0	34879.3	34879.9	34879.9	34884.3	34884.3	34868.3	34832.0
# assignments	115	124	116	36	62	187	115	130	238
% intensity *a/b/c* (±3)	88/4/8	92/4/4	88/8/4	88/4/8	*b*	88/4/8	88/4/8	83/7/10	92/4/5
OMC (MHz)	1.8	1.7	2.3	2.6	2.1	2.7	2.7	2.0	2.3

[a]Errors in rotational constants are ± 0.1 MHz except where indicated.

[b]Not determined due to low intensity of this band.

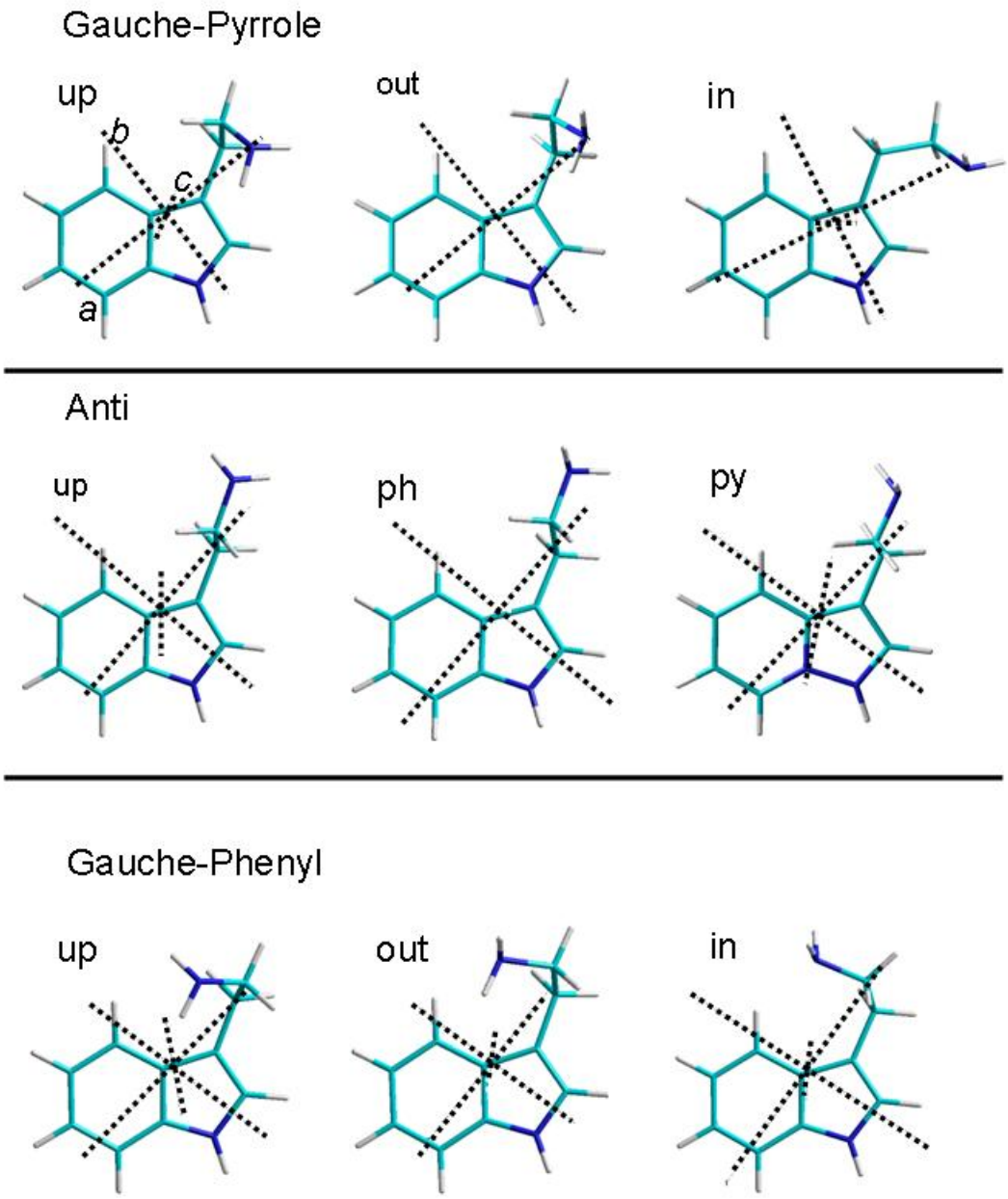

Figure 4-6. The nine conformers of TRA as calculated at the MP2+/631G level. See text for a description of the nomenclature used.**

Table 4-2. Calculated rotational constants, derived inertial defects, and relative energies of nine conformers of TRA in their ground electronic states at the MP2/6-31+G level.**

	GPyup	GPyout	GPyin	Antiup	Antiph	Antipy	GPhup	GPhout	GPhin
A (MHz)	1683.1	1713.6	2318.6	1756.0	1760.8	1764.9	1602.3	1589.3	1567.9
B (MHz)	693.3	691.7	575.0	615.3	618.3	615.4	739.3	761.2	750.5
C (MHz)	559.0	559.4	469.6	476.6	478.0	476.8	564.6	564.0	544.6
ΔI ($\mu Å^2$)	-125.2	-122.1	-20.8	-48.8	-47.1	-47.6	-103.9	-85.9	-67.6
ΔE (cm^{-1})	152	0	414	148	80	78	436	219	972

GPhout-GPhin, and GPhout-GPhin listed in Table 4-3, only the set of differences between GPhout and GPhup matches the experimental differences both in magnitude and sign ($\Delta A''$=-13.0, $\Delta B''$=21.9, and $\Delta C''$=-0.6 MHz; $\Delta\Delta I''$=18.0 $\mu Å^2$). Therefore, we assign bands C_{red} and F to conformers GPhout and GPhup, respectively, again confirming the absence of the GPhin conformer in the vibronic spectrum.

In the Anti class, several factors make the analysis complex. The most important of these is that five bands remain unassigned whereas there are only three conformers in this class. Additionally, the C_β-N bond in all conformers lies essentially along the *a*-axis, giving them very similar rotational constants (*cf.*, Table 4-2). We deal with these complexities with a full and iterative comparison of the differences in both the observed and calculated inertial parameters. First, we note that bands $C_{blue\text{-}red}$ and $C_{blue\text{-}blue}$, and D_{red} and D_{blue}, have very similar parameters; therefore, we group them together in the discussion which follows, using the average values of their parameters in the analysis. Then, we see from Table 4-3 that the differences in the ground state inertial parameters of bands D and E ($\Delta A''$=5.0, $\Delta B''$=2.5, and $\Delta C''$=1.1 MHz; $\Delta\Delta I''$=1.6 $\mu Å^2$) are matched only by the differences between conformers Antiph and Antiup ($\Delta A''$=4.8, $\Delta B''$=3.0, and $\Delta C''$=1.4 MHz; $\Delta\Delta I''$=1.9 $\mu Å^2$). Each of the three sets of differences from experiment matches only one theoretical set (C_{blue}-D with Antipy-Antiph, D-E with Antiph-Antiup, and C_{blue}-E with Antipy-Antiup). In general, the experimental and calculated rotational constants of the different conformers in all classes agree to within 1.5 % or less. Based on this analysis, bands C_{blue}, D, and E are assigned to conformers Antipy, Antiph, and Antiup, respectively. This assignment is consistent with the differences in the experimental ground state constants upon a three-fold rotation of two hydrogen atoms around the C_β-N bond. For example,

Table 4-3. Differences in the ground state rotational constants and inertial defects among the conformers of TRA within each class, compared to theory

Gauche-Pyrrole			
Experimental	**A-B**		
ΔA (MHz)	21.3		
ΔB (MHz)	0.1		
ΔC (MHz)	0.6		
ΔΔI (μÅ^2)	2.8		
Calculated	**out-up**	**up-in**	**out-in**
ΔA (MHz)	30.5	-635.5	-605.0
ΔB (MHz)	-1.6	118.3	116.7
ΔC (MHz)	0.4	89.4	89.7
ΔΔI (μÅ^2)	3.1	-104.3	-101.2

Gauche-Phenyl			
Experimental	**C_{red}-F**		
ΔA (MHz)	-12.9		
ΔB (MHz)	17.1		
ΔC (MHz)	-0.5		
ΔΔI (μÅ^2)	13.8		
Calculated	**out-up**	**up-in**	**out-in**
ΔA (MHz)	-13.0	34.4	21.4
ΔB (MHz)	21.9	-11.2	10.7
ΔC (MHz)	-0.6	20.0	19.5
ΔΔI (μÅ^2)	18.0	-36.2	-18.2

Anti			
Experimental	**C_{blue}-D**	**D-E**	**C_{blue}-E**
ΔA (MHz)	8.9	5.0	13.9
ΔB (MHz)	-2.2	2.5	0.3
ΔC (MHz)	-1.0	1.1	0.1
ΔΔI (μÅ^2)	0.8	1.6	2.4
Calculated	**py-ph**	**ph-up**	**py-up**
ΔA (MHz)	4.1	4.8	8.9
ΔB (MHz)	-2.9	3.0	0.1
ΔC (MHz)	-1.2	1.4	0.2
ΔΔI (μÅ^2)	-0.5	1.7	1.2

Antiup (conformer E), which has the two amine hydrogens on either side of the *a*-axis, can be transformed into either Antipy (conformer D) or Antiph (conformer C_{blue}) by a simple rotation of the NH_2 group about the C_β-N axis, placing one hydrogen atom on the *a*-axis and changing its ground state rotational constants.

Table 4-4 displays the structural assignment of the origin bands of TRA. Where pertinent, our assignments are consistent with those that have been made before,[3-10] including the recent microwave assignment of conformers A and B.[20] Previously, there was still an ambiguity surrounding the identities of the conformers responsible for bands C_{blue} and D. Here, we have completed the structural assignment by resolving this issue with the former being assigned to conformer Antipy and the latter to conformer Antiph.

From the assignment of each origin band to a unique conformer, we can reach an understanding of the interactions responsible for the intensity and fluorescence excitation energy shifts in TRA. The strongest bands in the fluorescence excitation spectrum in Fig. 4-1 are assigned to conformers GPyout (A) and GPyup (B). Moreover, we note that they are the most blue shifted. The structural feature that is common to both conformers is the N-H bond pointing towards the electron rich pyrrole ring. In contrast, the bands of conformers C-F which lack this interaction are weaker. Therefore, we conclude that the N-H---$\pi_{(py)}$ interaction is responsible for the stability of conformers GPyout and GPyup in both the S_0 and S_1 states. This effect is analogous to the findings in MPEA.[11] The stronger intensity of band A comes from an additional stabilizing interaction due to a weak intramolecular hydrogen bond between the lone pair of the nitrogen atom and the C_β hydrogen atom (*cf.*, Fig. 4-6). The effect of this secondary stabilizing interaction can also be seen in the pattern of the shifts among conformers within the Gauche-Phenyl and Anti classes.

Table 4-4. Assignments of specific bands in the fluorescence electronic spectrum of TRA to specific conformers (see Figs. 4-1 and 4-6).

Band	Conformer	Relative Frequency (cm^{-1})
A	GPyout	0
B	GPyup	-20
C_{red}	GPhout	-36
C_{blue}	Antipy	-36
D	Antiph	-31
E	Antiup	-47
F	GPhup	-84

The hybrid band ratios for each of the conformers are listed in Table 4-1. An examination of these data shows that these ratios are quite similar for each conformer of TRA; thus, the position and orientation of the side chain does not significantly affect the orientation of the S_1 - S_0 transition moment (TM). This transition is localized on the indole chromophore. Indole itself exhibits an *ab* hybrid band with a TM that makes an angle of 38.3° with the *a*-axis.[17]

The additional mass of the ethylamine side chain rotates this TM vector into the *abc* coordinate system of TRA by angles which are largely the same for all conformers. This lack of sensitivity also has been observed in 3-indole acetic acid where it was found that the TM orientations in conformers with side chains out-of-the-plane of the indole ring are more or less the same.[21] Similarly, all conformers exhibit similar values of ΔA, ΔB, and ΔC, indicating that the structural changes upon excitation mainly occur in the indole ring system. These results stand in sharp contrast to those for MPEA, where it was found that the S_1 - S_0 TM orientations and rotational constant differences are quite different among the different conformers.[11]

For the first time, two subbands have been observed in the spectra of bands C_{blue} and D in TRA. What is responsible for these? One possibility is that they originate from higher vibronic levels of other conformers; a second possibility is that they originate from new conformers of TRA, not observed before. These two possibilities can be ruled out on the basis of two different experiments. These are the previous hole-burning experiments,[10, 22] which have not revealed the presence of additional conformers, and the present experiments, which show that the two pairs of subbands that comprise bands C_{blue} and D each have very nearly the same rotational constants (*cf.*, Table 4-1). As we have seen, the rotational constants of TRA are very sensitive to conformational "choice".

The third possibility, which is most likely, is that the subbands result from a tunneling process that interconverts the amine protons of each conformer. The primary evidence supporting this interpretation are the 1:3 and 3:1 relative intensities of the split subbands. These have their origin in the statistical weights of affected nuclear spins. The tunneling motion that is responsible must be a coupled inversion and internal rotation motion since neither motion by itself can independently interconvert the amine protons. Splittings of this type, varying from 100 kHz to 1 GHz, have been observed previously in the microwave and infrared spectra of a number of primary amines.[23] Similar effects have been observed in the high resolution electronic spectra of many molecules and weakly bound complexes along other coordinates.[24,25] In electronic spectroscopy, the frequency separation of the two subbands represents the difference in the tunneling splittings in the two electronic states. Often, it is additionally observed that there are small differences in the rotational constants of the two subbands that can be used to determine the axes about which the motion is occurring. In both cases reported here, the A constants of the two subbands are different, suggesting a motion about *a*, but these differences are (presently) too imprecise to be analytically useful.

Three facts make the present observations especially intriguing. First, the splitting is observed in two conformers, and no others. The two conformers differ only in the orientation of their NH_2 groups with respect to the C_β-N bond. Second, the magnitude of the observed splitting in each pair of subbands is the same (~ 95 MHz). And third, the "sense" of the splittings is different; the relative intensity of the two subbands in the C_{blue} band is 1:3 whereas that of the two subbands in the D band is 3:1. The logical conclusion to be reached as a consequence of these three facts is that the conformers responsible for these bands, Antipy and Antiph, are interconverting, one into the other, owing to a reduced barrier along the large amplitude

coordinate. A schematic illustration of the resulting potential energy surface is shown in Fig. 4-7. Alternatively, it may be that the barrier along this coordinate is reduced by virtue of a coupling along the interconversion coordinate. In either event, it is apparent that this process is multidimensional, since there must be at least two connected levels in each well. Similar processes have not been observed before in large biomolecules.

The absence of such subbands among the conformers of the Gauche-Pyrrole and Gauche-Phenyl families indicates that interactions between the amine group and either the phenyl or pyrrole ring in those groups are significant, producing large energy differences between the conformers within each class. The localized wave functions that result prevent these conformers from communicating with each other. In contrast, Antiph and Antipy are less influenced by the phenyl and pyrrole π ring system because the amine group points away from the indole ring in both conformers. Theoretical calculations reflect this diversity in the energies of conformers within each class as can be seen in Table 4-2. Typically, members of the same family are predicted to have ground state energies that differ by 100-200 cm^{-1}, whereas the calculated energies of Antiph and Antipy differ by only 2 cm^{-1}. Even the Antiup conformer has a significantly higher energy than the other members of this family. Thus, the similarity in the energies of Antiph and Antipy in both electronic states must play a key role in the dynamics of the interconversion process; their 0^0_0 bands are degenerate to within 4 cm^{-1}. Small differences in the zero-point energies (not shown in Fig.4-7) in one or both electronic states, owing to differences in the energies of interaction of the ethylamine side chain with the two rings, are likely to be responsible for the reversal in the relative intensities of the two subbands in the two spectra.

A recent study of the ground state conformational landscape of TRA using the new stimulated emission pumping (SEP)-hole filling and SEP-induced population transfer techniques indicated that isomerization barriers are family and conformer specific.[26] The relative energies of TRA conformers also were determined. By measuring the isomerization thresholds of different reactant-product pairs (GPyout with GPyup, GPhout, GPhup, Antiup, Antipy, and Antiph, and GPyup with GPyout, GPhup, and GPhout), it was found that the lowest isomerization threshold (< 562 cm^{-1}) separates members within the Gauche-Phenyl family and that higher barriers connect conformers belonging to different families. The highest isomerization barriers (1219-1316 cm^{-1}) are between GPyout and any of the Anti conformers.

Taking the value F = 12.1 cm^{-1} for the NH_2 group, we can reproduce the observed splitting of 95 MHz in the two bands with barrier heights of 300 and 302 cm^{-1}, respectively. A recent *ab initio* estimate places these two barriers at ~ 650 cm^{-1}.[27] But large couplings among the different large amplitude modes (including the reaction coordinate) could reduce these barriers significantly. In fact, our most important result may be this very general one; that heretofore undiscovered but facile interconversion pathways exist between "degenerate" conformers on the energy landscapes of large molecules. Experiments on isotopically labeled tryptamines will be necessary to confirm this intriguing possibility in this system.

4.6. Conclusions.

We report high resolution $S_1 \leftarrow S_0$ fluorescence excitation experiments on TRA in the collision-free environment of a supersonic jet and a molecular beam. A complete description of the conformational landscape of TRA is given as each of the seven observed origin bands is assigned to a unique conformer of the isolated molecule through comparisons of the rotational constants and predictions from theory. A possible hindered motion interconverting the Antipy

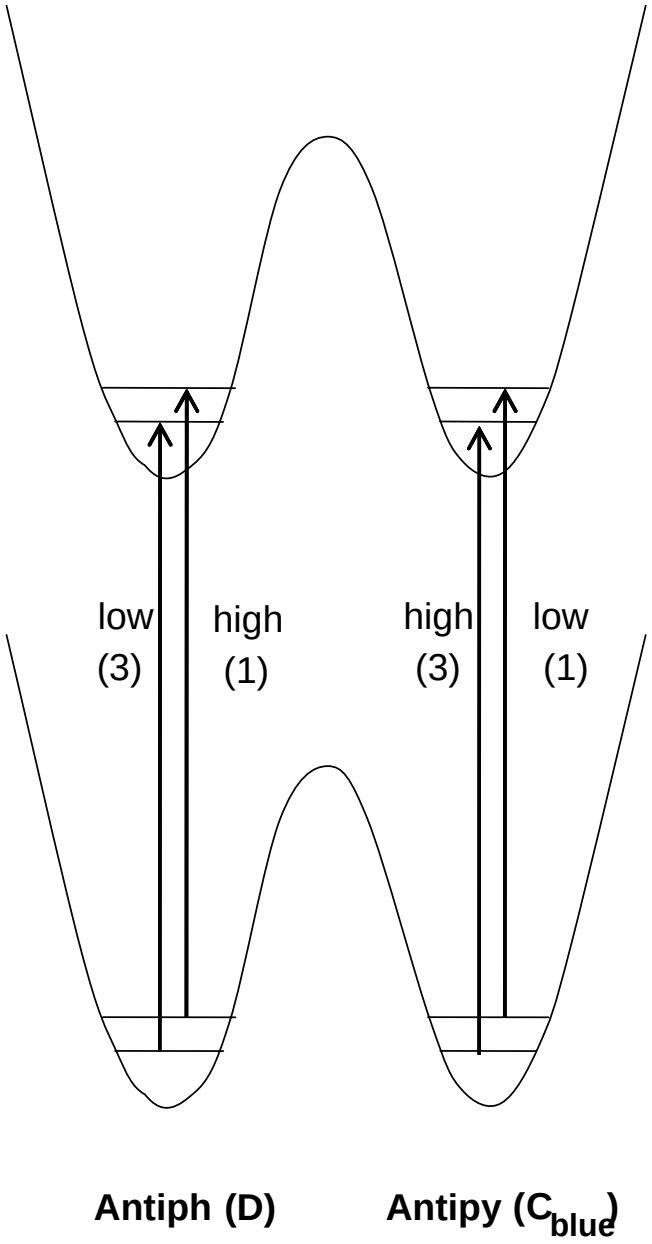

Figure 4-7. Hypothetical one-dimensional potential energy curves along the interconversion coordinate for the S_0 and S_1 states of Antipy and Antiph of TRA. Coupling to at least one other large amplitude vibrational coordinate leads to two nearly degenerate energy levels in each well. Low (1) and high (3), etc. refer to the relative energies and intensities of the two subbands in the electronic spectra of the two conformers.

and Antiph conformers is proposed to explain the appearance of subbands in the rotationally resolved spectra of bands C_{blue} and D. Motions of this type may lower the barriers to interconversion among nearly degenerate conformers of many other large molecules important in biology.

4.7. Acknowledgements.

We thank James Fitzpatrick, Jon Hougen, Cheolhwa Kang, Brooks Pate, John Yi, and Tim Zwier for helpful discussions. This work has been supported by NSF (CHE-0315584) to whom we are grateful. We are also grateful to John Simons for his enthusiastic support of our research over many stimulating years, and wish him well.

4.8. References.

(1) Clayton, A. H. A.; Sawyer, W. H. *European Biophysics Journal* **2002**, *31*, 9.

(2) Park, Y. D.; Rizzo, T. R.; Peteanu, L. A.; Levy, D. H. *J. Chem. Phys.* **1986**, *84*, 6539.

(3) Phillips, L. A.; Levy, D. H. *J. Chem. Phys.* **1986**, *85*, 1327.

(4) Phillips, L. A.; Levy, D. H. *J. Chem. Phys.* **1988**, *89*, 85.

(5) Wu, Y. R.; Levy, D. H. *J. Chem. Phys.* **1989**, *91*, 5278.

(6) Connell, L. L.; Corcoran, T. C.; Joiremans, P. W.; Felker, P. M. *Chem. Phys. Lett.* **1990**, *166*, 510.

(7) Connell, L. L.; Corcoran, T. C.; Joiremans, P. W.; Felker, P. M. *J. Phys. Chem.* **1990**, *94*, 1229.

(8) Felker, P. M. *J. Phys. Chem.* **1992**, *96*, 7844.

(9) Felker, P. M. *Chem. Rev.* **1994**, *94*, 1784.

(10) Carney, J. R.; Zwier, T. S. *J. Phys. Chem. A* **2000**, *104*, 8677.

(11) Yi, J. T.; Robertson, E. G.; Pratt, D. W. *Phys. Chem. Chem. Phys.* **2002**, *4*, 5244.

(12) Majewski, W. A.; Pfanstiel, J. F.; Plusquellic, D. F.; Pratt, D. W. *Laser Techniques in Chemistry*; A. B. Myers and T.R. Rizzo (Ed); J. Wiley & Sons: New York, **1995**, p. 101.

(13) Frisch, M. J.; Trucks, G. W.; Schlegel, H. B.; Scuseria, G. E.; Robb, M. A.; Cheeseman, J. R.; Zakrzewski, V. G.; J. A. Montgomery, J.; Stratmann, R. E.; Burant, J. C.; Dapprich, S.; Millam, J. M.; Daniels, A. D.; Kudin, K. N.; Strain, M. C.; Farkas, O.; Tomasi, J.; Barone, V.; Cossi, M.; Cammi, R.; Mennucci, B.; Pomelli, C.; Adamo, C.; Clifford, S.; Ochterski, J.; Petersson, G. A.; Ayala, P. Y.; Cui, Q.; Morokuma, K.; Malick, D. K.; Rabuck, A. D.; Raghavachari, K.; Foresman, J. B.; Cioslowski, J.; Ortiz, J. V.; Stefanov, B. B.; Liu, G.; Liashenko, A.; Piskorz, P.; Komaromi, I.; Gomperts, R.; Margin, R. L.; Fox, D. J.; Keith, T.; Al-Laham, M. A.; Peng, C. Y.; Nanayakkara, A.; Gonzalex, C.; Challacombe, M.; Gill, P. M. W.; Johnson, B.; Chen, W.; Andres, M. W. W. L.; Gonzalez, C.; Head-Gordon, M.; Replogle, E. S.; Pople, J. A. Gaussian 98, Revision A.10; Gaussian, Inc.: Pittsburgh, PA, **1998**.

(14) Watson, J. K. G. *Vibrational Spectra and Structure*; J.R. Durig (Ed); Elsevier: Amsterdam, 1977; Vol. 6, Chapter 1.

(15) Described in Plusquellic, D.F.; Suenram, R.D.; Mate, B.; Jensen, J.O.; Samuels, A.C. *J. Chem. Phys.* **2001**, *115*, 3057.

(16) Phillips, L. A.; Webb, S. P.; Martinez III, S. J.; Fleming, G. R.; Levy, D. H. *J. Am. Chem. Soc.* **1988**, *110*, 1352.

(17) Berden, G.; Meerts, W. L.; Jalviste, E. *J. Chem. Phys.* **1995**, *103*, 9596.

(18) Caminati, W.; di Bernado, S. *J. Mol. Struct.* **1990**, *240*, 253.

(19) Suenram, R. D.; Lovas, F. J.; Fraser, G. T. *J. Mol. Spectrosc.* **1988**, *127*, 472.

(20) Caminati, W. *Phys. Chem. Chem. Phys.* **2004**, *6*, 2806.

(21) Nguyen, T. V.; Yi, J. T.; Pratt, D. W. to be published.

(22) Carney, J. R.; Zwier, T. S. *Chem. Phys. Lett.* **2001**, *341*, 77.

(23) Andrews, A.M.; Fraser, G.T.; Pate, B.H. *J. Phys. Chem.* **1994**, *98*, 9979.

(24) Spangler, L. H.; Pratt, D. W. *Jet Spectroscopy and Molecular Dynamics.*; Hollas, J. M., Phillips, D., Eds.; Chapman and Hall: London, **1995**; p. 366.

(25) Kang, C.-H.; Pratt, D.W.; Schaefer, M. *J. Phys. Chem. A* **2005**, *109*, 767.

(26) Dian, B. C.; Clarkson, J. R.; Zwier, T. S. *Science* **2004**, *303*, 1169.

(27) McCarthy, V.N.; Jordan, K.D., work in progress.

5. Permanent Electric Dipole Moments of Four Tryptamine Conformers in the Gas Phase. A New Diagnostic of Structure and Dynamics.

Tri V. Nguyen and David W. Pratt*

Department of Chemistry, University of Pittsburgh
Pittsburgh, PA 15260 USA

5.1. Abstract.

Rotationally resolved electronic spectroscopy in the gas phase, in the absence and presence of an applied electric field, has been used to determine the charge distribution of a cross section of the energy landscape of tryptamine (TRA). We report the magnitude and direction of the permanent electric dipole moments of the four TRA conformers GPyout, GPyup, GPhup and Antiup in their S_0 and S_1 electronic states. Each dipole moment is unique, providing a powerful new tool for conformational analysis of biomolecules in the gas phase. A comparison of the results for the different conformers of TRA reveals that the position and orientation of the ethylamine side chain plays a major role in determining both the permanent and induced electric dipole moments of the different species in both electronic states.

Submitted to *The Journal of Chemical Physics.*

5.2. Introduction.

The permanent electric dipole moment of an isolated molecule is an important predictor of its behavior in physical, chemical and biological processes.[1] Because the magnitudes and directions of such moments are sensitive to molecular size and shape, they also can serve as a useful tool in conformational analysis. A recent example of this approach is found in the work of Reese, *et al*.[2] on the *cis* and *trans* isomers of 3-aminophenol. Excited state dipole moments also may play a role in controlling the donor/acceptor strength of "push-pull" systems and can lead to solvent reorganization in the condensed phase, in cases where significant charge redistribution is produced by the absorption of light. A recent example of such behavior in the gas phase has been reported by Kang, *et al*.[3] This work also provided a measurement of the induced dipole moment that is produced when a water molecule is weakly bound to the chromophore, in both its ground and electronically excited states.

Reported here are measurements of the permanent electric dipole moments of tryptamine (TRA) in its ground and electronically excited states. TRA (see Scheme I) is an interesting candidate for such a study because it is a large molecule with a rich energy landscape. Several conformers are present in free-jet expansions, making it possible (at least in principle) to differentiate them on the basis of differences in their dipole moments. At the same time, the side chain in TRA is sufficiently simple to track the specific interactions that might lead to differences in the values of the dipole moments among the different conformers of the isolated molecule.

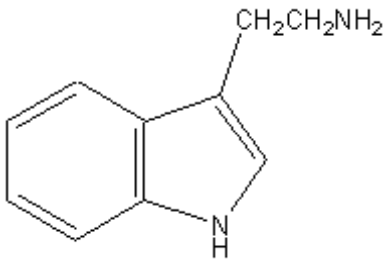

Scheme I

A detailed understanding of the energy landscape of TRA has been derived from a series of pioneering experiments on the isolated gas phase molecule.[4-10] Figure 5-1 shows the vibrationally resolved $S_1 \leftarrow S_0$ fluorescence excitation spectrum of TRA. The labeling scheme is taken directly from Park, *et al*.[4] in which the ordering A-F is used to designate the electronic origins of six conformers of TRA based on power saturation studies. Band A, the most intense and highest energy band, is located at ~ 34915 cm^{-1}. The other origin bands are shifted to the red of band A, at - 20 (B), - 31 (D), - 36 (C), - 47 (E), and - 84 cm^{-1} (F) with respect to band A. The presence of a seventh conformer was established when rotational band contour studies showed that band C is actually composed of two overlapping origins.[5] These two bands are called C_{red} and C_{blue} (*cf.*, Fig. 5-1). In a later study,[7] each of the seven bands was assigned to a unique conformer; band A to GPyout, band B to GPyup, band C_{red} to GPhout, band C_{blue} to Antipy, band D to Antiph, band E to Antiup and band F to GPhup. (The nomenclature used here is identical to that introduced by Carney and Zwier.[6]) Additionally, Dian, *et al.*[9,10] have made measurements of the energy thresholds to conformational isomerization involving several reactant-product pairs.

Permanent electric dipole moments of isolated molecules can be determined by a variety of techniques. Microwave spectroscopy has been a mainstay in obtaining information about the ground state.[11] However, despite a recent microwave study by Caminati,[12] no dipole moments have been reported for TRA. Compagnon, *et al.*[13] have used a molecular beam electric

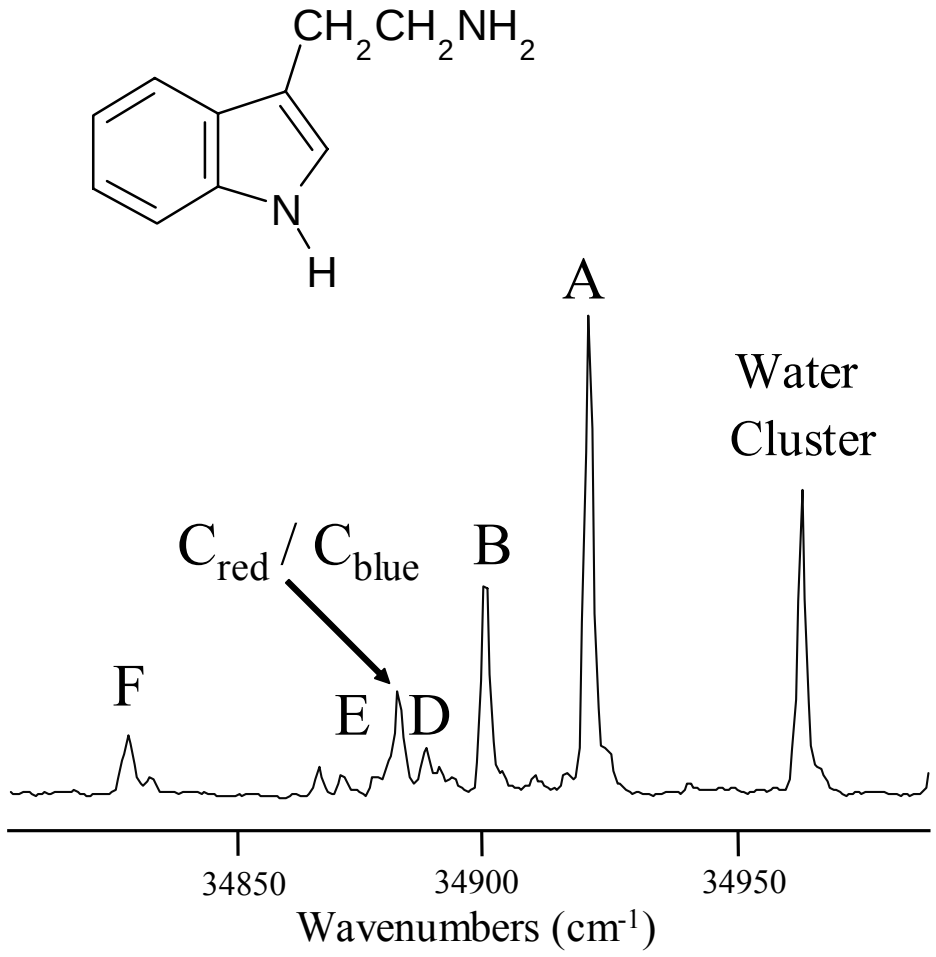

Figure 5-1: Fluorescence excitation spectrum of tryptamine cooled in a supersonic free jet. The origins of the transitions due to the seven conformers are marked as A-F in order of decreasing intensities. Also shown is the origin band of the single water cluster (From Ref. 7)

deflection technique to measure the dipole moment of the most stable conformer of tryptophan. In this work, we have measured the permanent electric dipole moments of four conformers of TRA in their ground and electronically excited states using the Stark effect on their fully resolved electronic spectra.[14]

5.3. Experiments.

TRA was purchased from Aldrich Chemical Co. and used without further purification. Rotationally resolved electronic spectra of the origin bands of TRA were recorded using a molecular beam apparatus that has been described previously in detail.[15] The sample was heated to ~ 150 ºC, seeded into ~ 400 torr of argon, and expanded into a vacuum through a 240 μm nozzle. The molecular beam was expanded through a 1 mm skimmer 2 cm downstream of the nozzle into a differentially pumped vacuum system. It was crossed 15 cm downstream of the nozzle with a modified continuous wave ring dye laser operating with R6G and intracavity doubled in BBO, yielding ~ 200 μW of ultraviolet radiation. The fluorescence collection optics consisted of two spherical mirrors positioned above and below the intersection of the molecular and laser beams. In order to maximize the light collection efficiency, the focus of the top mirror is located at the intersection of the two beams while the bottom mirror is focused at a 2 mm hole drilled in the center of the top mirror. The emitted signal was collected by a PMT. This spatially selective setup results in a collection efficiency of 33% and a Doppler-limited resolution of ~ 18 MHz. Absolute frequency calibration was performed by simultaneously recording the fluorescence spectrum of I_2 (accuracy ~ 30 MHz) and the laser interference fringes from a stabilized etalon with a spectral range of 299.7520 ± 0.0005 MHz in the fundamental of the dye.

The Stark cell[14] consists of two spherical mirrors, identical to those used in the zero-field experiment, with two stainless steel (Type 304) wire grids (diameter = 5 cm, mesh #50, wire diameter = 0.001 in.) placed between the mirrors. One grid is above and the other grid is below the plane of the molecular and laser beams, separated by ~1 cm with ceramic spacers. Two power supplies (Fluke 412B, 415B) were used to hold one grid at a positive voltage and the other at a negative voltage relative to a common ground. The electric field is perpendicular to the polarization of the laser radiation, yielding a $\Delta M = \pm 1$ selection rule. [14] Electric field strengths were calibrated using the known value of μ_a in the ground state of aniline and the combination-difference method of spectral assignment, which yields a determined plate separation of 0.982 ± 0.004 cm.

5.4. Results.

Figure 5-2 shows the Stark splitting of the high resolution fluorescence excitation spectrum of band A of TRA. The top trace is the overall spectrum at zero field. The bottom traces show an expanded portion of this spectrum at both zero field and fields of 509 and 1018 V/cm, together with fits of the spectra at 0 and 1018 V/cm. The transitions shown are $|J'\rangle \leftarrow |J''\rangle = |1\rangle \leftarrow |0\rangle$ and $|2\rangle \leftarrow |1\rangle$. Well-resolved single transitions in the zero-field spectrum exhibit frequency shifts, splittings and/or broadenings in the presence of a field. An example is provided by the $|J'K'_aK'_c\rangle \leftarrow |J''K''_aK''_c\rangle = |202\rangle \leftarrow |101\rangle$ transition in Fig. 5-2. As the field strength is increased, these effects become more pronounced, and may be used to determine both the magnitudes and the directions of the dipole moments in the molecular frame, in both electronic states, as described below.

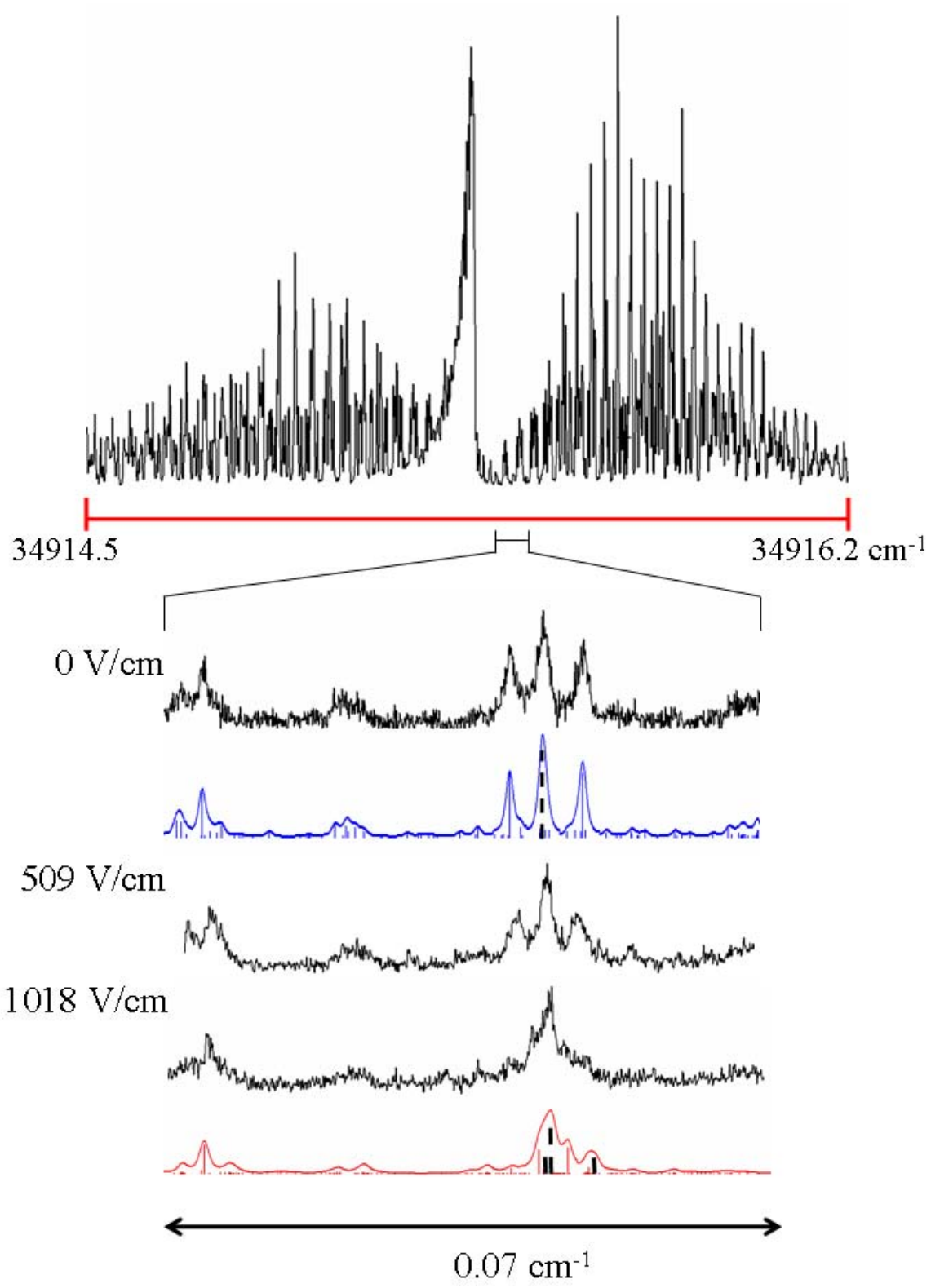

Figure 5-2: Stark splitting of a portion of the R branch of band A of TRA at 509 and 1018 V/cm compared with the zero-field spectrum. Also shown are calculated spectra at zero field and at a field of 1018 V/cm.

Figure 5-3 shows the Stark effect on the least intense origin band of TRA, band F. The top trace shows the zero-field spectrum. The bottom traces show a portion of the spectrum of band F at full resolution along with the frequency fit spectrum, at both 0 and 1018 V/cm. The transitions shown are $|J'\rangle \leftarrow |J''\rangle = |4\rangle \leftarrow |3\rangle$ and $|5\rangle \leftarrow |4\rangle$. Again, the application of a field produces frequency shifts, splittings and/or broadenings of the fully resolved spectra, which in this case are significantly more complex owing to the higher J values.

A special computer program has been written to fit these spectra.[14,16] The fitting process begins with a simulation of the spectrum generated from the ground and excited state rotational constants and estimates of the ground and excited state dipole moment components. Estimates of the dipole moment components were obtained from *ab initio* calculations.[17] Because a Stark-split spectrum has a significantly larger number of transitions than a zero-field spectrum, more care must be taken when making assignments. The initial assignments were made for transitions in the least congested portions of the spectrum. Once a significant number of assignments had been made, a least squares analysis was performed. Additional assignments were made and/or previous assignments were altered, and the least squares fitting routine was repeated until the differences (OMC) between the experimental and simulated spectra were minimized. From an examination of the bottom traces in Figs. 5-2 and 5-3, it is evident that there are very few single transitions present in the Stark spectra. This congestion becomes even more severe at higher J quantum numbers. Therefore, we have limited our assignments to transitions with low J quantum numbers ($J'' \leq 10$) that displayed distinct features in the experimental spectrum.

Tables 5-1 and 5-3list the ground and excited state dipole moments that were determined from the fits of bands A, B, E and F at different field strengths using these procedures. The fits are characterized by OMC values of 4.8, 7.7, 3.5, and 3.3 MHz, respectively. The resulting

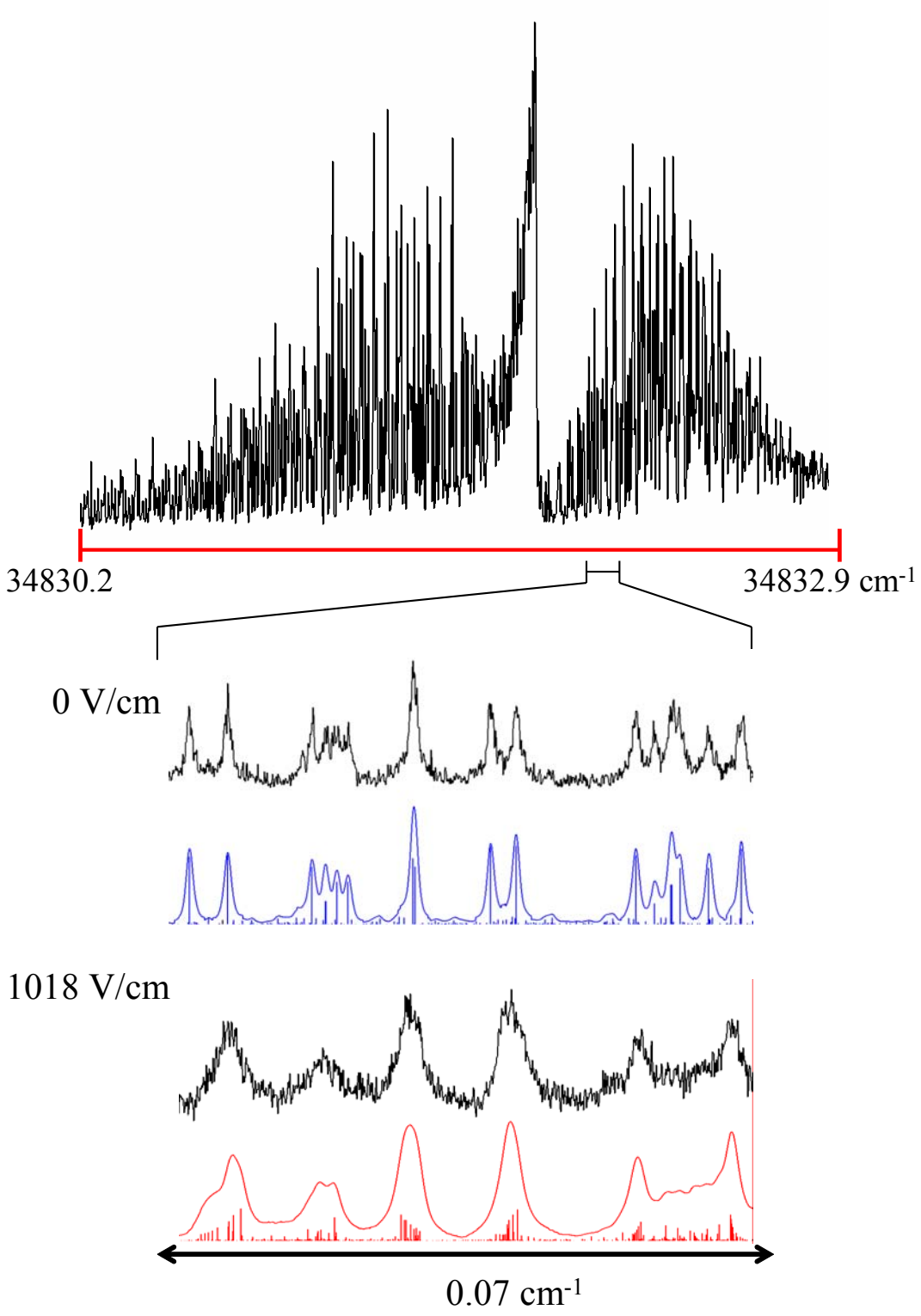

Figure 5-3: Stark splitting of a portion of the R branch of band F of TRA at 1018 V/cm compared with the zero-field spectrum. Also shown are the calculated spectra at the two field strengths.

Table 5-1: Experimental and theoretical values of the electric dipole moments, and estimated relative energies, of four conformers of tryptamine in the ground S_0 electronic state. Calculations were performed at the MP2 6-31G* level.

Band	A		B		E		F	
Conformer	GPyout		GPyup		Antiup		GPhup	
Experiment								
μ_a (D)	0.60	(0.10)	0.40	(0.10)	0.70	(0.10)	0.90	(0.10)
μ_b (D)	1.33	(0.01)	2.53	(0.02)	2.38	(0.09)	2.06	(0.03)
μ_c (D)	0.56	(0.06)	0.75	(0.02)	0.63	(0.10)	0.64	(0.03)
μ (D)	**1.60**	(0.20)	**2.70**	(0.10)	**2.60**	(0.10)	**2.40**	(0.10)
Theory								
μ_a (D)	0.50		0.42		0.64		0.91	
μ_b (D)	1.01		2.86		2.59		2.39	
μ_c (D)	0.73		0.84		1.01		0.76	
μ (D)	**1.34**		**3.02**		**2.85**		**2.67**	
ΔE (cm^{-1})	0		152		148		436	

(ground state) dipole moments are 1.6, 2.7, 2.6, and 2.4 D, respectively. For comparison, the dipole moment of the most prominent conformer of unsolvated tryptophan has been estimated to be 3.99 D.[13]

5.5. Discussions.

The ground state permanent electric dipole moments of TRA listed in Table 5-1 fall into two classes. The three "Up" conformers have values lying between 2.4 and 2.7 D whereas the "Out" conformer has a value of 1.6 D. The differences in these values lie well outside of experimental error, 0.1-0.2 D. Thus, measured values of the dipole moments may be used to distinguish one conformer from another, especially when the different components of the dipole moments (*i.e.*, the directions of the dipole moments in the molecular frame) are also known (*cf.*, Table 5-1).

The second thing to notice about the measured values of $\boldsymbol{\mu}$ in the ground state of TRA is that the values for the "Up" conformers are all greater than the corresponding value for indole whereas the value for the "Out" conformer is less than the corresponding value for indole. (The dipole moment of indole in the ground state is 1.963 D.[3,18]) This result clearly shows that the ethylamine side chain makes a significant contribution to the measured dipole moments of TRA, increasing or decreasing the dipole moment of indole depending on the position and orientation of the side chain with respect to the ring. This is not a surprising result, given that the nitrogen atom on the ethylamine side chain has a lone pair of electrons.

What makes these differences intriguing is that they provide a new way to characterize the energy landscape of TRA. Previously, it has been shown by several techniques that the nine lowest energy conformers of TRA can be classified into three families based on the position of the ethylamine side chain relative to the indole ring (Gauche Phenyl, Gauche Pyrrole and Anti). The three families are further subdivided based on the orientation of the nitrogen lone pair with

respect to the ring ("In", "Up" and "Out").[6] Heretofore, it has been assumed that the different members of each family would have very similar properties, but that these properties would differ significantly from one family to another. An example of such a property is the set of rotational constants that describe each conformer; the rotational constants of the different members of a particular family are very similar, but vary significantly from one family to another.[7] The present results show that there is at least one other property, the dipole moment, which differs significantly among the different members of the *same* family.

Theory (at the MP2/6-31G* level)[17] adequately reproduces these differences in ground state dipole moments (*cf.,* Table 5-1). Even though the calculated magnitudes of $\boldsymbol{\mu}$ are larger than the true values by an average of ~ 14 % , the three "Up" conformers have values that are similar ($\boldsymbol{\mu}_{GPyup}$ = 3.02, $\boldsymbol{\mu}_{Antiup}$ = 2.85 and $\boldsymbol{\mu}_{GPhup}$ = 2.67 D) and the "Out" conformer has a value that is very different ($\boldsymbol{\mu}_{GPyout}$ = 1.34 D). Furthermore, the calculations accurately reproduce the relative magnitude of the dipole moments ($\boldsymbol{\mu}_{GPyout} < \boldsymbol{\mu}_{GPhup} < \boldsymbol{\mu}_{Antiup} < \boldsymbol{\mu}_{GPyup}$).

Differences in these values may be explained by using a vector addition model to predict the dipole moments of the different conformers of TRA based on the known dipole moments of their "component parts". This model has been used previously to predict the dipole moment of aminobenzonitrile from the measured values for aniline and benzonitrile.[19] A similar approach was used to predict the dipole moment of indole-H_2O.[3] In the case of TRA, the component parts are indole and ethylamine. The ground state dipole moment of indole has previously been measured by microwave and high resolution UV spectroscopy.[3,18] The reported magnitude of $\boldsymbol{\mu}$ is 1.963 D and the angle that $\boldsymbol{\mu}$ makes with the *a* axis is $+33.0^0$. The dipole moments of the *trans* and *gauche* conformers of ethylamine have also been measured by microwave spectroscopy. The reported values are μ_a = 1.057 and μ_b = 0.764 D for the *trans* conformer[20] and μ_a = 0.11, μ_b

= 0.65 and μ_c = 1.014 D for the *gauche* conformer.[21] Then, the magnitudes and directions of the total dipole moments in the different conformers of TRA can be calculated by transforming the dipole moments of the component parts (in their respective inertial axis systems) into the corresponding inertial axis system of TRA and adding the vectors together. In this case, the Euler angles that describe the relative orientations of the different inertial tensors were obtained from energy optimized structures of indole, ethylamine, and TRA. The *gauche* ethylamine results were used for GPyout and the *trans* ethylamine results were used for GPhup, GPyup, and Antiup. Additionally, it was assumed that the dipole moment in ethylamine points towards the nitrogen lone pair, which accords with chemical intuition. A graphical example of this approach is illustrated in Fig. 5-4.

Table 5-2 summarizes the results of these calculations. The predicted dipole moments of the four measured conformers of TRA are $\boldsymbol{\mu}_{GPyout}$ = 1.20, $\boldsymbol{\mu}_{GPhup}$ = 2.57, $\boldsymbol{\mu}_{GPyup}$ = 2.70 and $\boldsymbol{\mu}_{Antiup}$ = 2.75 D. These values are in approximate agreement with the experimental results; 1.6, 2.4, 2.7 and 2.6 D, respectively. From this agreement, we conclude that the observed dipole moment of each conformer of TRA is approximately equal to the vector sum of the dipole moments of indole and ethylamine, providing that each of the component parts is properly oriented with respect to each other. Thus, substantial charge reorganization does not take place when these "parts" are joined by covalent chemical bonds in the ground electronic state, making measured dipole moments a powerful probe of biological molecule structure and dynamics.

The observed differences between the predicted and observed values may have their origin in the neglect of a C-H bond dipole that is inherent in our vector addition model. But they may also stem from small "induced" moments; *i.e.*, from small charge rearrangements that occur when the component parts are bonded together. Note, for example, that the predicted value for

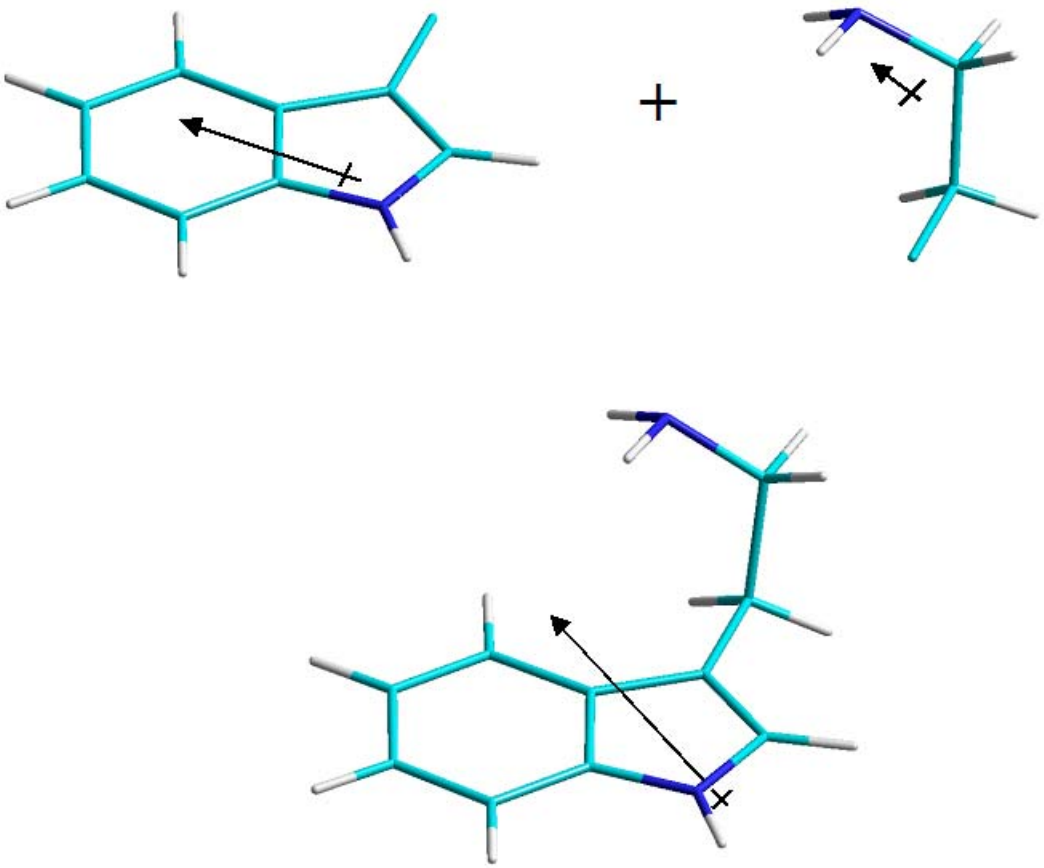

Figure 5-4: Illustration of the vector addition model on the GPyout conformer.

Table 5-2: Predicted electric dipole moments of four conformers of tryptamine in the ground electronic state, based on a vector addition model. See text for details.

Conformer	GPyout	GPyup	Antiup	GPhup
μ_a (D)	1.00	1.20	0.54	1.14
μ_b (D)	0.63	2.02	2.63	2.02
μ_c (D)	0.61	1.34	-0.60	1.12
$\boldsymbol{\mu}$ (D)	1.33	2.70	2.75	2.57

GPyout is less than that which is observed, whereas the predicted values for the "Up" conformers are mostly larger than those that are observed. Clearly, the component dipoles are mostly "antiparallel" in GPyout, since its dipole moment is less than that of indole, leading to the expectation that a "negative" induced dipole will result. In contrast, the component dipoles are mostly "parallel" in the "Up" conformers, leading to "positive" induced dipoles, as (mostly) observed. Thus, measured induced dipole moments may also be a powerful probe of the properties of large molecules.

The permanent electric dipole moments of all four conformers of TRA in their electronically excited (S_1) states also were determined from fits of the Stark-split spectra; these are listed in Table 5-3. The magnitudes of the dipole moments of all four conformers decrease upon excitation. This is not a surprising finding given that the magnitude of the dipole moment in indole decreases by 0.11 D when the photon is absorbed.[3] Decreases of order 0.1-0.2 D also are observed in TRA. But a closer examination of the data in Table 5-3 reveals a more interesting observation, namely how this decrease is distributed amongst the dipole moment components. μ_b experiences a small decrease with values of -5% for GPyout, -7% for GPyup, -1% for Antiup and -1% for GPhup. The magnitude of the variations in μ_c are similar, with values of -18% for GPyout, +18% for GPyup, +4% for Antiup and -3% for GPhup. However, the changes in μ_a are much more significant. μ_a decreases by -87% in GPyout, -100% in GPyup, -62% in Antiup and -49% in GPhup. Now, the *a*-axis of TRA is mostly parallel to the ethylamine side chain and approximately perpendicular to the long axis of indole; *cf.,* Fig. 5-5. Thus, these results suggest that interactions between the ethylamine side chain and the indole ring are more pronounced in the S_1 state. There seems to be a re-distribution of electron density along the *a*-axis, arising from

Table 5-3: Experimental and theoretical values of the electric dipole moments of four conformers of tryptamine in the S_1 electronic state. Calculations were performed at the CIS 6-31G* level.

Band	A		B		E		F	
Conformer	GPyout		GPyup		Antiup		GPhup	
Experiment								
μ_a (D)	0.10	(0.10)	0.10	(0.10)	0.30	(0.10)	0.50	(0.10)
μ_b (D)	1.26	(0.01)	2.34	(0.02)	2.34	(0.09)	2.03	(0.03)
μ_c (D)	0.46	(0.06)	0.87	(0.02)	0.66	(0.10)	0.62	(0.03)
μ (D)	**1.40**	(0.20)	**2.50**	(0.10)	**2.50**	(0.10)	**2.20**	(0.10)
Theory								
μ_a (D)	0.38		0.54		0.67		1.09	
μ_b (D)	1.36		2.95		2.60		2.47	
μ_c (D)	0.99		0.86		1.03		0.63	
μ (D)	**1.73**		**3.12**		**2.88**		**2.77**	

a shift of electrons from the ethylamine side chain to the indole π system. Only in this way are we able to explain the selective changes in μ_a that are observed when the photon is absorbed.

Figure 5-5 shows S_1 - S_0 electron density differences maps for the four conformers of TRA, calculated using *ab initio* methods at the CIS 6-31G* level. These are described as $0.354(\Psi^2_{LUMO} - \Psi^2_{HOMO-1}) + 0.646(\Psi^2_{LUMO+1} - \Psi^2_{HOMO})$ for GPyout, $0.357(\Psi^2_{LUMO} - \Psi^2_{HOMO-1}) + 0.643(\Psi^2_{LUMO+1} - \Psi^2_{HOMO})$ for GPyup, $0.349(\Psi^2_{LUMO} - \Psi^2_{HOMO-1}) + 0.651(\Psi^2_{LUMO+1} - \Psi^2_{HOMO})$ for GPhup and $0.356(\Psi^2_{LUMO} - \Psi^2_{HOMO-1}) + 0.644(\Psi^2_{LUMO+1} - \Psi^2_{HOMO})$ for Antiup. Clearly evident from these maps is the shift in electron density from the pyrrole ring to the phenyl ring that is responsible for the change in the dipole moment of indole when the photon is absorbed. But these maps fail to capture the charge transfer from the ethylamine to the indole ring that is implicated in the present measurements on the four conformers of TRA. Further study of this issue is required.

5.6. Conclusions.

Studies of the Stark effect on the high resolution electronic spectra of tryptamine have made possible accurate measurements of the permanent electric dipole moments of four conformers of the isolated molecule in their ground (S_0) and excited (S_1) electronic states. Each dipole moment is different, providing a powerful new tool for conformational analysis of biomolecules in the gas phase. The reported differences in both the magnitude and direction of the observed dipoles are attributed to differences in the positions and orientations of the ethylamine side chain that is attached to the indole frame. Substantial changes in the directions (but not the magnitudes) of the observed dipoles occur on absorption of light, an effect that may be attributed to enhancement of π hydrogen bonding in the electronically excited state. The

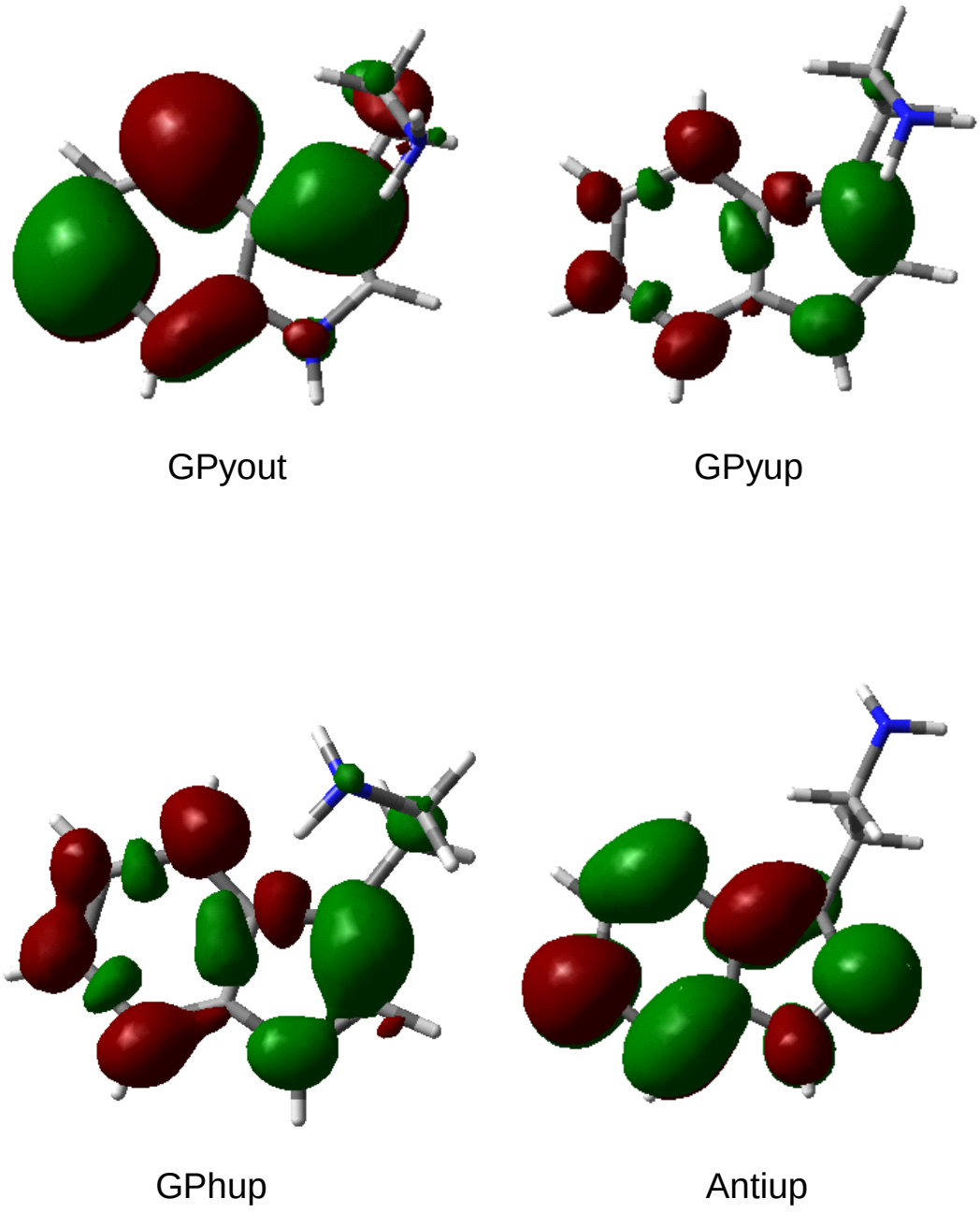

Figure 5-5: Electron density difference maps for the for the $S_1 \leftarrow S_0$ transition of the GPyout, GPyup, GPhup and Antiup as calculated by *ab initio* calculation. Dark contours indicate regions of electron gain, and light contours indicate region of electron loss.

results also provide an interesting new perspective on “through-bond” vs. “through-space” interactions in isolated molecules.

5.7. Acknowledgment.

This work has been supported by NSF (CHE-0315584). We thank D. R. Borst, K.D. Jordan, C.-H. Kang, T. M. Korter, V. McCarthy, D. M. Mitchell and J. T. Yi for assistance and helpful discussions.

5.8. References.

1. G. U. Bublitz and S. G. Boxer, *Ann. Rev. Phys. Chem.* **48**, 213 (1997).

2. J. A. Reese, T. V. Nguyen and D. W. Pratt, *J. Am. Chem. Soc.* **126**, 11387 (2004).

3. C.-H. Kang, T. Korter and D. W. Pratt, *J. Chem. Phys.* **122**, 174301 (2005).

4. Y. D. Park, T. R. Rizzo, L. A. Peteanu and D. H. Levy, *J. Chem. Phys.* **84**, 6539 (1986).

5. L. A. Phillips and D. H. Levy, *J. Chem. Phys.* **89** (85) (1988).

6. J. R. Carney and T. S. Zwier, *J. Phys. Chem. A* **104**, 8677 (2000).

7. T. V. Nguyen, T. M. Korter and D. W. Pratt, *Mol. Phys.* **103**, 1603 (2005).

8. M. Schmitt, M. Bohm, C. Ratzer, C. Vu, I. Kalkman and W. L. Meerts, *J. Am. Chem. Soc.* **127**, 10356 (2005).

9. B. C. Dian, A. Longarte and T. S. Zwier, *Science* **296**, 2639 (2002).

10. B. C. Dian, J. R. Clarkson and T. S. Zwier, *Science* **303**, 1169 (2004).

11. W. Gordy and R. L. Cook, *Microwave Molecular Spectra*, 3rd ed. ,Wiley-Interscience, New York, 1984.

12. W. Caminati, *Phys. Chem. Chem. Phys.* **6**, 2806 (2004).

13. I. Compagnon, F. C. Hagemeister, R. Antoine, D. Rayane, M. Broyer, P. Dugourd, R. R. Hudgins and M. F. Jarrold, *J. Am. Chem. Soc.* **123**, 8440 (2001).

14. T. M. Korter, D. R. Borst, C. J. Butler and D. W. Pratt, *J. Am. Chem. Soc.* **123**, 96 (2001).

15. W. A. Majewski, J. F. Pfanstiel. D. F. Plusquellic and D. W. Pratt, in *Laser Techniques in Chemistry,* J. Wiley & Sons, New York, 1995, p. 101.

16. D. R. Borst and D. W. Pratt, to be published.

17. M. J. Frisch, G. W. Trucks, H. B. Schlegel, G. E. Scuseria, M. A. Robb, J. R.Cheeseman, V. G. Zakrzewski, J. J. A. Montgomery, R. E. Stratmann, J. C. Burant, S. Dapprich, J. M. Millam, A. D. Daniels, K. N. Kudin, M. C. Strain, O. Farkas, J. Tomasi, V. Barone, M. Cossi, R. Cammi, B. Mennucci, C. Pomelli, C. Adamo, S. Clifford, J. Ochterski, G. A. Petersson, P. Y. Ayala, Q. Cui, K. Morokuma, D. K Malick, A. D. Rabuck, K. Raghavachari, J. B. Foresman, J. Cioslowski,

J. V. Ortiz, B. B. Stefanov, G. Liu, A. Liashenko, P. Piskorz, I. Komaromi, R. Gomperts, R. L. Martin, D. J. Fox, T. Keith, M. A. Al-Laham, C. Y. Peng, A. Nanayakkara, C. Gonzalez, M. Challacombe, P. M. W. Gill, B. Johnson, W. Chen, M. W. Wong, J. L. Andres, M. Head-Gordon, E. S. Replogle, and J. A. Pople, *Gaussian 98*, Revision A.10, Gaussian, Inc., Pittsburgh, PA, 1998.

18. W. Caminati and S. di Bernardo, *J. Mol. Struct.* **240**, 253 (1990).

19. D. R. Borst, T. M. Korter and D. W. Pratt, *Chem. Phys. Lett.* **350**, 485 (2001).

20. E. Fischer and I. Botskor, *J. Mol. Spectrosc*. **91**, 116 (1982).

21. E. Fischer and I. Botskor, *J. Mol. Spectrosc*. **104**, 226 (1984).

6. Rotationally resolved fluorescence excitation spectroscopy of the tryptamine-water Complex: a simple lock and key model.

Tri V. Nguyen and David W. Pratt*

Department of Chemistry, University of Pittsburgh
Pittsburgh, PA 15260 USA

6.1. Abstract.

The rotationally resolved $S_1 \leftarrow S_0$ electronic spectrum of the single water complex of the biomolecule tryptamine (TRA) has been observed and assigned. TRA itself has seven conformers in the gas phase; however, upon complexation the energy landscape collapses yielding only one unique TRA-H_2O structure. Analyses of the high resolution spectra of TRA-H_2O and deuterated TRA-D_2O suggest that the water molecule is attached *via* two hydrogen bonds, one with the ethylamine side chain (O-H$\cdots$$NH_2$) and the other with the pyrrole ring (H-O$\cdots$H-C) in both electronic states. No tunneling motion of the attached water molecule is observed suggesting that the water effectively "locks" the GPyout conformerof the bare molecule into place, thereby inhibiting the formation of water complexes of other conformations of TRA.

6.2. Introduction.

One of the intriguing aspect of water as a solvent is its ability to influence the solute *via* different types of hydrogen bonds. This characteristic is rooted in the amphoteric nature of the water molecule. Our interest is to determine how the different types of interactions might be manifested upon complex formation with a flexible molecule. One such flexible molecule is tryptamine (TRA). The complexity of the TRA conformational landscape originates in the flexibility of the ethylamine side chain, shown below.

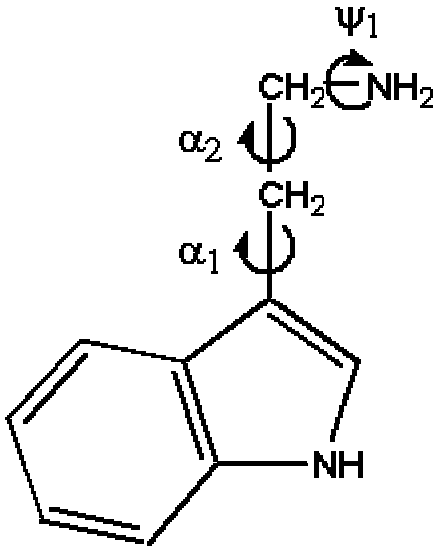

Scheme I

The TRA monomer has been the subject of many studies. Park *et al.* were the first to record the vibrationally resolved $S_1 \leftarrow S_0$ fluorescence excitation spectrum.[1] They showed that multiple origin bands were present in the environment of a supersonic jet. Subsequently, partially resolved contours of these bands[2] and of deuterated tryptamine (dTRA)[3] were used to assign the various conformers of TRA. Rotational coherence measurements extended the analysis.[4-6] A more detailed conformational profile was given once R2PI, RIDIR and UV-UV hole burning investigations were combined with the results from previous studies.[7] Recently, we have used rotationally resolved fluorescence excitation spectroscopy to give a complete description of the

energy landscape of TRA in which each of the seven origin bands were assigned to a unique conformer.[8]

Sipior and Sulkes[9] investigated water complexes of TRA by using vibrationally resolved $S_1 \leftarrow S_0$ fluorescence excitation spectroscopy. They observed a single origin band upon complex formation at 34 959 cm^{-1}. This finding was corroborated by Peteanu and Levy[10] who used R2PI spectroscopy. TRA-H_2O complex was also studied by rotational coherence spectroscopy,[5,6] by RIDIR, [11] and by high resolution spectroscopy.[12] In this work, we have used rotationally resolved fluorescence excitation spectroscopy to study the TRA-H_2O complex. We report information on the identity of the TRA conformer present in the complex, the position and orientation of the water molecule.

6.3. Experiments.

Tryptamine and D_2O were purchased from Sigma-Aldrich and used without further purification. The high resolution apparatus has been described elsewhere [13]. The molecular beam was formed by flowing Ar (~400 Torr) over room-temperature water or deuterated water and then tryptamine (heated to ~150 ºC), and, finally, expanded into a vacuum through a 240 μm nozzle. The molecular beam was expanded through a 1 mm skimmer 2 cm downstream of the nozzle into a differentially pumped vacuum system. It was crossed 15 cm downstream of the nozzle with a modified continuous wave ring dye laser operating with R6G and intracavity doubled in BBO, yielding ~200 μW of ultraviolet radiation. The fluorescence collection optics consisted of two spherical mirrors positioned above and below the intersection of the molecular and laser beams. In order to maximize the efficiency, the focus of the top mirror is located at the intersection of the two beams while the bottom mirror is focused on a 2 mm hole drilled in the

center of the top mirror. The emitted signal was collected by a PMT. This spatially selective setup results in a collection efficiency of 33% and a Doppler-limited resolution of ~ 18 MHz. Absolute frequency calibration was performed by simultaneously recording the fluorescence spectrum of I_2 (accuracy ~ 30 MHz) and the laser interference fringes from a stabilized etalon with a spectral range of 299.7520 ± 0.0005 MHz in the fundamental of the dye.

6.4. Results.

The electronic origin band of TRA-H_2O is blue shifted by ~ 37 cm^{-1} with respect to the strongest origin band (Band A) of the bare molecule.[9] Figure 6-1 shows the high resolution fluorescence excitation spectrum of band A. Spanning ~1.7 cm^{-1}, the spectrum exhibits typical *a*-type band features, P- and R- branches on either side of an intense central Q-branch. Initially, approximately 4000 *a*-type transitions based on inertial parameters of TRA conformers were generated to account for the observed spectrum. The FWHM of a single transition spans ~30 MHz. Quantum number assignments of single transitions in the simulated spectrum to corresponding transitions in the experimental spectrum were made using a Windows' based program, jb95, which employs the Watson Hamiltonian.[14] Subsequently, a least-square fitting procedure was used to optimize these frequency assignments throughout the P-, Q-, and R-branch. Initially, more than 150 assigned transitions were assigned, resulting in an OMC (observed minus calculated) of 2.0 MHz, a standard deviation of 0.1 MHz for all rotational constants. However, all of the intensity in the experimental spectrum could not be accounted for by only *a*-type transitions. An autocorrelation analysis to check for the possible existence of subbands was inconclusive.[15] An intensity analysis was performed in which *b*- and *c*- type transitions were added to the previously generated fit. The hybrid band character determined

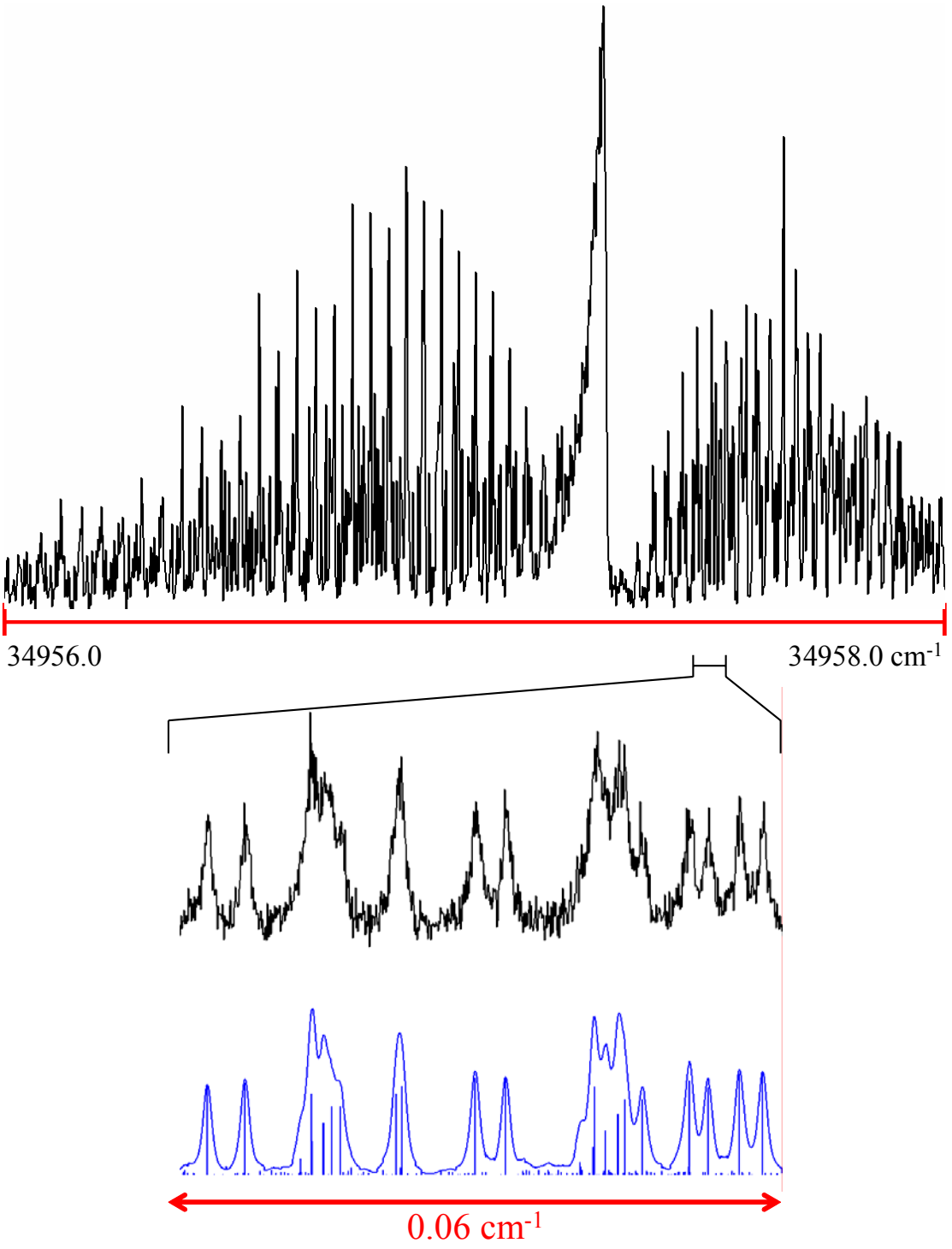

Figure 6-1: Rotationally resolved fluorescence excitation spectrum of tryptamine-H_2O in a molecular beam.

from this intensity analysis indicates a relative ratio of 87/9/4 for *a/b/c* type selection rules with all intensity being accounted for. The lower traces of Fig. 6-1 represent an expanded portion of the experimental spectrum of TRA-H_2O along with the frequency fit spectrum to illustrate the quality of the fit. The lineshape profile was characterized by a Doppler-broadened component of 18 MHz (Gaussian) and a lifetime-broadened component of 20 MHz (Lorentzian). The observed Lorentzian component indicates a fluorescence lifetime of ~ 8 ns.

A similar procedure was used to fit the spectrum of dTRA-D_2O shown in Fig. 6-2. There is some ambiguity as to the nature of complex formed. Based on the RCS studies, Connel *et al*[5]. suggest that the three amine protons in TRA are exchanged by deuterons; thus, the complex formed is the deuterated dTRA-D_2O. A list of inertial parameters derived from the fits of the two spectra is given in Table 5-1.

6.5. Discussions.

The major results of this study are the rotational constants of the TRA-H_2O and dTRA-D_2O complexes in their ground and excited states. Also, no subbands were found in the rotationally resolved spectra of TRA-H_2O. We now discuss how these data may be used to provide information about the structural and dynamic properties of the complex.

Water position in the complex. First, we use the rotational constants of TRA-H_2O in its ground electronic state to determine and approximate geometric structure of the complex. The measured values are A″ = 1462.7, B″ = 482.7 and C″ = 397.5 MHz (*cf.* Table 6-1). These values are all very different from the corresponding values of TRA itself. For example, the "A" conformer of TRA (GPyout)[8] has A″ = 1730.6, B″ = 681.8 and C″ = 551.4 MHz. All three of these values are larger than the corresponding values for the complex, reflecting its larger mass.

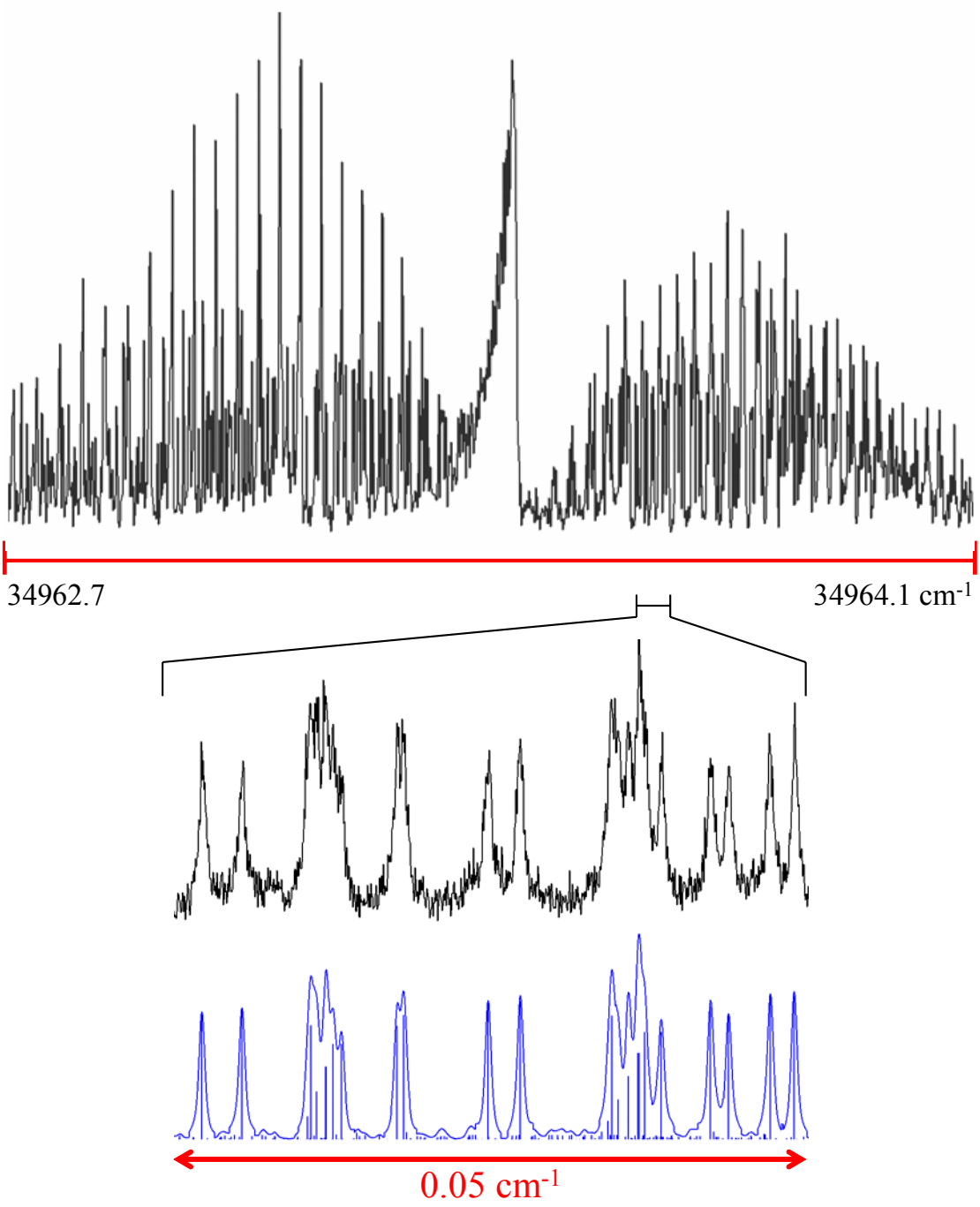

Figure 6-2. Rotationally resolved fluorescence excitation spectrum of tryptamine-D_2O in a molecular beam.

Table 6-1: Inertial parameters of TRA-H_2O and of dTRA-D_2O in their ground (S_0) and excited (S_1) electronic states[a].

	TRA-H_2O		dTRA-D_2O	
	S_0	S_1	S_0	S_1
A, MHz	1462.7	1455.9	1386.4 (1.6)	1380.6 (1.6)
B, MHz	482.7	478.0	458.4	453.8
C, MHz	397.5	393.8	379.1	375.5
κ	-0.840	-0.841	-0.842	-0.844
ΔI, *u*Å^2	-121.1	-121.0	-133.8	-133.9
Origin, cm^{-1}	34957.1		34963.5	
OMC, MHz	2.0		1.5	
% intensity *a/b/c* (± 3)	87/9/4		87/5/8	

[a]Errors in rotational constants are ± 0.1 MHz except where indicated.

Next, we use the differences in the rotational constants of TRA and TRA-H_2O to determine the center-of-mass (COM) coordinates of the water moiety in the principal axis frame of the bare molecule using Kraitchman's equations.[16] The key assumption in using this procedure is that complex formation does not alter the structure of the parent bare molecule.[17] Since TRA has seven conformers and the coordinates obtained from the Kraitchman's analysis can be in any one of the eight unique quadrants due to the three-dimensional shape of TRA, there are theoretically 56 possible water positions, and more in the event of an induced fit.

The absence of subbands in the water complex spectrum indicates that the water does not sample any motion that exchanges its hydrogen atoms. Moreover, the water complex origin band is blue shifted with respect to the corresponding bands of the seven conformers of TRA. Recall that the origin band of indole-H_2O is red shifted by ~ 132 cm^{-1} relative to that of the bare molecule and that it exhibits two subbands due to tunneling. The water molecule is attached to the indole frame *via* a quasi-linear N—H···OH_2.[18] If the water molecule in TRA-H_2O were also attached to the indole ring, this would lead to a LIF pattern with seven water complex bands that are similarly red-shifted relative to their bare molecule origin bands. Thus, the water molecule must be attached to the ethylamine side chain. This finding agrees with the study by Zwier and co-workers[11] that indicated the presence of a HOH···NH_2 hydrogen bond in the TRA-H_2O complex using RIDIR technique.

The absence of subbands in the rotationally resolved spectrum also implies that tunneling does not occur in the TRA-H_2O complex because the barrier is either too low or too high to distinguish the sub-torsional energy levels at our resolution. If low, one OH group would be freely rotating around the hydrogen bond, or the two water hydrogen atoms are exchanging without constraint. This is highly unlikely since the RIDIR data would have shown this distinct

spectroscopic signature.[11] If the barrier is high, a double hydrogen bonded system is implicated, with one HOH···NH_2 hydrogen bond and a second bond linked to either the ethylamine side, the pyrrole ring or the phenyl ring. Again, recall that there is only one water complex origin; thus, the second hydrogen bond cannot be within the side chain. From this analysis, we can eliminate the "up" conformers (GPyup and GPhup) and all three Anti conformers of TRA as possible sites to which the water may bond.

We have therefore reduced the number of possible TRA conformers participating in the complex from seven to two, GPhout and GPyout. Next, we use Kraitchman's equations to quantitatively locate the COM coordinates of water in the principal axis frames of GPhout and GPyout. The results are listed in Table 6-2. Also, Figures 6-3 and 6-4 illustrate all 8 COM positions relative to GPhout and GPyout respectively as taken from the data in Table 6-2. Recall that the water molecule is attached to ethylamine side chain and forms a second h-bond with either the pyrrole or the phenyl ring. A careful inspection of Fig. 6-4 reveals that none of the 8 possible COM positions of the water in GPhout leads to a chemically reasonable structure of TRA-H_2O. Conversely, a careful examination of Fig. 6-3 shows that structures 6 and 8 are the most likely candidates for the TRA-H_2O complex. The COM position is close to the ethylamine side chain and to the pyrrole ring. We have effectively reduced the number from 56 mathematically possible positions to 2 chemically relevant coordinates for the COM of the water molecule. Moreover, these two positions would result in structures that are very similar as they only differ by ~0.48 Å along the *c*-axis of the complex (*cf.* Table 6-2). Figure 6-5 shows the likely structure of the complex where the water molecule acts both as an acid (HOH···NH_2) and a base (CH···OH_2). This result agrees with other studies.[5,6,11,12]

Table 6-2. Center of mass (COM) coordinates of the water molecule in the principal axis frames of the bare parent molecule and the TRA-H_2O complex.

State	Coordinate	GPyout		Gphout	
		Bare molecule frame (Å)[a]	Complex frame (Å)[a,b]	Bare molecule frame (Å)[a]	Complex frame (Å)[a,b]
S_0	|**a**|	4.068 ± 0.002	4.037 ± 0.002	4.572 ± 0.001	4.308 ± 0.005
	|**b**|	2.290 ± 0.006	1.211 ± 0.002	1.10 ± 0.01	0.523 ± 0.006
	|**c**|	0.51 ± 0.02	0.24 ± 0.01	1.355 ± 0.008	0.716 ± 0.005
	|**r**|	4.696 ± 0.002	4.221 ± 0.002	4.889 ± 0.004	4.399 ± 0.001
S_1	|**a**|	4.071 ± 0.002	4.035 ± 0.002	4.568 ± 0.001	4.305 ± 0.004
	|**b**|	2.286 ± 0.006	1.220 ± 0.002	1.13 ± 0.01	0.546 ± 0.005
	|**c**|	0.52 ± 0.02	0.25 ± 0.01	1.331 ± 0.008	0.706 ± 0.005
	|**r**|	4.698 ± 0.002	4.223 ± 0.002	4.891 ± 0.004	4.397 ± 0.001

[a]Errors in the coordinates were determined by propagating the errors in the measured rotational constants through the Kraitchman's analysis.
[b]Determined from the transformation matrix relating the two principal axis systems.

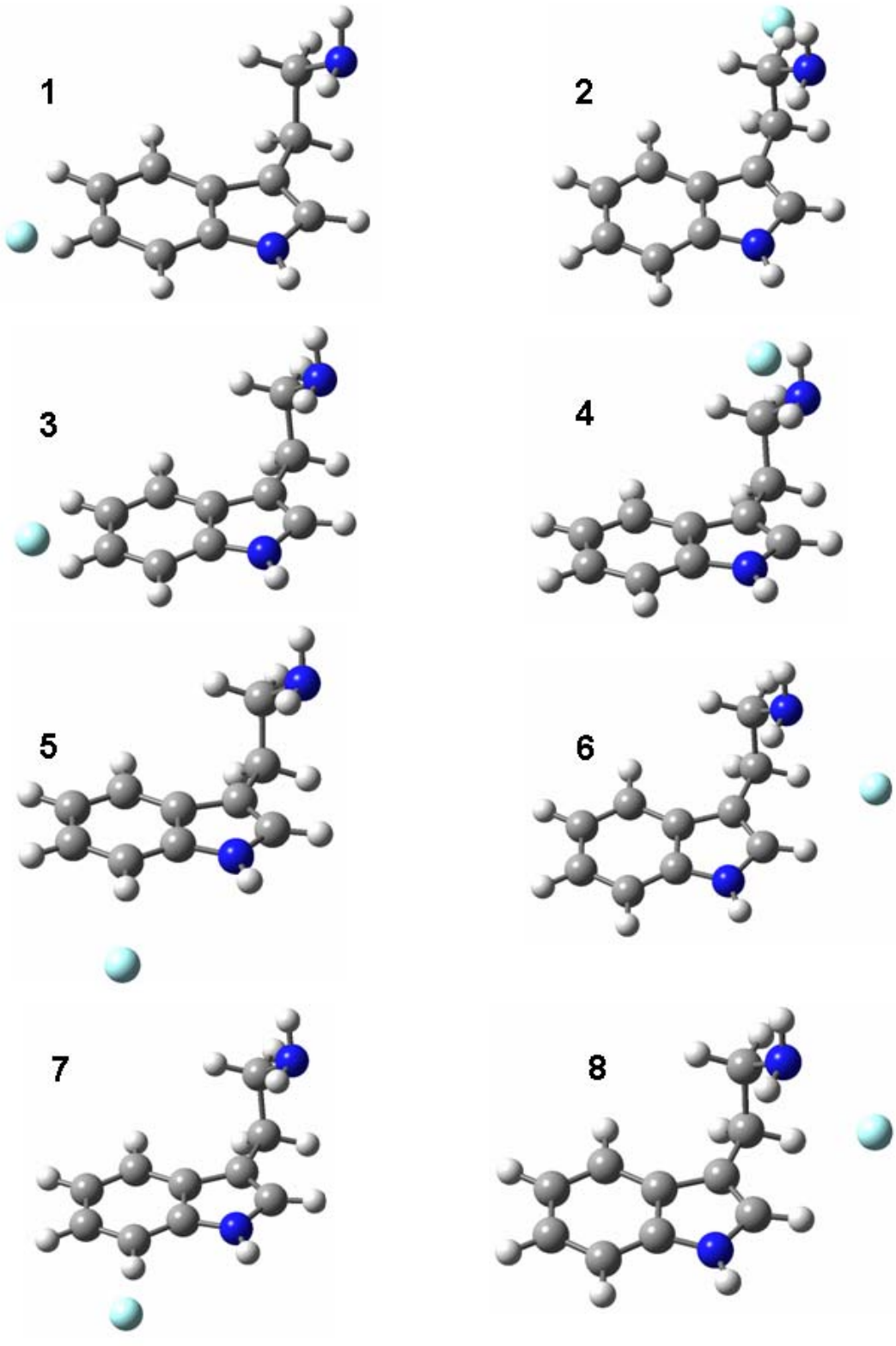

Figure 6-3: Illustrations of the possible COM positions of water in the principal axis frame of the GPyout conformer as derived from the Kraitchman's analysis (see text).

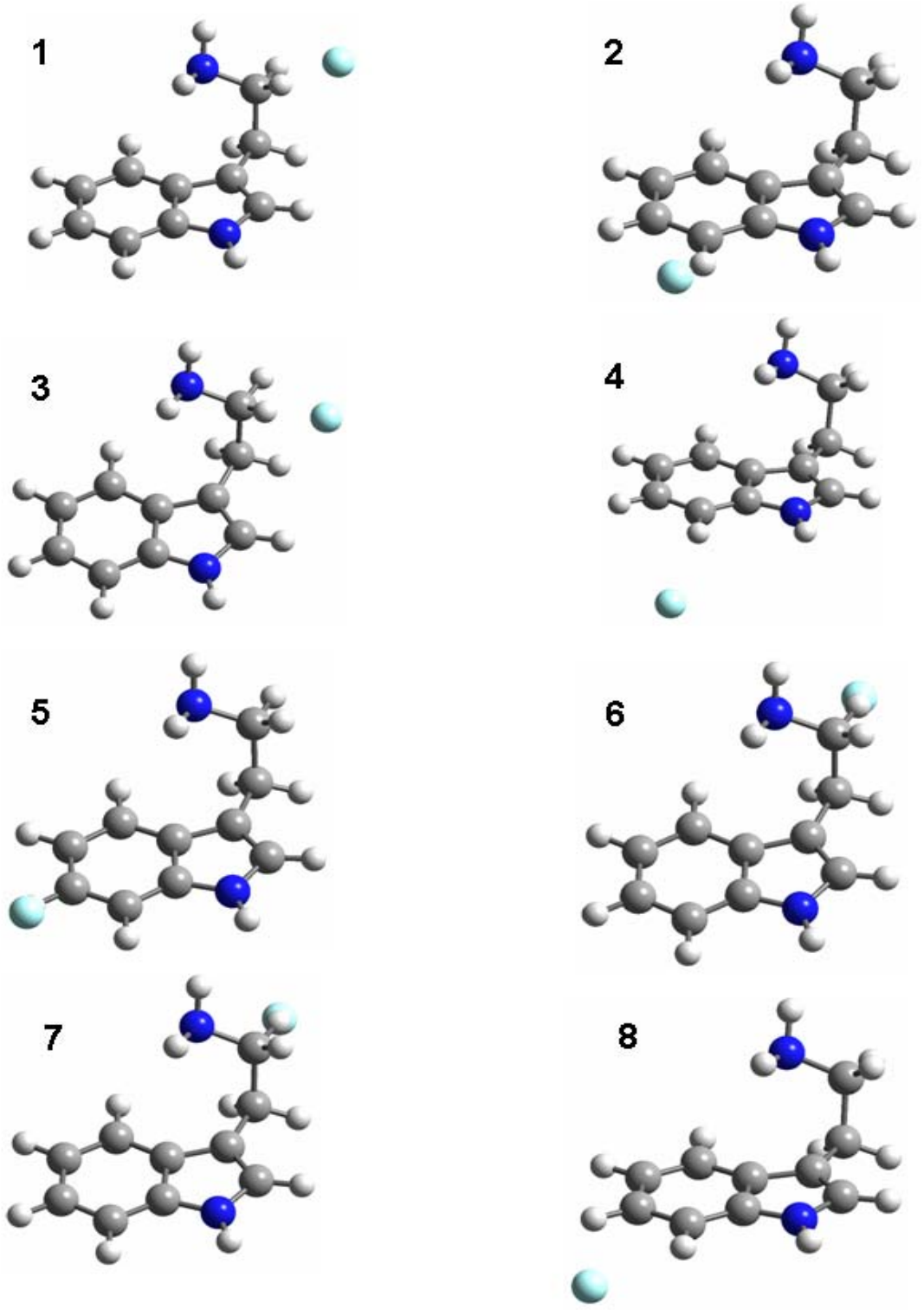

Figure 6-4: Illustrations of the possible COM positions of water in the principal axis frame of the GPhout conformer as derived from the Kraitchman's analysis (see text).

Water orientation in TRA-H_2O. Additional information about the orientation of the attached water molecule is provided by the isotopic substitution experiment. A comparison of the ground state rotational constants of TRA-H_2O and dTRA-D_2O listed in Table 6-1 shows that all three rotational constants decrease upon deuterium substitution. This result is consistent with the direction and magnitude of the changes in the rotational constants of the complex compared to the bare molecule as the water molecule is located "off-axis". There is a large body of work on the topic of the effect of deuterium substitution on strong intermolecular hydrogen bonds by X-ray crystallography,[19] gas-phase microwave,[20-21] and gas-phase rotationally resolved electronic spectroscopy[22] indicating that hydrogen bonds expand upon deuterium substitution. This effect can be attributed to a change in the zero-point vibration of the heavier deuterium atom.

We can exploit this particular property to determine the orientation of the water molecule by comparing the experimental rotational constants of TRA-H_2O and dTRA-D_2O through Kraitchman's equations. Table 6-3 lists the COM coordinates of the D_2O along with the differences in the coordinates of H_2O and D_2O. The latter values have been adjusted to match the undeuterated GPyout reference frame by using the rotational constants of dTRA. [3, 12] The displacements along the *a*- and *b*-axis are similar (~ 0.05 Å) and smaller than along the *c*-axis (0.15 Å). This data confirms the proposed structure shown in Fig. 6-5 where one h-bond is mostly along the *c*-axis and the second h-bond is in-between the *a*- and *b*-axis.

The vibrational motions along the two hydrogen bonds directly affect each other and the magnitude of the COM displacements. By examining these changes in the COM coordinates, we can gain information on the relative strength of the two hydrogen bonds and, as a by-product, on the orientation of the water molecule. Here, the HOH···NH_2 bond coordinate (~ along the *c*-axis) experiences a greater displacement and is stronger than the CH···OH_2 bond; therefore, the

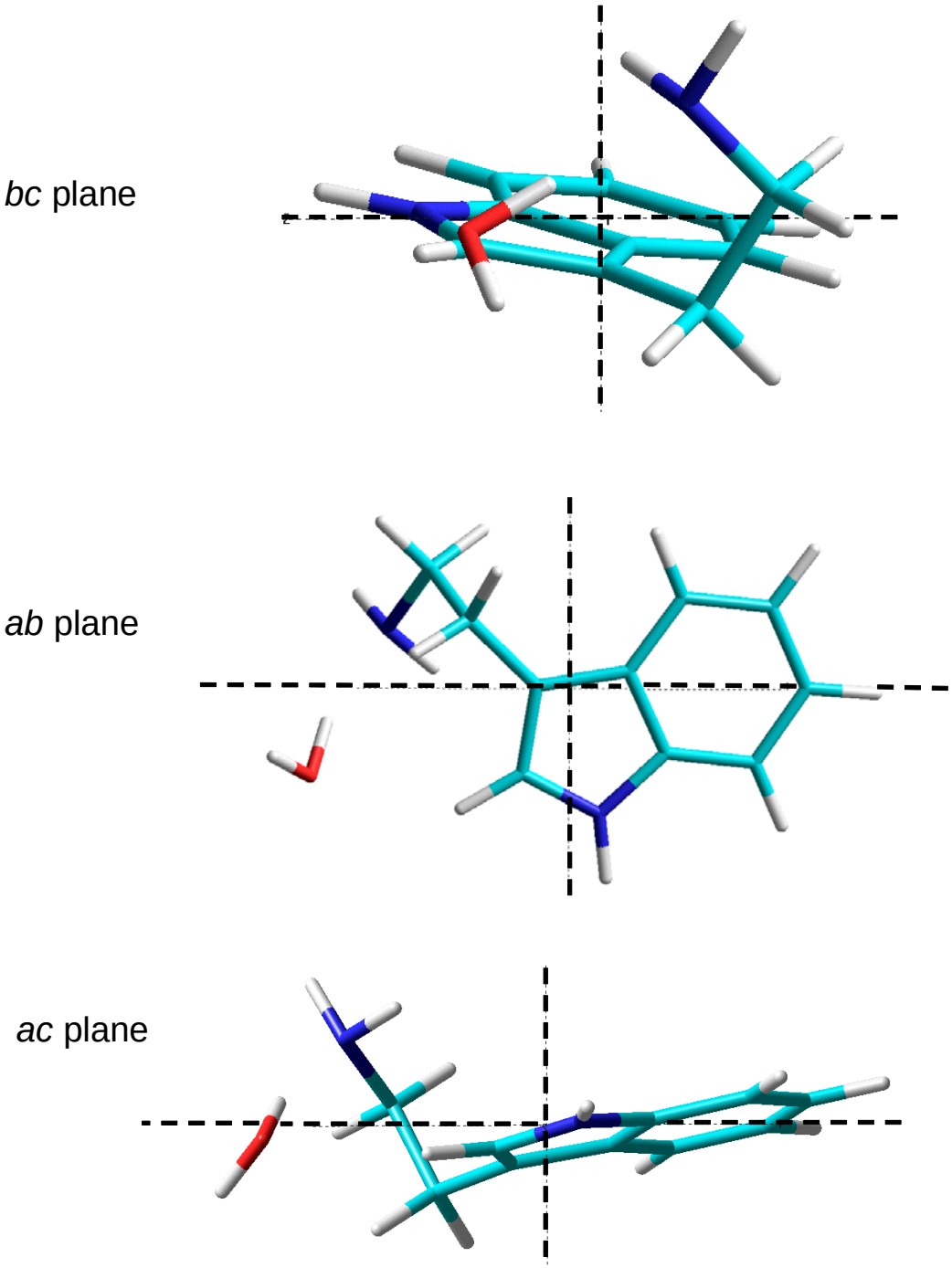

Figure 6-5: Illustrations of the GPyout-H_2O complex in the *ab*, *bc* and *ac* plane.

Table 6-3. Center of mass (COM) coordinates of the water and deuterated water molecules in the principal axis frames of the bare GPyout conformer and the TRA-D_2O complex. Differences in the COM coordinates between TRA -D_2O and TRA -H_2O are also listed.

		GPyout-D_2O		D_2O- H_2O Adjusted[c]
State	Coordinate	Bare molecule frame (Å)[a]	Complex frame (Å)[a,b]	Bare molecule frame (Å)[a]
S_0	|**a**|	4.095 ± 0.002	4.144 ± 0.006	-0.046
	|**b**|	2.470 ± 0.007	1.230 ± 0.002	0.048
	|**c**|	1.01 ± 0.01	0.419 ± 0.006	0.15
	|**r**|	4.889 ± 0.006	4.346 ± 0.002	0.049
S_1	|**a**|	4.106 ± 0.002	4.147 ± 0.006	-0.041
	|**b**|	2.463 ± 0.006	1.248 ± 0.003	0.052
	|**c**|	1.02 ± 0.01	0.423 ± 0.006	0.13
	|**r**|	4.895 ± 0.006	4.351 ± 0.002	0.052

[a]Errors in the coordinates were determined by propagating the errors in the measured rotational constants through the Kraitchman analysis.
[b]Determined from the transformation matrix relating the two principal axis systems.
[c]Adjusted for triple deuteration in the bare molecule by using the rotational constants of dGPyout from Reference 12.

former is a straighter and more linear bond while the latter has some angular feature.

This result is consistent with the observation that the origin band of the complex is blue shifted (by ~ 41 cm^{-1}) relative to the bare molecule. The overall intermolecular hydrogen bonding system in the S_1 state is weaker than in the S_0 state. Typically, this behavior is observed in complexes where the water molecule acts more like an acid (hydrogen donor).[23,24,25] In this arrangement, the water acts more like an acid as the HOH···NH_2 bond is stronger than the CH···OH_2 bond (water as a base). This data shows that it is the synchronization of the two hydrogen bonds that is the cause of the collapse of the complex conformational landscape of TRA into a single complex structure. Furthermore, the disparity in the strength and nature of the two hydrogen bonds effectively prevents the water hydrogen atoms from tunneling since exchanging hydrogen atoms about the C_2 axis of the water molecule requires the breaking of two hydrogen bonds. Spectroscopically, this (lack of) phenomenon led to the absence of any splitting and subbands in the rotationally resolved TRA-H_2O spectrum. But, more information such dipole moment is needed to determine whether or not the species to which the H_2O is attached is one of the known TRA structures, or something completely different. In the language of biology, is this a "lock and key" or is it an "induced fit."

6.6. Conclusions.

The rotationally resolved fluorescence excitation spectrum of tryptamine-water (TRA-H_2O) has been observed and assigned. No splitting and subbands were detected. The analysis identifies the TRA host conformer, the position and orientation of the water molecule. In the double hydrogen bonding system, the water molecule is linked to the ethylamine side chain of

the GPyout conformer (band A) via an HOH···NH_2 bond and to the pyrrole ring via a CH···OH_2 bond.

6.7. Acknowledgment.

We thank Cheolhwa Kang, Tim Korter, and John Yi for helpful conversations. This work has been supported by NSF (CHE-0315584).

6.8. References.

[1] Y. D. Park, T. R. Rizzo, L. A. Peteanu, and D. H. Levy, J. Chem. Phys. 84, 6539 (1986).

[2] L. A. Phillips and D. H. Levy, J. Chem. Phys. 85, 1327 (1986); L. A. Phillips and D. H. Levy, J. Chem. Phys. 89 (85) (1988).

[3] Y. R. Wu and D. H. Levy, J. Chem. Phys. 91, 5278 (1989).

[4] L. L. Connell, T. C. Corcoran, P. W. Joiremans, and P. M. Felker, Chem. Phys. Lett. 166, 510 (1990); P. M. Felker, Chem. Rev. 94, 1784 (1994).

[5] L. L. Connell, T. C. Corcoran, P. W. Joiremans, and P. M. Felker, J. Phys. Chem. 94, 1229 (1990).

[6] P. M. Felker, J. Phys. Chem. 96, 7844 (1992).

[7] J. R. Carney and T. S. Zwier, J. Phys. Chem. A 104, 8677 (2000).

[8] T. V. Nguyen, T. M. Korter, and D. W. Pratt, Molecular Physics 103 (11-12), 1603 (2005).

[9] J. Sipior and M. Sulkes, J. Chem. Phys. 88, 6146 (1988).

[10] L. A. Peteanu and D. H. Levy, J. Phys. Chem. 92, 6554 (1988).

[11] T. S. Zwier, J. Phys. Chem. A 105, 8827 (2001).

[12] M. Schmitt, M. Bohm, C. Ratzer, C. Vu, I. Kalkman, and W. L. Meerts, J. Am. Chem. Soc. (2005).

[13] W. A. Majewski, J. F. Pfanstiel, D. F. Plusquellic, and D. W. Pratt, *Laser Techniques in Chemistry*. (J. Wiley & Sons, New York, 1995).

[14] D. F. Plusquellic, (to be published).

[15] R. M. Helm, H. P. Vogel, and H. J. Neusser, Chem. Phys. Lett. 270, 285 (1997).

[16] W. Gordy and R. L. Cook, *Microwave Molecular Spectra*, 3rd ed. (Wiley-Interscience, New York, 1984).

[17] B. B. Champagne, D. F. Plusquellic, J. F. Pfanstiel, D. W. Pratt, W. M. van Herpen, and W. L. Meerts, Chem. Phys. 156, 251 (1991).

[18] T. Korter, D. W. Pratt, and J. Kupper, J. Phys. Chem. A 102, 7211 (1998).

[19] K. J. Gallagher, *Hydrogen Bonding*. (Pergamon, Belfast, 1959).

[20] T. R. Dyke, Top. Curr. Chem. 120, 85 (1984).

[21] C. C. Costain and G. P. Srivastava, J. Chem. Phys. 41, 1620 (1964).

[22] A. Held and D. W. Pratt, J. Chem. Phys. 96, 4869 (1991).

[23] J. A. Dickinson, M. R. Hockridge, E. G. Robertson, and J. P. Simons, J. Phys. Chem. A 103, 6938 (1999).

[24] A. V. Federov and J. R. Cable, J. Phys. Chem. A 104, 4943 (2003).

[25] M. Becucci, G. Pietraperzia, M. Pasquini, G. Piani, A. Zoppi, R. Chelli, E. Castelluci, and W. Demtroder, J. Chem. Phys. 120, 5601 (2004); C. G. Eisenhardt, G. Pietraperzia, and M. Becucci, Phys. Chem. Chem. Phys. 3, 1407 (2001); B. M. Giuliano and W. Caminati, Angew. Chem. Int. Ed. 44, 603 (2005); J. W. Ribblett, W. E. Sinclair, D. R. Borst, J. T. Yi, and D. W. Pratt, In preparation (2005).